# A COMPARATIVE MODELING STUDY OF THE DOSE DEPENDENT EFFECTS OF ANTIARRHYTHMICS ON A CARDIAC CELL

by

BINAYA TULADHAR

Master of Science, 2011
University of Massachusetts Lowell
Lowell, MA

Submitted to the Graduate Faculty of the
College of Science and Engineering
Texas Christian University
in partial fulfillment of the requirements
for the degree of

Master of Science

May 2019

A COMPARATIVE MODELING STUDY OF THE DOSE DEPENDENT EFFECTS OF ANTIARRHYTHMICS ON A CARDIAC CELL

by

Binaya Tuladhar

Dissertation Approved:

Dr. Hana M Dobrovolny, Advisor

Dr. Peter M Frinchaboy

Dr. Anton Naumov

Dr. Ken Richardson

For The College of Science and Engineering

# ACKNOWLEDGEMENTS

I would like to express my special appreciation and thanks to my advisor Dr. Hana Dobrovolny, who have been a tremendous mentor and for her continuous support of my study, for her motivation and patience. Her continuous guidance helped me all the time of my research and in writing this dissertation.

I would also like to thank Dr. Peter Frinchaboy, Dr. Anton Naumov, and Dr. Ken Richardson for serving as my committee members. Dr. Frinchaboy has been a great help for my successful python coding for my simulations as I learned a lot from his computational physics lecture.

Finally, I would like to thank the Department of Physics and Astronomy for providing me an opportunity for higher study and the research in this university.

# Contents

# List of Figures

# List of Tables

# List of Abbreviations

| | |
|---|---|
| **AP** | Action Potential |
| **APD** | Action Potential Duration |
| **ATP** | Adenosine Triphosphate |
| **AV** | Atrioventricular |
| **BCL** | Basic Cycle Length |
| **CRS** | Critical Ring Size |
| **DI** | Diastolic Interval |
| **DRC** | Dynamic Restitution Curve |
| **ECG** | Electrocardiogram |
| **JSR** | Junctional Sarcoplasmic Reticulum |
| **NSR** | Network Sarcoplasmic Reticulum |
| **PP** | Pacing Protocol |
| **RC** | Restitution Curve |
| **RRD** | Reverse Rate Dependence |
| **SA** | Sinoatrial |
| **SCD** | Sudden Cardiac Death |
| **SR** | Sarcoplasmic Reticulum |
| **SRC** | S1-S2 Restitution Curve |
| **VA** | Ventricular Arrhythmia |
| **VF** | Ventricular Fibrillation |

# Chapter 1

# Introduction

## 1.1 Electrophysiology of the Heart

The human heart is a complex and nonlinear system. The heart pumps blood throughout the body, supplying oxygen and nutrients to the tissues and removing carbon dioxide and other waste. The mechanical contraction of the heart is mediated by electro-chemical excitation that travels through the specialized conduction systems and the muscles. These excitation waves cause a coordinated contraction of the muscle in a normal heart. A heartbeat starts with an electrical pulse in the sinoatrial (SA) node. The SA node is located in the atria and is referred to as the heart's "natural pacemaker, " as it initiates impulses for the heartbeat. The SA node of the heart sends an electrical signal in order to initiate a new heart beat 60–100 times/min. The electrical pulse spreads to the atria and to the ventricles through the atrioventricular (AV) node and specialized conduction pathways, such as the bundle of His and Purkinje fibers. The electric pulse is followed by a physical contraction of each cardiac cell. During contraction of a single cell, the

chemical energy in the form of adenosine triphosphate (ATP) available in the cell has to be transformed into mechanical work. If the electrical activity is orderly, all the cells will contract in an orderly fashion, allowing the heart to pump the blood to other parts of the body. When the heartbeat is above 100, or below 60, times/min, then we say the heartbeat is abnormal. When it exceeds 350 beats/min, sudden death may occur.

## 1.2 The Cardiac Cell

Individual cardiac cells are bound to each other to form cardiac muscle tissue. Cardiac cells are approximately brick-shaped and are stacked in the heart like a brick wall. The cell is 100 μm in length and 22 μm in diameter. These cells are joined by channel proteins, called gap junctions, to facilitate the movement of electrical impulses from one cell to the next, allowing an electrical signal to propagate through the entire heart. The electric signal initiates a process in each cell which is referred to as an "action potential ". Gap junctions are intercellular connections between cardiac cells and connect the cytoplasm of two cells directly, allowing various ions and electrical impulses to directly pass through a gate between them. A gap junction channel is composed of two connexons. These connexons are connexin proteins. The gap junction channels are more concentrated along the ends of the cells than along the sides, giving a directional propensity for the propagation of electric impulse. These cells are excitable, as they are stable in their rest state, but a small and finite stimulus will cause a transient response. In the resting state, these cells exhibit an electrical potential across the membrane. The existence of this potential is due to the electrical and chemical forces balancing each other without any

movement of ions crossing the cell membrane. The typical value of the resting potential in most cardiac cells is about $-85$ mV to $-90$ mV.

## 1.3 The Action Potential

The electrical activity of the cell can be measured by measuring the potential difference between the inside and the outside of the cell. A single ventricular cell has various concentrations of $Na^+$, $K^+$, and $Ca^{2+}$ ions in the intracellular and in the extracellular regions of the cell, separated by a cell membrane. The electric pulse originating from the SA node reaches the ventricles through the conducting pathways and forces the ions to flow in and out of the cell membrane through the ion channels, causing a change in the membrane potential. The response of this membrane potential over the time duration of each heartbeat is called an "action potential ". The action potential (AP) can be defined as an electrical pulse at the cellular level, generated by the movement of ions through the transmembrane ion channels in the cardiac cells. Electrocardiogram (ECG) represents the electrical activity of the whole heart and provides the summation of all the AP of all the cardiac cells, and the information from the ECG reflects the characteristics of the AP. Fig. 1.1 shows the action potential generated from our simulation of the mathematical model, the Bernus model under study. Cardiac cells are considered polarized when they are at rest and no electrical activity takes place. This is called the "resting potential ". The electrical and chemical gradients of the ions are in equilibrium during the resting period of the cell, and as a result, the transmembrane voltage is maintained at approximately $-90$ mV. The action potential plot in Fig. 1.1 shows the electrical changes in the cell

during the cycle of depolarization and repolarization.

The action potential consists of five phases, from 0 to 4, as shown in Fig. 1.1. Phase 4 is the resting phase of the cell, and during this phase, the cell is ready to receive an electrical stimulus. During this phase, the cell membrane is permeable to $K^+$ ions more than it is to the other ions. For this reason, the resting potential is close to $K^+$ potential, approximately $-90$ mV in the human ventricular cell. Phase 0 of the action potential is characterized by a sharp upstroke, during which the fast $Na^+$ ions enter the cell through sodium ion channels in the cell membrane and the cell then depolarizes. The depolarization causes the membrane potential to reach a peak positive value. The sodium channels are voltage dependent because they open only when the membrane voltage attains a certain voltage, called the "threshold voltage ". Then some $K^+$ comes out of the cell, and the cell begins an early; and partial, repolarization, as seen in phase 1. During this phase, the cell begins to contract. Then the slow $Ca^{2+}$ ions enter the cell, causing a prolonged phase of slow repolarization, characterized by a plateau in phase 2 until the membrane potential falls to 0 mV. This is the distinctive feature of the cardiac action potential. During phase 3, more $K^+$ ions come out of the cell and cause the further repolarization of the cell, characterized by its downslope, and the cell finally comes back to its resting potential.

The action potential duration (APD) is defined as the amount of time in which the voltage remains above a threshold membrane voltage. In this study, the threshold voltage is chosen at 90% recovery from the peak voltage to the resting voltage, usually denoted by $APD_{90}$. The time duration between two consecutive stimuli is known as the "basic cycle length (BCL) " or the "pacing period (PP) ". The time duration from the end of

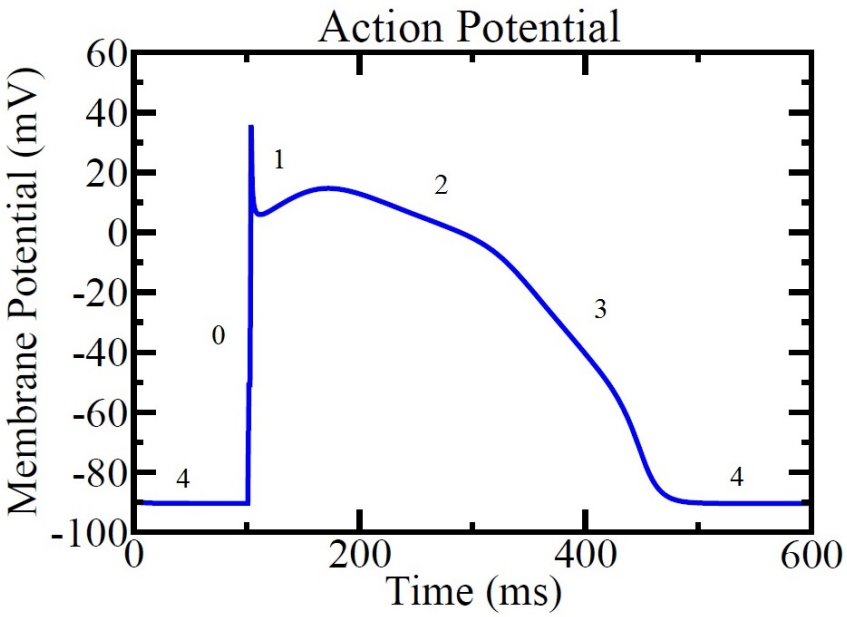


Figure 1.1: The change in transmembrane potential over time is called an action potential. The action potential has five different phases.

the previous action potential to the beginning of the current action potential is called the "diastolic interval (DI) ". A typical response to the pacing of a cardiac cell is shown in Fig. 1.2. For a constant basic cycle length, the pacing relation is given by

$$APD + DI = BCL \tag{1.1}$$

## 1.4 Cardiac Arrhythmia and Antiarrhythmic Drugs

Cardiac arrhythmia is an abnormal heart rhythm and refers to a deviation from the normal sequence of electrical impulses. When the electrical impulses coordinating the heartbeats do not work properly, they cause the heart to beat either too fast or too

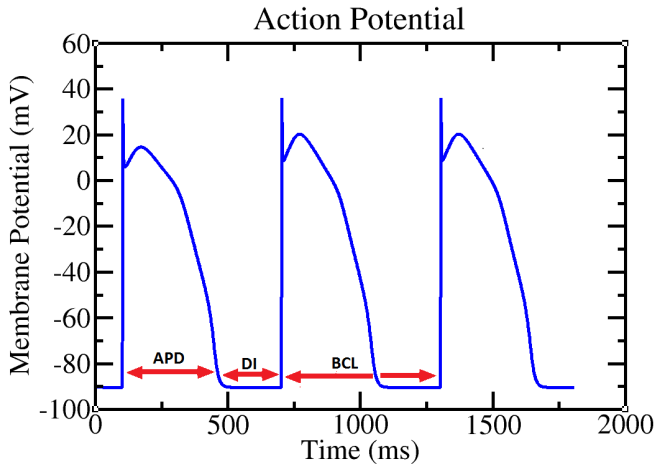


Figure 1.2: The relation between APD, DI and BCL.

slow and sometimes irregularly. In the human heart, arrhythmia due to heartbeat above 100 times/min is called "tachycardia " and arrhythmia due to a heartbeat below 60 times/min is called "bradycardia ". Sudden cardiac death (SCD), primarily caused by cardiac arrhythmias, is one of the leading causes of mortality in the United States. It is responsible for over half of the total deaths due to cardiovascular disease and accounts for over 325,000 deaths annually (1, 2). Ventricular fibrillation (VF), which severely distorts the contraction rhythm of cardiac muscle (3), is the main cause of these mortalities. This leads to full loss of the heart's pumping function. Fig. 1.3 shows the various forms of cardiac arrhythmias, corresponding to deviations from a normal heartbeat. As seen in Fig. 1.3, there are different forms of tachycardia as the heart rate increases; and when the heart rate is above 350 times/min, ventricular fibrillation occurs, which can cause SCD in humans.

Antiarrhythmic agents are pharmaceuticals that are used to prevent cardiac arrhythmias. These drugs are used to treat abnormal heart rhythms, which result from the

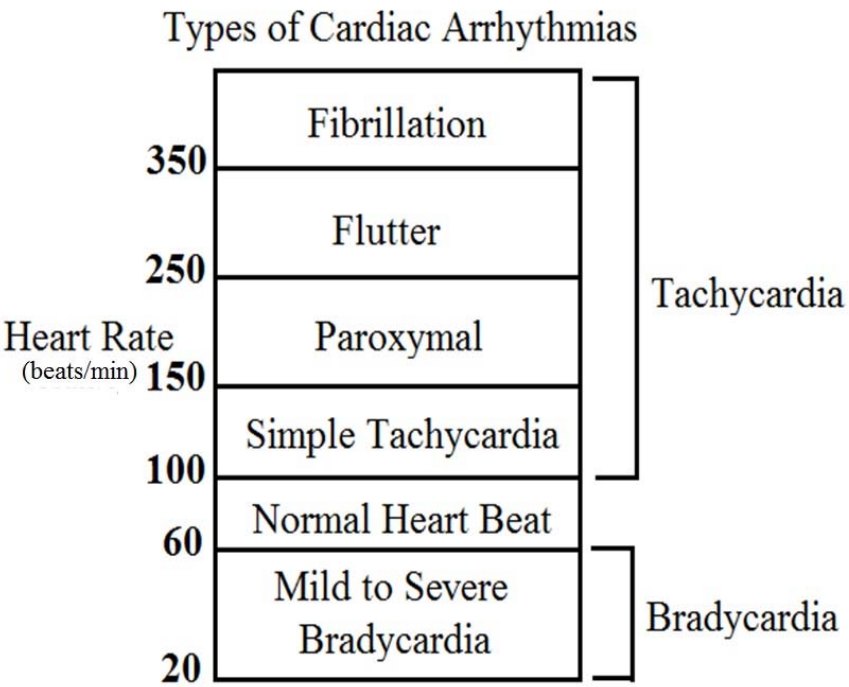


Figure 1.3: Types of cardiac arrhythmias can result from changes in heart rhythm.

irregular electrical activity of the heart. Several antiarrhythmic drugs alter cell membrane ion conductances, causing changes in the electrophysiological response of the cell. There are four main classes of antiarrhythmic drugs, grouped according to their electrophysiological mechanism of action, also know as Vaughan-Williams classification (4). Antiarrhythmic drugs are grouped by the effect they have on the ion channels and on cardiac action potentials.

1. Class I: Sodium channel blockers.
2. Class II: Beta blockers.
3. Class III: Potassium channel blockers
4. Class IV: Calcium channel blockers.

### 1.4.1 Use of Antiarrhythmic Drugs and their Limitations

Various antiarrhythmic medications have been identified and are commonly used (5–7) in the treatment of patients with life-threatening heart rhythms. While the clinical effect of these medications must be well-documented to gain FDA approval (6, 8, 9), and the biochemical effect of the compounds are also typically well-known (10–13), there remains a large gap in our understanding of how the drugs affect dynamics at the cellular and tissue levels.

One of the major limitations of antiarrhythmic drugs is proarrhythmia (14–17), which is a worsening or induction of arrhythmia by drug application. In many cases, these drugs prevent the recurrence of arrhythmia effectively; however, the drugs may produce the side

effects. The proarrhythmic nature of these antiarrhythmic drugs is an important factor that limits their proper use. Therefore, the development of new antiarrhythmic drugs that minimize, and even eliminate, the risk of proarrhythmia depends on understanding the mechanisms of how these drugs induce proarrhythmia. The proarrhythmic risks of sodium channel blockers have been studied using the drug flecainide, which showed an increased mortality risk in dogs (14, 18). Potassium channel blockers can produce torsade de pointes which may deteriorate into ventricular fibrillation (19, 20). There is little direct evidence of calcium channel blockers contributing to significant proarrhythmia, but excessive concentrations of these drugs may cause varying degrees of atrioventricular block (21). Additionally, several clinical studies have noted increased mortality with various classes of antiarrhythmic drugs (8, 9).

## 1.5 Bifurcation Theory

Bifurcation theory deals with the mathematical study of changes in the qualitative behavior of dynamical systems which are nonlinear in nature. A nonlinear dynamical system is a dynamical system in which the output is not proportional to the input. When a dramatic qualitative change in appearance takes place due to a small change in a system's parameters, a bifurcation is said to occur. Cardiac cells are nonlinear systems, as they have nonlinear voltage and current profiles, and they also have the property of sudden transitions to different cardiac rhythms (22).

The application of nonlinear dynamics in understanding cardiac arrhythmia has grown tremendously over the last few decades. The generation of electrical activity in cardiac

cells is through a very highly complex system. The system consists of many parts which are interconnected and often has a nonlinear dependence on one or more variables, such as the transmembrane voltage of cardiac cell membrane or ionic concentrations. Bifurcation theory is useful in describing the electrical instability in cardiac cells. We can treat the basic cycle length (BCL) as a bifurcation parameter. During periodic electrical stimulation of a cardiac cell, $M$ stimuli can elicit $N$ responses of action potentials, referred to as $M$:$N$ behavior. Bifurcation mediates the transition from one response to another response pattern under the changes in BCL (23). During slow pacing of a cardiac cell, 1:1 behavior is observed, and each APD is identical to the other. With rapid pacing, APD shortens and bifurcation occurs, which can give rise to different responses: either a 2:2 or 2:1 response (24). APD alternates in a long-short pattern during 2:2 behavior, in a state called "alternans " at a constant BCL. The transition from a 1:1 response to a 2:2 response is of particular interest to researchers, as alternans has been shown to be a precursor to arrhythmia (25–27).

## 1.6 Restitution

Cardiac alternans, which is a long and short alternation in the (APD), may be a precursor to the development of ventricular arrhythmias (VAs), leading to SCD (1, 25, 28–33). During slow pacing of cardiac cells, each stimulus generates a single AP with all APD equal. However, at faster pacing, there is a decrease in APD as well as DI giving rise to restitution. Restitution plays a crucial role in the function of heart at normal heart rate with a shorter APD and a longer DI, providing enough time for refilling the heart

with blood. However, with increasing heart rates, DI shortens quickly compared to APD and the normal response pattern 1:1 can change to 2:2 giving rise to altenans. Some recent clinical studies have shown that there is a correlation between alternans in the electrocardiogram (ECG) and its tendency to promote ventricular fibrillation (25, 34, 35). Electrical restitution plays an important role in heart function and describes the nonlinear functional relationship between APD and the preceding diastolic interval (DI). The function is known as the APD restitution curve (RC). In an RC, we study the relationship between APD and DI when the basic cycle length (BCL) is varied. The steepness of the RC is thought to play an important role in determining the onset of arrhythmia. Nolasco and Dahlen (36) mathematically predicted the onset of alternans using the APD restitution relationship. The stability analysis of their mapping model predicted the occurrence of alternans when the slope of the RC is greater than 1 (37), termed as the restitution condition. When the slope of the RC exceeds 1, the 1:1 pattern becomes unstable and heart rhythm behaves abnormally. There are several protocols to measure different types of restitution curves (RC), each of which measures an individual RC, the most common being the dynamic and the S1-S2 RCs (38, 39). We can study the different aspects of mechanisms for changing the APD by these methods.

The mathematical relationship between APD and the preceding DI is written as

$$APD_{n+1} = F(DI_n) \tag{1.2}$$

where $F$ is the function that relates APD to the preceding DI, known as the restitution curve. $APD_{n+1}$ denotes APD on the $(n+1)th$ pace.

If a cardiac cell is stimulated periodically with a basic cycle length BCL, then the summation of the APD and DI at any beat $n$ during 1:1 response is given by,

$$BCL = APD_n + DI_n \tag{1.3}$$

Inserting Eq. (1.2) into Eq. (1.3), we see that the dynamics is governed by a 1-dimensional map (28, 37) and is given by

$$APD_{n+1} = F(BCL - APD_n) \tag{1.4}$$

It was shown by Guevara (37) that when the slope of the RC is less than 1, the 1:1 response pattern is stable. However, for such a model, there is only one RC regardless of the pacing protocol (40).

A new type of mapping model was proposed by Gilmour et al. (41), to describe their experiments using dog hearts, and they proposed that the 1:1 response pattern becomes unstable when the RC, using the dynamic restitution protocol, is greater than 1. A model of this form was later derived analytically (42) from an ionic model of the cardiac membrane. This mapping model assumes that APD depends on the preceding DI as well as on the preceding APD. The mapping model displays rate dependent restitution because there is an explicit dependence of $F$ on both $APD_n$ and $DI_n$, which is of the form

$$APD_{n+1} = F(APD_n, DI_n) \tag{1.5}$$

Inserting Eq. (1.3) into Eq. (1.5), this model is still represented by a 1-dimensional map and is given by

$$APD_{n+1} = F(APD_n, BCL - APD_n) \tag{1.6}$$

In several experiments and modeling studies (39, 43–45), when the slope of the RC was equal to or greater than 1, the rapid pacing induced alternans and fibrillation in isolated ventricles, whereas alternans and fibrillation did not occur when the slope of the RC was less than 1 (39, 43, 44). These experiments also indicated that fibrillation in ventricles can be suppressed by flattening the RC by lowering its slope below 1. Researchers suggested that the maximum slope of the electrical RC is an indicator of the risk of arrhythmia and plays an important role in the development of new antiarrhythmic drugs (46, 47). By analyzing the steepness of the RC, we can study the initiation and maintenance of alternans (42). The flattening of the RC results in the disappearance of alternans and helps to maintain a steady state APD for normal heart rhythm, and therefore, the study of the slope of the RC plays an important role in anti-arrhythmic therapy (48). The restitution hypothesis conceived by Nolasco and Dahlen, however, has been shown to fail in some recent experiments (24, 40, 49, 50), suggesting that the slope of the RC does not predict alternans.

### 1.6.1 Dynamic Restitution

After the cell is paced at a fixed interval for some time period, a steady state is attained, and during this state, there a correspondence between APD and DI. The dynamic restitution curve (DRC) is determined by steady state APD and DI. The steady state APD

and DI are measured at each BCL as the BCL is varied. So for a given cardiac cell we obtain a single DRC.

### 1.6.2 S1-S2 Restitution

The immediate effect of a perturbation in BCL on a system which was previously at the steady state is measured by the S1-S2 restitution curve. The incomplete recovery of ionic currents causes this immediate response to perturbation (51). In the S1-S2 restitution method, the cell is paced at constant basic cycle length (S1) until the steady state is reached. This is followed by a single stimulus (S2) at a different BCL. The interval between S1 and S2 is varied, and the APD produced by the S2 BCL and the preceding DI is used to obtain a point on the RC. The choice of different S1 BCLs results in different restitution curves (40, 52, 53).

In cardiac cells, the APD does not depend only on the previous DI, but also with the short-term pacing history, such that each APD plays an important role in determining the next APD (38, 54). This property is called "short-term cardiac memory". S1-S2 restitution curves with different S1 BCLs would be very much similar in the absence of short-term cardiac memory.

### 1.6.3 Previous Experimental Work

Experimental examination of the effect of antiarrhythmics on action potential duration (APD) is fairly commonplace, although results are not very consistent. Several studies have examined the effect of class I antiarrhythmics on APD (55–65) with some studies

observing an increase of APD with application of the drug (55, 59–61), others observing a decrease in APD (55, 57, 58, 62), yet others observing no change in APD (63–65), and one study even observing biphasic dose-dependent behavior (56). There is somewhat less confusion about the effect of potassium channel blockers on APD, with the majority of studies finding prolongation of APD in the presence of a class III drug (59, 66–74). Two studies have seen other effects of potassium channel blockers: one study noted biphasic dose-dependent behavior in the presence of azimilide (75), while another study noted a decrease in APD during treatment with amiodarone (70). Finally, most studies using class IV antiarrhythmics indicate that these drugs shorten APD (59, 62, 76), although one study observed biphasic dose-dependent behavior in the presence of verapamil (59).

There have also been a number of experimental studies that examined the rate-dependent effect of antiarrhythmics. Such studies, measuring the effect of a drug on APD at several different pacing rates, are particularly common for class III antiarrhythmics where a phenomenon called reverse rate dependence (RRD) has been observed (66–69, 71–73, 76–79). RRD refers to a decrease in the effect of a drug at rapid pacing, where we would actually like for the drug to be most effective. While RRD has frequently been observed for class III antiarrhythmics, there are other studies that have noted positive rate dependence (72), or no rate dependence (73), for drugs in this class. Some studies examining the rate dependent effect of class I agents also showed mixed results, with RRD observed in cardiac tissue from some animals, but not others (78, 80), and positive rate dependence observed in yet another study (74). There are no studies of the rate-dependent effect of class IV antiarrhythmics on APD.

There are a number of experimental and modeling studies (39, 43–45, 49, 81) which

studied the restitution hypothesis. When the slope of the RC was equal to or greater than 1, the rapid pacing induced alternans and fibrillation in isolated ventricles, whereas alternans and fibrillation did not occur when the slope of the RC was less than 1. These experiments also indicated that fibrillation in ventricles can be suppressed by flattening the RC. However, there are cases, where the slope of the RC is greater than 1, and still there is an absence of alternans. The experiments on frog cardiac tissue (24) and rabbit heart tissue (49) showed no alternans, even though the slope of the RC is greater than 1. There are experiments on bullfrog (40) and canine cardiac Purkinje fibers (50), where the slope of the RC does not approach 1, even though alternans are present. These experiments contradict the restitution hypothesis.

### 1.6.4 Importance of Mathematical Modeling of Antiarrhythmic Drugs

A limitation of the experimental studies is the small number of drug concentrations used to determine the effect of a drug. Some of the mixed findings might arise from the limited number of doses used in these studies. Additionally, the use of spatially extended tissue to measure single-cell effects makes it difficult to isolate drug effects from the effects of spatial coupling or the effects of spatial heterogeneity. These limitations make it difficult to form a complete understanding of how a drug alters the electrophysiological properties of a single cell. Mathematical models can help fill in some of the gaps left by experimental data since a wide range of doses can easily be simulated. Some modeling studies have simulated the effect of antiarrhythmics (82–90), although many follow the

lead of experiments and examine only a few doses (87–90), providing an incomplete understanding of the full range of effects of an antiarrhythmic.

Chay explained the proarrhythmic action of some class I and IV antiarrhythmic drugs and how some potassium channel blockers can control reentrant arrhythmias through simulations of cardiac cells arranged in a ring (84, 85). Chay modeled the antiarrhythmic drugs by varying conductances of $Na^+$, $Ca^+$, and explained how blocking of these currents can be proarrhythmic by means of a bifurcation approach and simulation of the model. At a certain ring size, termed the critical ring size (CRS), the infinite ring behavior breaks down suddenly. Sodium and calcium channel blockers shorten this CRS, whereas the potassium blockers lengthen this CRS. Shortening of CRS refers to a drug being proarrhythmic whereas lengthening of CRS explains the drug being antiarrhythmic.

Trenor et al. (82) carried out computational work to develop an in-silico tool for the safety assessment of preclinical antiarrhythmic drugs using the O'Hara model for human ventricular cells (91). Their computational work illustrated the proarrhythmic potential of antiarrhythmic drugs by examining the impact of the ratio of potassium channel blockers and sodium channel blockers on APD. A detailed model of cardiac electrophysiology was also used in computer simulations by Mirams et al. (83) where they predicted the risk of proarrhythmic effects of the antiarrhythmic drug.

Brennan et al. (92) reviewed detailed models of antiarrhythmic drug action on cardiac electrophysiology. They presented mathematical modeling that has been used to investigate the interaction of drugs with $Na^+$ and $K^+$ channels and how they alter the electrophysiological behavior of cardiac cells and tissues. Brennan et al. (93) modified the Ten Tusccher and Panfilov model (94) and used it for simulation of the potassium

blocker sotalol. They found that sotalol induced changes in the AP of ventricular cells at different BCLs. A comparison of the response of the Brennan model at different BCLs was made with experimental data from excised human hearts (95).

In our study, we use the Bernus model (96) of a single human ventricular cell and the Fox model (97) of a single canine ventricular cell to implement different doses of sodium, potassium and calcium channel blockers through a parameter called "efficacy". From our computational work, we are able to study the change in the APD, rate dependence, perform a bifurcation analysis, and study the restitution properties of APD on both types of cells.

## 1.7 Modeling of Cardiac Cells

### 1.7.1 The Hodgkin and Huxley model

The mathematical modeling of biological excitable media, such as neurons and cardiac cells, started in 1952 with the Hodgkin-Huxley model of the squid giant axon (98). The Hodgkin-Huxley model describes the generation of action potentials in neurons. Hodgkin and Huxley demonstrated that the macroscopic ionic currents in the squid giant axon are due to changes in $Na^+$, $K^+$ conductances in the membrane of the axon. Based on their experiments, Hodgkin-Huxley developed a detailed mathematical model of the $Na^+$ and $K^+$ conductances. Both of these conductances are voltage and time-dependent. Their pioneering work led to the development of a coupled set of differential equations that describe the ionic basis of the action potential.

We can think that each individual ion channel is either open or closed in the cell and contains one or more than one physical gate. These gates then regulate the flow of ions through the channel. The gates are protein pores in the cell membrane and have openings that are wide enough for the ions to pass through. The concept of "gating variables" is introduced by Hodgkin and Huxley and subsequently used thereafter in other mathematical models. Each gating variable $y$, which is the probability function of opening or closing the gate, can be constructed in order to define the fractional opening of the channels as a function of the voltage and time. The value of a gating variable is a dimensionless quantity that ranges between 0 and 1 with 0 corresponding to all ion channels closed, and 1 corresponding to all ion channels open.

From their experiments on the squid giant axon, Hodgkin and Huxley found that sodium and potassium conductances could be reproduced by using gating variables that obey first order differential equations. The differential equations are of the form

$$\frac{\mathrm{d}y(t)}{\mathrm{d}t} = \frac{y_\infty - y(t)}{\tau_y}, \tag{1.7}$$

where $y_\infty$ describes the steady state value of $y$, and $\tau_y$ is a time constant.

The parameters $y_\infty$ and $\tau_y$ characterize a gate. The parameter $y$ characterizes the state of this gate at a particular time. $y_\infty$ and $\tau_y$ are implicitly time-dependent because they depend on the membrane potential. We can write the above equation in the form of a rate equation. This equation describes the opening and the closing of the gates at various times and as a function of cell membrane voltage. Therefore the gates control

the kinetics of ionic flow through the ion channels.

$$\frac{\mathrm{d}y(t)}{\mathrm{d}t} = \alpha_y(1-y) - \beta_y y, \tag{1.8}$$

where $\alpha_y$ is the rate at which the ion channel gates change from closed to open state and $\beta_y$ describes the rate at which the gates change from open to closed state. Together, they give the total rate of change in the ion channels during an action potential. They are both rate constants that vary with membrane voltage only and have dimension of $[\text{time}]^{-1}$. Their values are based on empirical data.

If the membrane voltage $V_m$ is maintained at some fixed value $V$, then the fraction of gates of the ion channel in the open state will reach a steady state value (i.e., $dy/dt = 0$) as $t \to \infty$.

The equation Eq. (1.8) can then be written as follows.

$$y_\infty = \frac{\alpha_y}{\alpha_y + \beta_y}. \tag{1.9}$$

The time approaching this equilibrium value is described by a simple exponential with time constant $\tau_y$ given by:

$$\tau_y = \frac{1}{\alpha_y + \beta_y}. \tag{1.10}$$

An individual ion channel in an open state contributes a small, but fixed, value to the total conductance, while channels in the closed state contribute nothing. For a large number of channels, the conductance is thus proportional to the number of channels that are in the open state. So the conductance is therefore proportional to the probability that

the gates associated with the channels are open. Therefore the macroscopic conductance $G_{ion}$ due to ion channels with the gating variable $y$ is proportional to the product of each of the individual gate probabilities $y$:

$$G_{ion} = g_{ion}\Pi y_i, \tag{1.11}$$

where $g_{ion}$ provides the maximum conductance that is possible when all the ion channel gates are open.

In the Hodgkin and Huxley model, the three gating variables $n$, $m$ and $h$ describe the behavior of three different ion gates, the $K^+$ channel gate, the $Na^+$ channel activation gate and the $Na^+$ channel inactivation gate, respectively. There are no $Ca^{2+}$ ions in the neuron cells, so this model lacks the presence of $Ca^+$ that is present in the cardiac cells. The potassium channel conductance was expressed as a power function of the gating variable $n$. Hodgkin and Huxley found that the potassium channel conductance could be expressed as

$$G_K = g_K n^4, \tag{1.12}$$

where $g_K$ denotes the maximum conductance of the potassium channel.

The conductance of the sodium channel is a function of two gating variables, activation gating variable $m$ and inactivation gating variable $h$. Hodgkin and Huxley gave the empirical expression for the conductance of the sodium channel as

$$G_{Na} = g_{Na} m^3 h, \tag{1.13}$$

where $g_{Na}$ denotes the maximum conductance of the sodium channel. The probability of opening of activation gates increases with depolarization, while the probability of opening of inactivation gates decreases with depolarization.

These three gating variables are determined as follows using Eq. (1.8) (98)

$$\frac{\mathrm{d}n}{\mathrm{d}t} = \alpha_n(1-n) - \beta_n n \tag{1.14}$$

$$\frac{\mathrm{d}m}{\mathrm{d}t} = \alpha_m(1-m) - \beta_m m \tag{1.15}$$

$$\frac{\mathrm{d}h}{\mathrm{d}t} = \alpha_h(1-h) - \beta_h h \tag{1.16}$$

These $\alpha$'s and $\beta$'s are the rate constants, and they are voltage dependent. Their empirical functions, which were fitted to data from experiments on squid giant axon (98), are

$$\alpha_n = \frac{0.01(V+10)}{\exp[(V+10)/10-1]} \tag{1.17}$$

$$\beta_n = 0.125\exp[V/80] \tag{1.18}$$

$$\alpha_m = \frac{0.01(V+25)}{\exp[(V+25)/10-1]} \tag{1.19}$$

$$\beta_m = 4\exp[V/18] \tag{1.20}$$

$$\alpha_h = 0.07\exp[V/20] \tag{1.21}$$

$$\beta_h = \frac{1}{\exp[(V+30)/10+1]}. \tag{1.22}$$

Hodgkin and Huxley suggested that the electrical behavior of the cell membrane of the squid giant axon may be represented by an electrical equivalent circuit as shown in Fig. 1.4. In the figure, a capacitor is used to describe the charge storage capacity of the

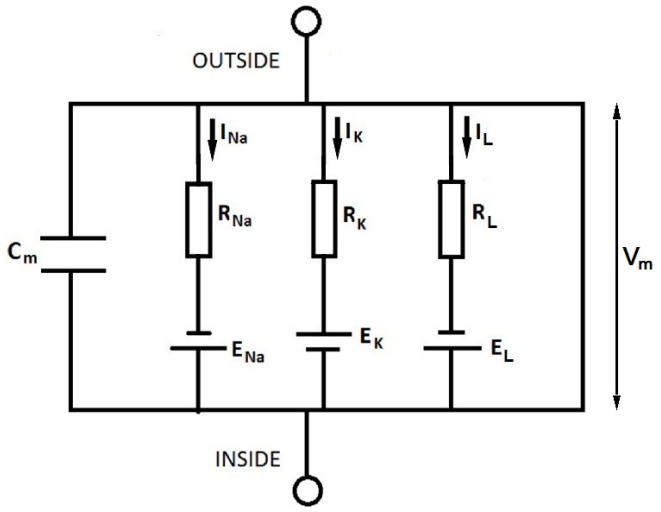


Figure 1.4: Equivalent electrical circuit showing a cell membrane of squid giant axon. The capacitor $C_m$ describes the capacitance of the cell membrane. Two variable resistors $R_{Na}$, and $R_K$, are the voltage dependent $Na^+$ and $K^+$ conductances. The fixed resistor $R_L$ is the voltage independent leakage conductance and the three batteries represent reversal potentials for the corresponding conductances (98).

cell membrane. The voltage-dependent $Na^+$ ion, $K^+$ ion conductances are represented by two variable resistors and voltage independent leakage conductance $L$ is represented by a fixed resistor $R_L$.

The current is carried through the cell membrane capacitance and also by the passage of ions through the resistances $R_{Na}$, $R_K$ and $R_L$ in parallel with the membrane capacitance. The ionic currents are potassium current $I_K$, a sodium current $I_{Na}$, and a small leakage current $I_L$ which was later identified as chlorine current $I_{Cl}$.

The current $I$ is related to electrical potential $V$ by Ohm's law, given by

$$I = \frac{V}{R}, \tag{1.23}$$

where $R$ is the resistance.

In order to calculate the value of the potential contributing to $Na^+$, $K^+$ and leak channel ion flow, we take the difference between the membrane potential $V_m$ ($V$=$V_m$)and the equilibrium potential $E_{ion}$. The equilibrium potential, also known as Nernst potential is the potential that exists due to the concentration gradients of ions across the membrane. Hence, we have the modified Ohm's law as follows.

$$I = \frac{V_m - E_{ion}}{R}. \tag{1.24}$$

The conductance of ion channels across the membrane is given by the reciprocal of the resistance, $G_{Na}$=$1/R_{Na}$, $G_K$=$1/R_K$ and $G_L$=$1/R_L$. In terms of conductances, the sodium current $I_{Na}$, the potassium current $I_K$, and the leakage current $I_L$ are given by

$$I_{Na} = G_{Na}(V_m - E_{Na}) \tag{1.25}$$

$$I_K = G_K(V_m - E_K) \tag{1.26}$$

$$I_L = G_L(V_m - E_L), \tag{1.27}$$

respectively. Using Eq. (1.12), and Eq. (1.13) the sodium current, and the potassium current are given by

$$I_{Na} = m^3 h g_{Na}(V_m - E_{Na}) \tag{1.28}$$

$$I_k = n^4 g_K(V_m - E_K), \tag{1.29}$$

and the leakage current is given by

$$I_L = g_L(V_m - E_L). \tag{1.30}$$

According to Hodgkin and Huxley, sodium conductance showed a more complex behavior than potassium conductance. The sodium conductance showed a transient response, whereas the potassium conductance showed a sustained response with step changes in the voltage. They found that sodium channels inactivate whereas the potassium channels do not. In order to model this process, they postulated that the sodium channels are controlled by two gating variables: $m$, an activation gate and $h$, an inactivation gate, both of which depend on the membrane potential. The activation variable $m$ is found to increase with membrane potential and the inactivation variable $h$ found to decrease with the membrane potential. Hodgkin and Huxley modeled the sodium conductance using three $m$ gates and one $h$ gate as shown in the above equation by the exponent of $m$ and $h$ respectively. The potassium channels are controlled by a single gating variable $n$ and its value increases with the membrane potential. They modeled the potassium channel conductance with four identical $n$ gates shown by the exponent of $n$ in the equation.

The total current $I$ is the sum of the current that charges the cell membrane capacitance and the currents due to individual ions,

$$I = I_C + I_{ions}, \tag{1.31}$$

where

$$I_{ions} = I_{Na} + I_K + I_L \tag{1.32}$$

$I_C$ is the capacitive current which is the rate of change of charge $q$ at the surface of membrane surface given by

$$I_C = \frac{dq}{dt}. \tag{1.33}$$

This charge $q$ is stored in the membrane capacitance and is related to the instantaneous membrane voltage $V_m$ and membrane capacitance $C_m$ by

$$q = C_m V_m. \tag{1.34}$$

Therefore, the capacitive current is given by

$$I_C = C_m \frac{dV_m}{dt}. \tag{1.35}$$

Substituting for $I_C$ in Eq. (1.31) gives

$$I = C_m \frac{dV_m}{dt} + I_{Na} + I_K + I_L. \tag{1.36}$$

Substituting for ionic currents from Eq. (1.28), (1.29) and (1.30), we get

$$I = C_m \frac{dV}{dt} + m^3 h g_{Na}(V - E_{Na}) + n^4 g_K(V - E_K) + I_K + g_L(V - E_L). \tag{1.37}$$

If an externally stimulated current $I_{stim}$ is applied to the circuit then this current is

equal to $I$, which is the total current within the circuit. The Hodgkin and Huxley model is a representation of the action potential in the squid giant axon, and this model can be applied to many different excitable cells with some modification, as the underlying mechanisms of ion transport remain the same. The first mathematical model of cardiac cells was developed in 1960 by Denis Noble (99) by describing the action potentials of the Purkinje fibers. Action potentials in cardiac cells differ considerably from action potentials found in nerve cells. The major difference is the presence of calcium ions in the cardiac cells. The calcium ions play an important role in the repolarization phase of the action potential. The calcium influx into the cell prolongs the duration of the action potential and therefore produces a characteristic plateau phase which is missing in the action potential of the neurons. Because of the presence of calcium ions in cardiac cells, the duration of the action potential is very long compared to the duration of action potential found in neurons.

A number of different types of cardiac cell models from different species have been developed to represent different areas of the heart, including the atria and ventricles, the SA node, as well as the specialized conducting cells in the bundle of His and Purkinje systems. There is an increase in the complexity of mathematical models that are used to describe the electrical dynamics of cardiac cells with the discovery of new ion channels and the ionic processes.

The Beeler-Reuter model (100) is the first ventricular model based on experimental data from the guinea pig describing four ionic currents that include the addition of a $Ca^{2+}$ current and six gating variables to the Hodgkin and Huxley model. Luo-Rudy (101) developed their model for guinea pig ventricular cells based on the Beeler-Reuter

model with six ionic currents. In the following sections, we will discuss the Bernus model of a human ventricular cell and the Fox model of a canine ventricular cell.

### 1.7.2 The Bernus Model

Priebe and Beuckelmann published the first human ventricular model, based on the Luo-Rudy 2 model (102), an extension of the earlier Luo-Rudy 1 model (101) of guinea pig ventricular cells, in 1998 (103) with 17 variables, including the membrane voltage and 9 gating variables. The Bernus model (96) is the reduction of the Priebe-Beuckelmann (PB) model published in 2002. The number of variables was reduced to a total of 6 that includes the membrane voltage and 5 gating variables. Bernus found that their model is 4.9 times faster for numerical computation and is more stable than the PB model. The Bernus model consists of 9 different currents described as follows.

#### 1.7.2.1 The Fast $Na^+$ Current

The fast sodium current in the Bernus model is given by

$$I_{Na} = g_{Na} m^3 v^2 (V_m - E_{Na}), \tag{1.38}$$

where $g_{Na}$ is the maximum conductance of $Na^+$ ions, $V_m$ is the transmembrane potential and $E_{Na}$ is the Nernst potential for $I_{Na}$. $m$ is the activation gating variable and $v$ is the inactivation gating variable.

The three activation gates and one inactivation gate are proposed by Hodgkin and Huxley for neurons and are applicable to cardiac cells (100). According to Hodgkin and

Huxley, the exponent of $m$ represents three identical activation gates and the exponent of $v$ represents two identical inactivation gates in a sodium channel. Later, it was interpreted that the exponent three refers to the three arms of the sodium channel protein that rotate in order to block the channel or leave the channel open for $Na^+$ ions to pass through. The channel undergoes conformational changes as the transmembrane voltage changes, causing the arms to rotate. The position of the arms is probabilistic and the probability depends on the transmembrane voltage. In order to have the gate open, we require that all three arms rotate to the open position so that the $Na^+$ ions can pass through.

As shown in Fig. 1.5, the activation gates $m$, are closed and the inactivation gates $v$ are open when the cell membrane is at its resting membrane potential. The activation gates $m$, begin to open gradually and $Na^+$ ions enter the cell through the ion channel and the depolarization of membrane voltage is initiated. The $Na^+$ current reaches a maximum value when the activation gates $m$ are completely open. As $Na^+$ current reaches the maximum value, the inactivation gates $v$ begin to close and the passage of $Na^+$ ions gradually decrease. The passage of $Na^+$ ions stop when the inactivation gates $v$ are completely closed.

#### 1.7.2.2 The Slow $Ca^{2+}$ Current

The slow calcium current is given by

$$I_{Ca} = g_{Ca} d_\infty f f_{Ca} (V_m - E_{Ca}), \tag{1.39}$$

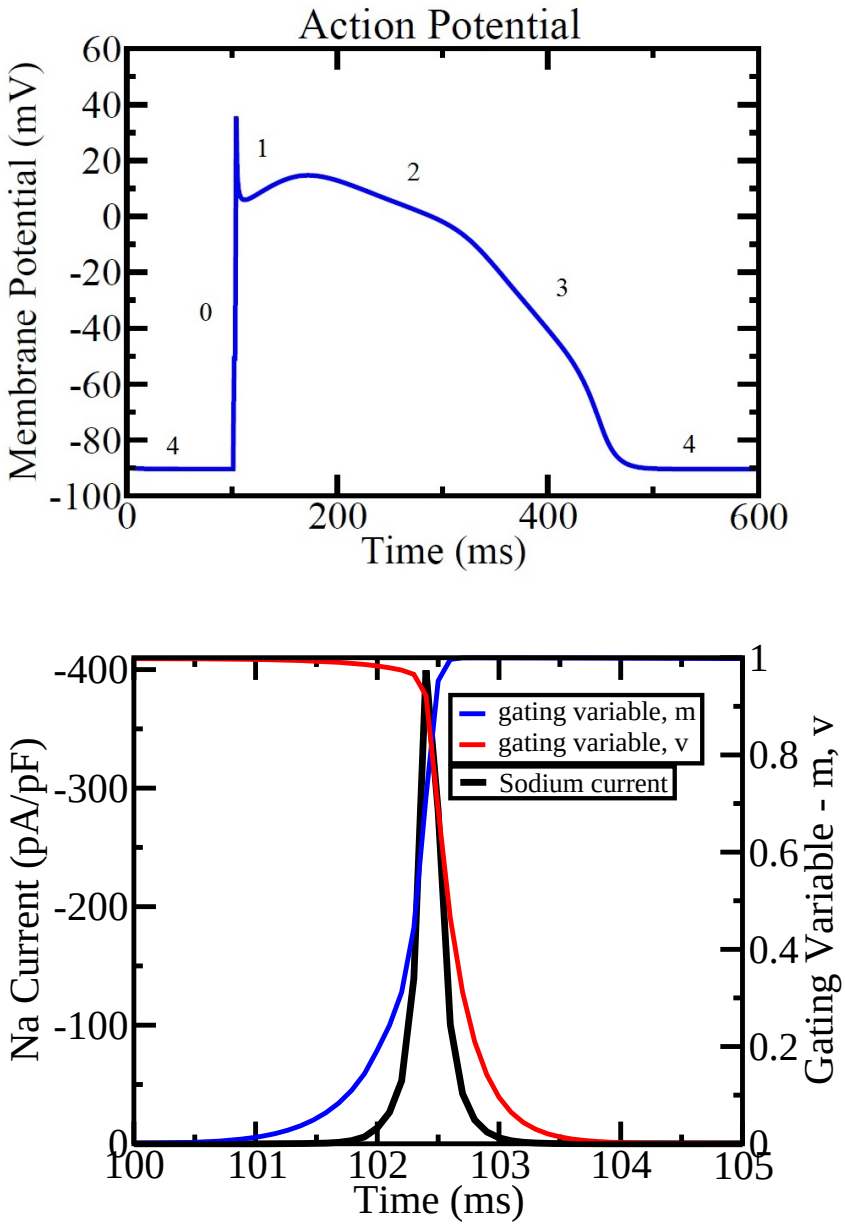


Figure 1.5: (top) Action potential of a ventricular cell, (bottom) activation gating variable $m$, inactivation gating variable $v$ and the flow of $Na^+$ current.

where $d_\infty$ is the activation variable and $f$ is the inactivation variable. $f_{Ca}$ is a proportional factor independent of $V_m$ and is calculated using

$$f_{Ca} = \frac{1}{1 + [Ca^{2+}]_i/0.0006}, \tag{1.40}$$

where $g_{Ca}$ is the conductance of $Ca^{2+}$ ions, $f$ is the inactivation variable and $E_{Ca}$ is the Nernst potential for $Ca^{2+}$ ion. $d_\infty$ depends on membrane potential only whereas $f$ depends on both membrane voltage and time.

From Fig. 1.19, we see that the inactivation gate $f$ opens and the $Ca^{2+}$ ions enter through the ion channels. The $Ca^{2+}$ current reaches a maximum value and then decreases gradually showing a plateau characteristic of the action potential. The $Ca^{2+}$ current decreases with fewer ions entering the cell and finally becomes zero, even though the gate remains open.

#### 1.7.2.3 The Transient Outward $K^+$ Current

The transient outward current is one of the potassium currents, when the $K^+$ flows out of the cell during phase 1 (Fig. 1.1) repolarization of the action potential.

$$I_{to} = g_{to} r_\infty to (V_m - E_{to}). \tag{1.41}$$

This current has two gating variables; $r_\infty$ is the activation variable and $to$ is the inactivation variable. $g_{to}$ is the conductance of $I_{to}$ current. $E_{to}$ is the Nernst potential for $I_{to}$ current. $r_\infty$ depends on membrane potential only whereas $to$ depends on both membrane voltage and time.

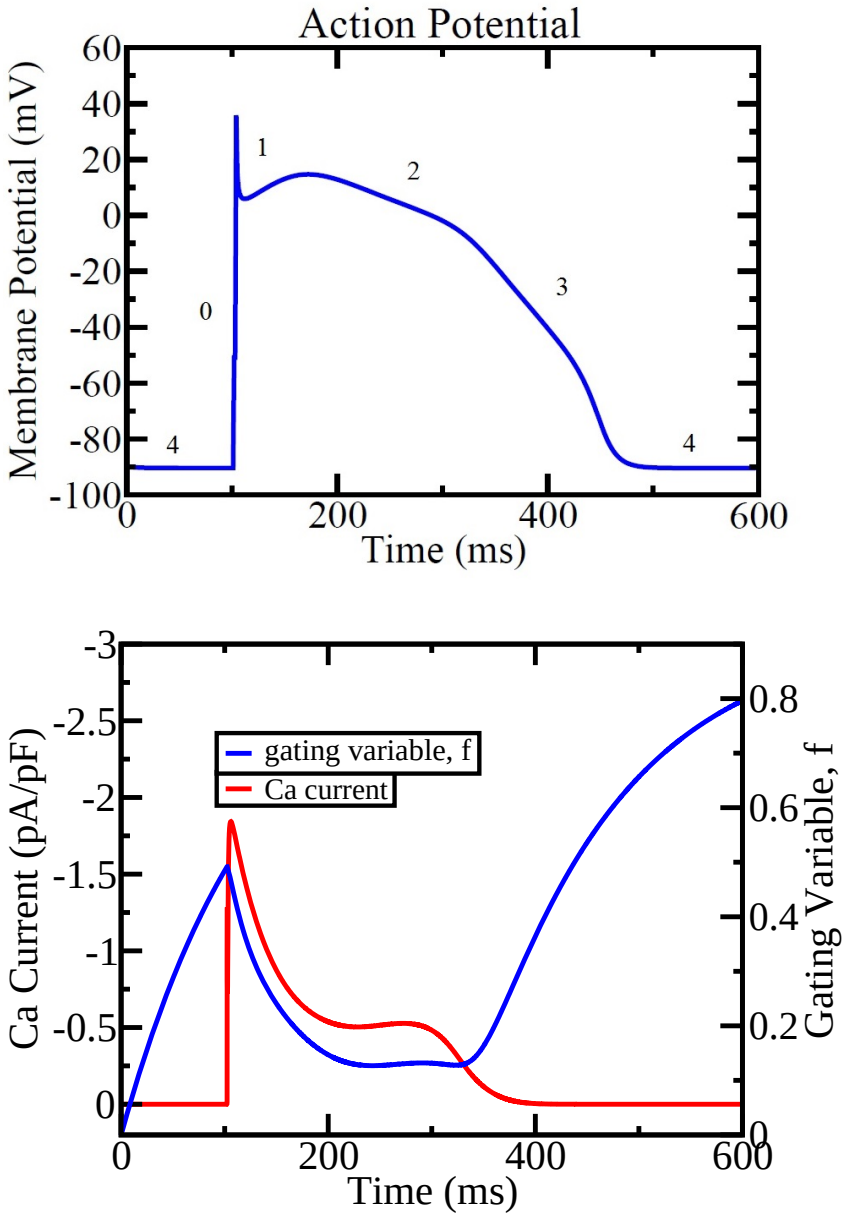


Figure 1.6: (top) Action potential of a ventricular cell, (bottom) gating variable $f$, and the flow of $Ca^{2+}$ current.

As shown in Fig. 1.7, the inactivation gate *to* is initially open and the potassium ions flow out of the channels. The $I_{to}$ current reaches a maximum value after which the current decreases with the closing of the gates until the current becomes zero.

#### 1.7.2.4 The Delayed Rectifier $K^+$ Current

The delayed rectifier current is due to the flow of $K^+$ ions during the phase 3 (Fig. 1.1) repolarization of the action potential.

$$I_K = g_K X^2 (V_m - E_K), \tag{1.42}$$

where $g_K$ is the conductance of $I_K$ current and $X$ is the activation gating variable. $E_K$ is the Nernst potential for $K^+$ ions.

The exponent of the gating variable $X$ explains that the potassium channel has two arms that can rotate and either block the channel or leave it open for $K^+$ ions to pass through. With the slower opening of the gate $X$, the efflux of $K^+$ ions increases (Fig. 1.8) and thereby increases the potassium current. After reaching a maximum value the current begins to decrease with the closing of the $X$ gate.

#### 1.7.2.5 The Inward Rectifier $K^+$ Current

This $K^+$ current is the outward current unlike the name suggests. The name arises because " inward rectification" is the property that the outward current of these channels is blocked at high membrane potentials.

$$I_{K1} = g_{K1} K1_\infty (V_m - E_K), \tag{1.43}$$

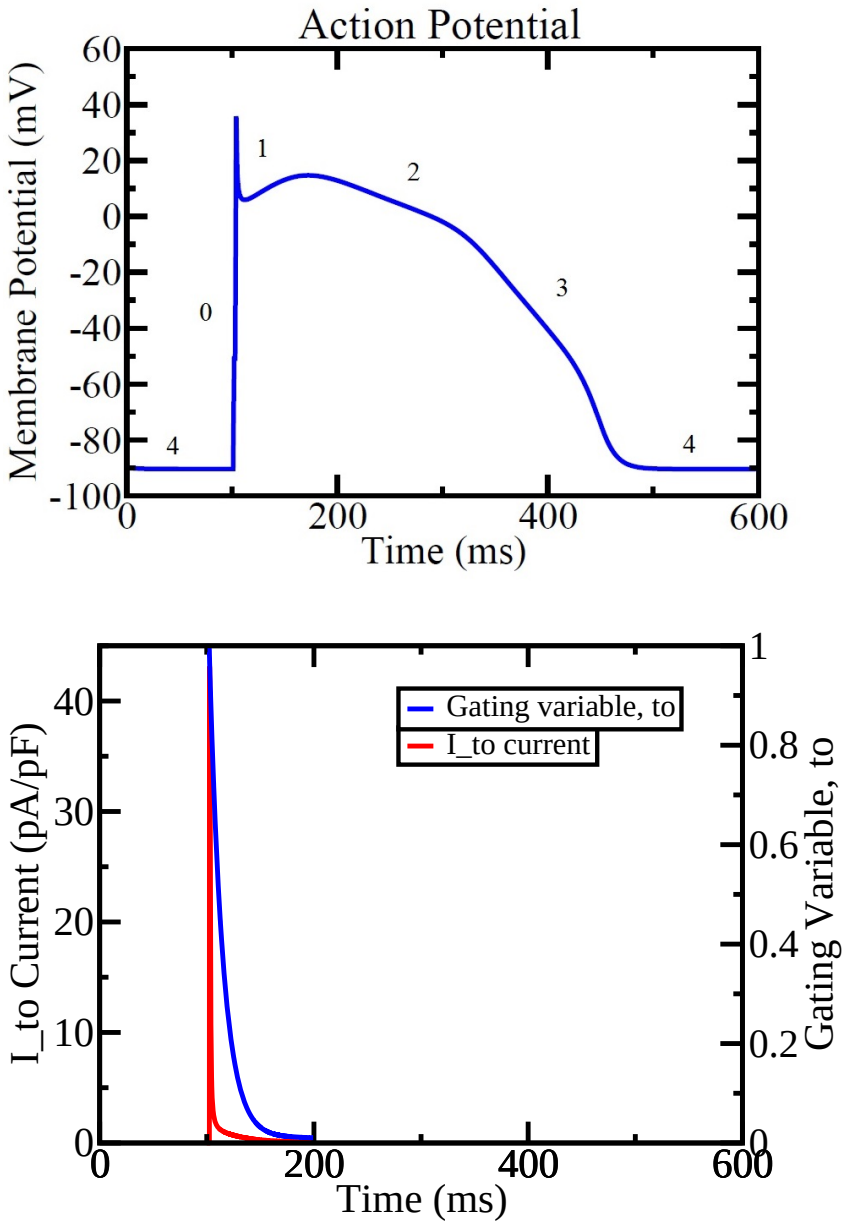


Figure 1.7: (top) Action potential of a ventricular cell, (bottom) gating variable *to*, and the flow of transient outward potassium current $I_{to}$.

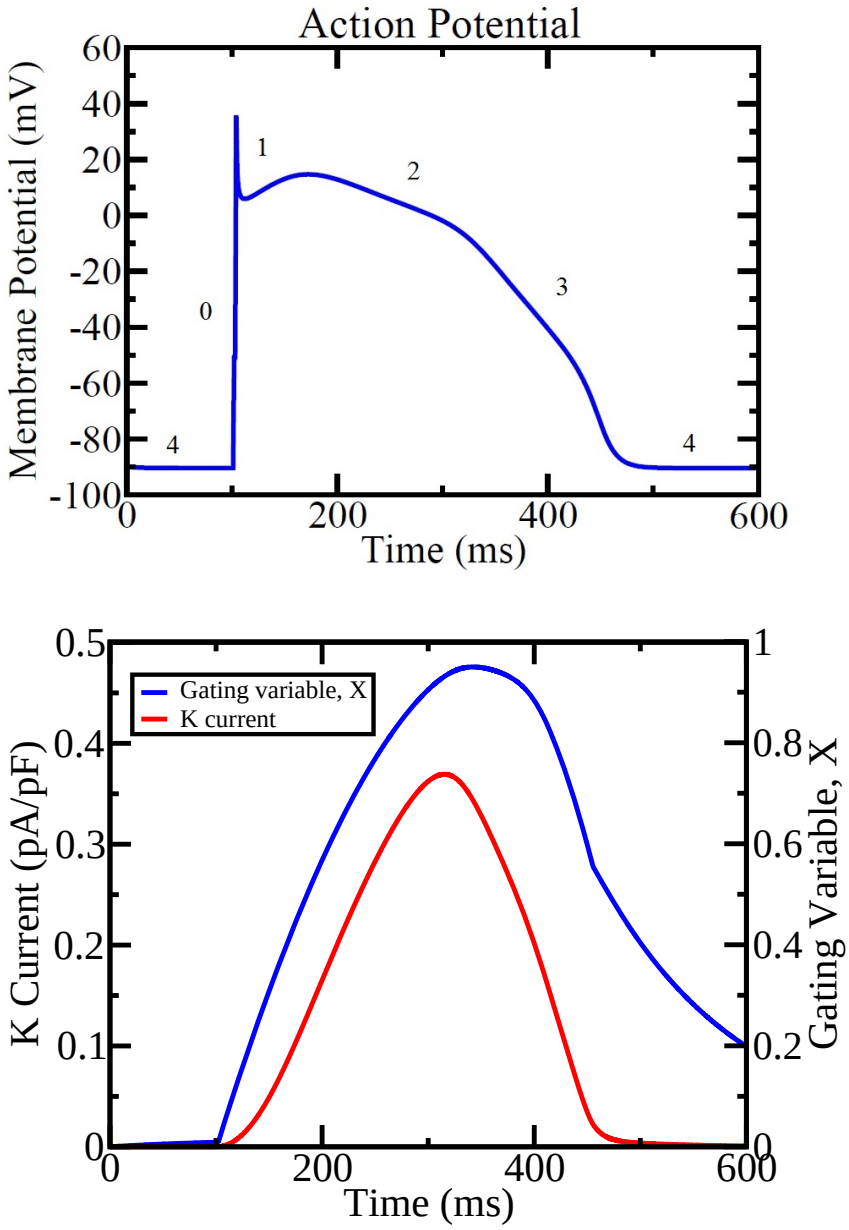


Figure 1.8: (top) Action potential of a ventricular cell, (bottom) gating variable $X$, and the flow of $K^+$ current.

where $g_{K1}$ is the conductance for $I_{K1}$ current. $K1_\infty$ is the inactivation gate of the current $I_{K1}$ and depends on membrane potential only. This current has no explicit time dependence and its dynamic behavior depends only on the membrane potential. This current flows out of the cell during the infux of $Na^+$ and during the resting potential period (Fig. 1.9).

#### 1.7.2.6 The $Na^+$ - $K^+$ Pump

The activity of the pump is stimulated by extracellular $K^+$ ions and intracellular $Na^+$ ions and depends on the membrane potential. The $Na^+$ - $K^+$ pump allows three $Na^+$ ions to exit out of the membrane in exchange for two $K^+$ that enter the cell. The pump works during the various phases of the action potential (Fig. 1.10) and allows enough $Na^+$ to get accumulated on the outside of the cell for the next depolarization.

$$I_{NaK} = g_{NaK} f_{NaK} f'_{NaK}, \tag{1.44}$$

where $g_{NaK}$ is the conductance for $I_{NaK}$ current. $f_{NaK}$ is the voltage dependent parameter of $I_{NaK}$ and $f'_{NaK}$ is the parameter depending upon the fixed ion concentrations of $Na^+$ and $K^+$ ions.

#### 1.7.2.7 $Na^+$ - $Ca^{2+}$ Exchanger

$$I_{NaCa} = g_{NaCa} f_{NaCa}, \tag{1.45}$$

where $g_{NaCa}$ is the conductance of $I_{NaCa}$ current. $f_{NaCa}$ is the voltage dependent parameter and also depends upon the fixed ion concentrations of $Na^+$ and $Ca^{2+}$ ions.

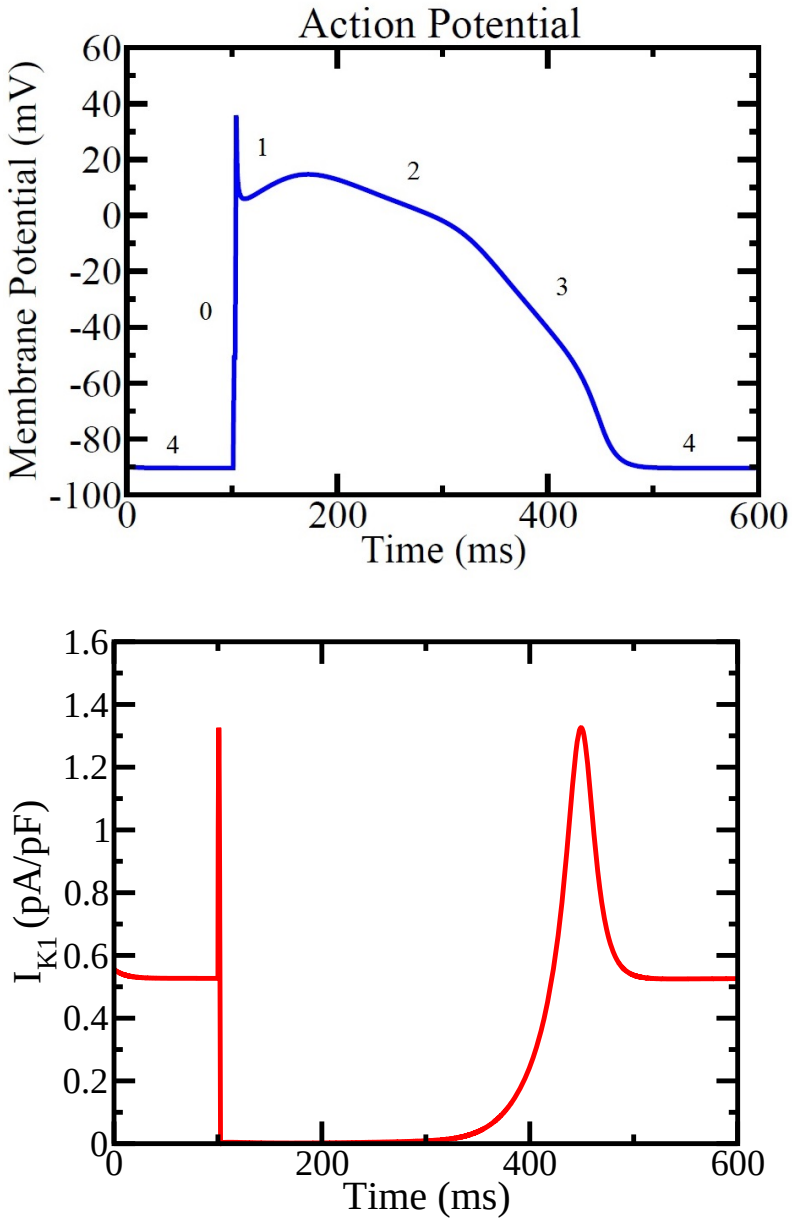


Figure 1.9: (top) Action potential of a ventricular cell, (bottom) the flow of K1 current from the cell.

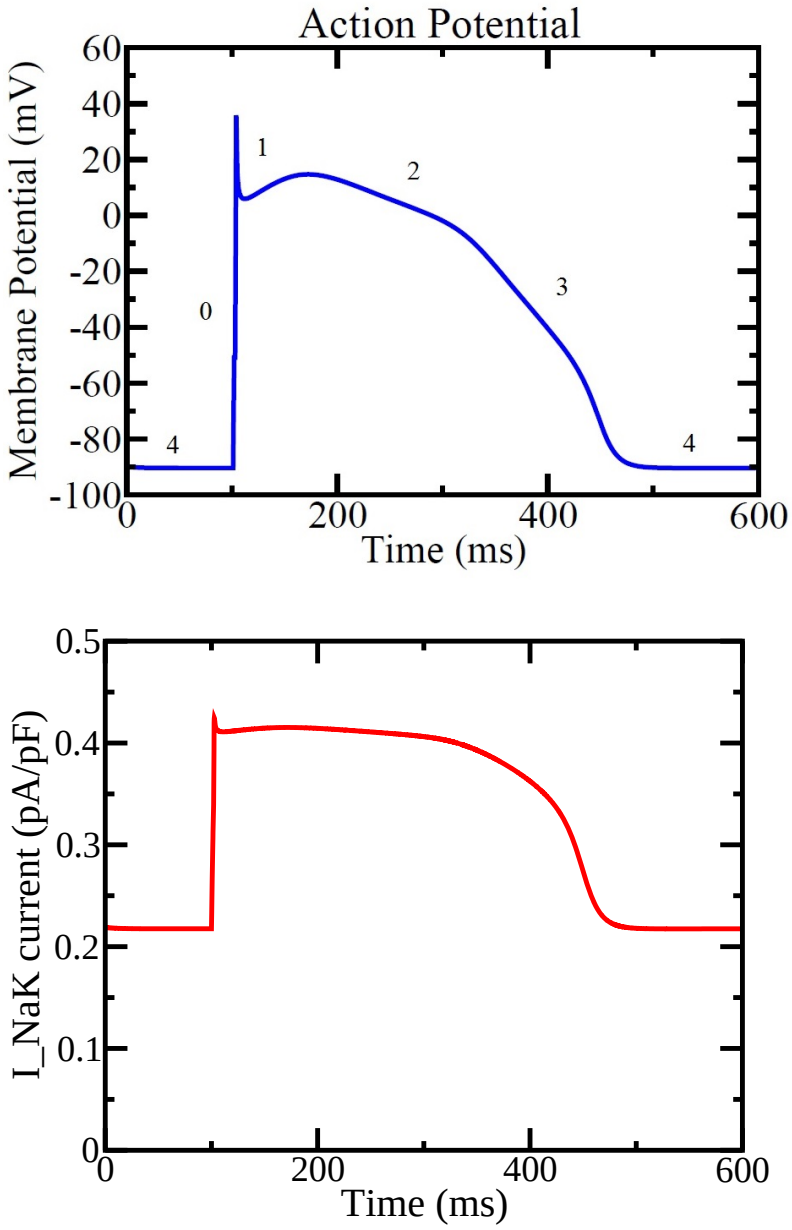


Figure 1.10: (top) Action potential of a ventricular cell, (bottom) flow of $NaK$ current.

The $Na^+$- $Ca^{2+}$ exchanger removes a single $Ca^{2+}$ ion in exchange for the import of three $Na^+$ ions into the cell. When the membrane potential is negative, the $Na^+$- $Ca^{2+}$ exchanger sends $Ca^{2+}$ out as $Na^+$ enters the cell. The exchanger works in the opposite direction once the cell is depolarized with membrane potential becoming positive,. i.e., $Na^+$ ions leave and $Ca^{2+}$ enters the cell. As shown in (Fig. 1.20), the exchanger current flows during various phases of the action potential.

#### 1.7.2.8 The $Ca^{2+}$ and $Na^+$ Background Currents

The $Ca^{2+}$ background current $I_{Ca,b}$ is introduced into the model for balancing $Ca^{2+}$ extrusion through $I_{NaCa}$ at resting potential.

$$I_{Ca,b} = g_{Ca,b}(V_m - E_{Ca}), \tag{1.46}$$

where $g_{Ca,b}$ is the conductance of $I_{Ca,b}$ current. The flow of $Ca^{2+}$ background current during various phases of action potential is shown in (Fig. 1.12).

Similarly, $Na^+$ background current is introduced for maintaining the resting level of intracellular $Na^+$ ions. The $Na^+$ ions exit the cell through the pump and entry into the cell through the exchanger maintains the resting level of intracellular $Na^+$ ions.

$$I_{Na,b} = g_{Na,b}(V_m - E_{Na}), \tag{1.47}$$

where $g_{Na,b}$ is the conductance of $I_{Na,b}$ current. The flow of $Na^+$ background current during various phases of action potential is shown in (Fig. 1.13).

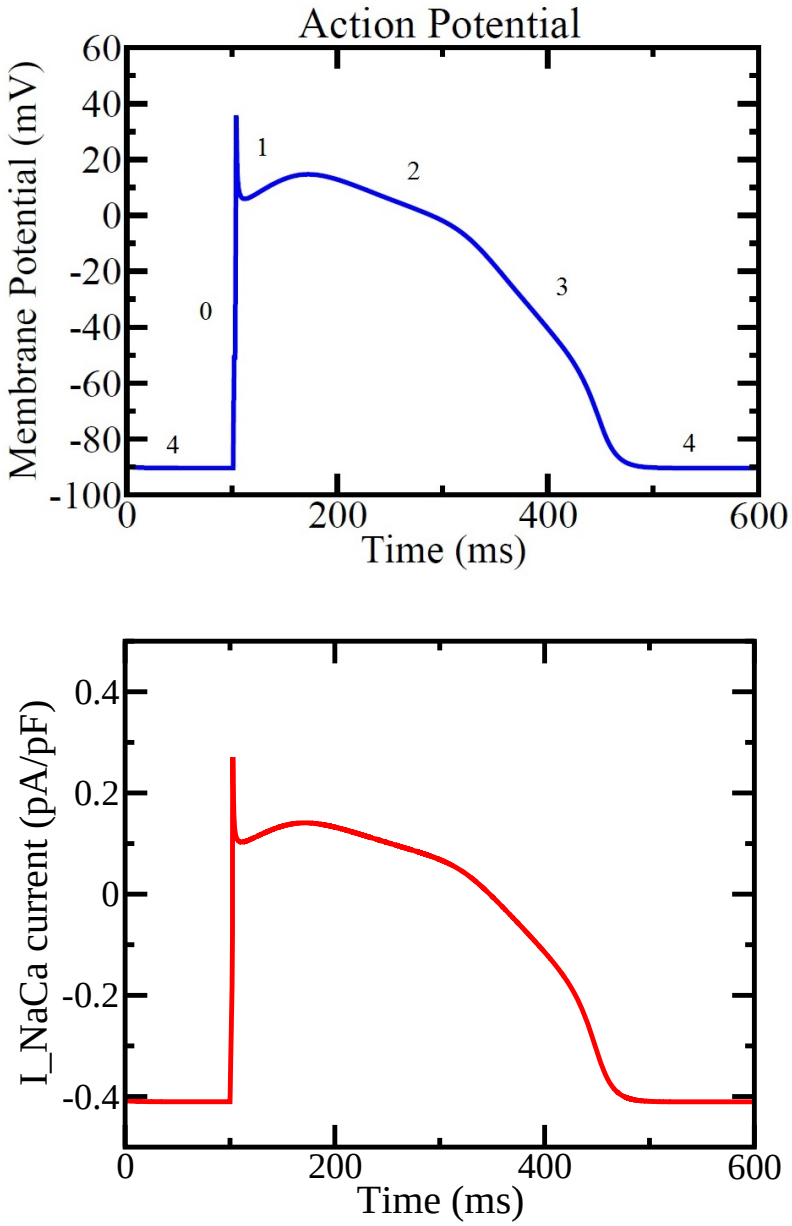


Figure 1.11: (top) Action potential of ventricular cell, (bottom) flow of $NaCa$ current.

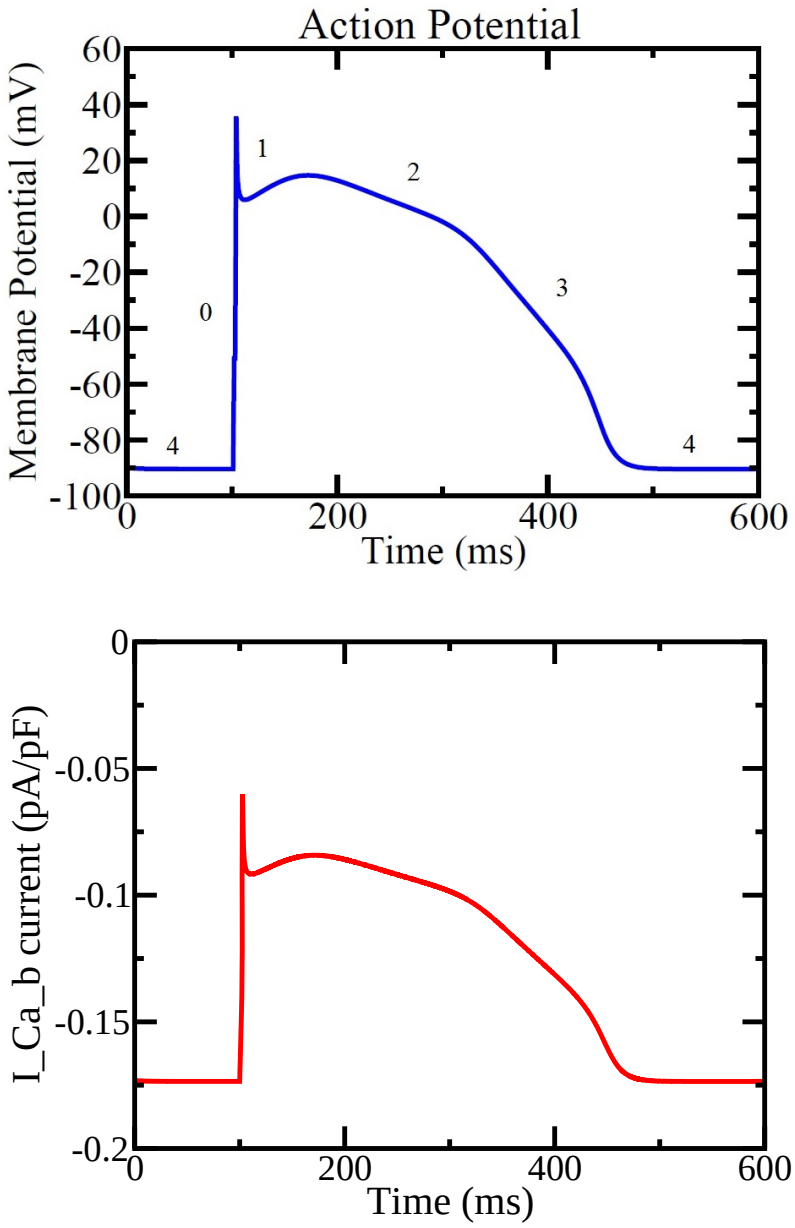


Figure 1.12: (top) Action potential of a ventricular cell, (bottom) flow of $Ca^{2+}$ background current.

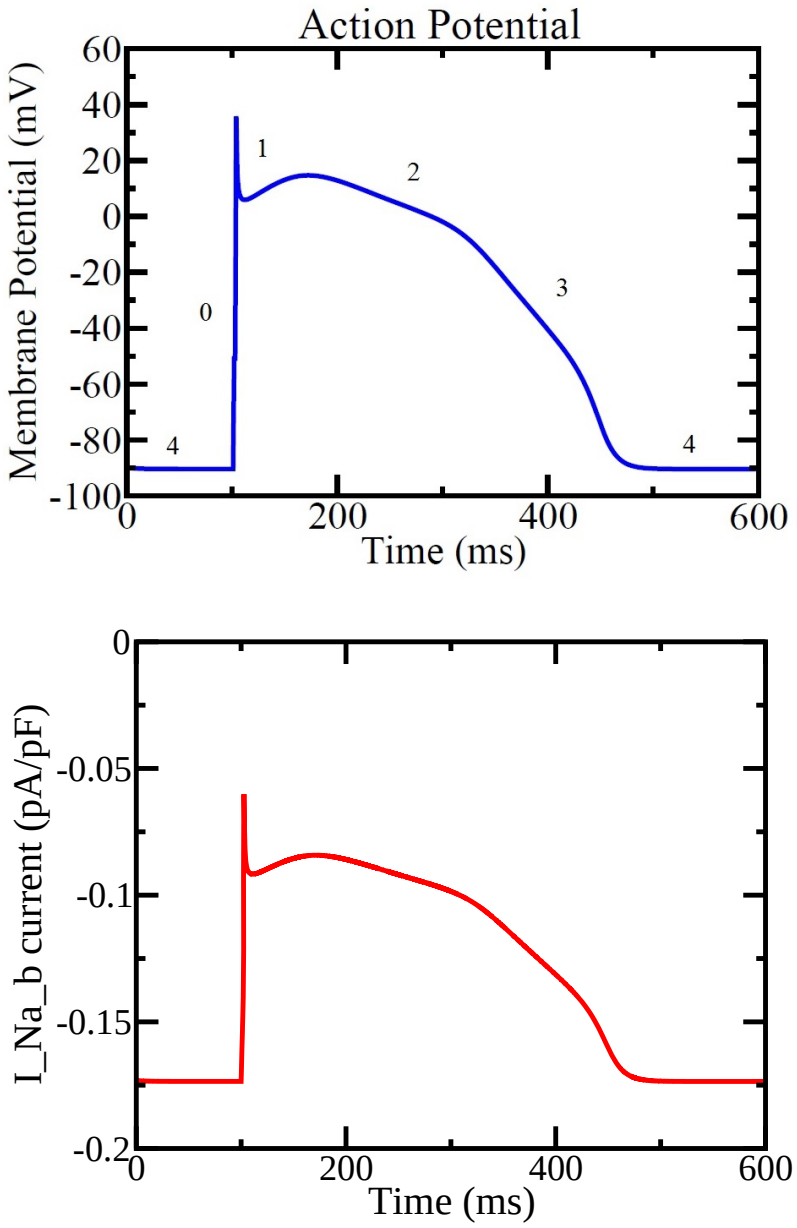


Figure 1.13: (top) Action potential of a ventricular cell, (bottom) flow of $Na^+$ background current.

### 1.7.3 The Fox Model

The Fox model (97) is based on a previous canine ventricular cell developed by Winslow et al. (104) which is a modified Luo-Rudy model (102) and includes a simplified description of intracellular calcium handling which is based on the rabbit ventricular cell (105). This model uses 13 different ionic currents and 13 variables. The variables include the membrane voltage, cytoplasmic and sarcoplasmic reticulum $Ca^{2+}$ concentrations and 10 gating variables. This model exhibits sustained APD alternans at fast pacing rates which are not present in Winslow and Luo-Rudy models.

#### 1.7.3.1 The $Na^+$ current

The sodium current in the Fox model is given by

$$I_{Na} = g_{Na} m^3 h j (V_m - E_{Na}), \tag{1.48}$$

where $g_{Na}$ is the maximum conductance of $Na^+$ ions, $V_m$ is the transmembrane potential and $E_{Na}$ is the Nernst potential for $I_{Na}$. $m$ is the activation gating variable, $h$ is the fast inactivation gating variable, and $j$ is the slow inactivation gating variable (Fig. 1.14).

#### 1.7.3.2 The Inward rectifier $K^+$ Current

The $K^+$ current in this model was formulated from Freeman et al. (106) data of German shepherd dogs, that indicate smaller outward current at depolarizing potentials.

$$I_{K1} = g_{K1} K1_\infty \frac{[K]}{[K^+]_e + K_{mK1}} (V_m - E_K), \tag{1.49}$$

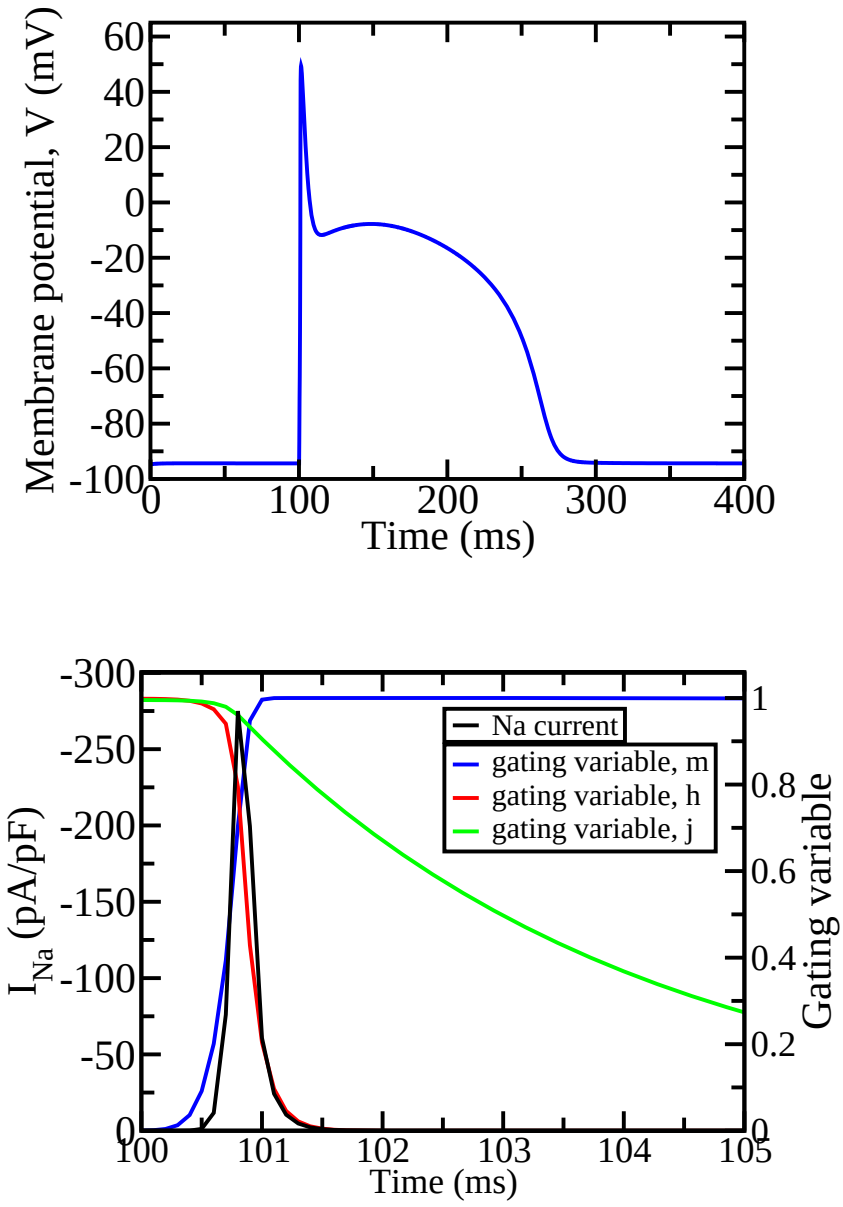


Figure 1.14: (top) Action potential of a ventricular cell, (bottom) activation gating variable $m$, fast inactivation gating variable $h$, slow inactivation gating variable $j$ and the flow of $Na^+$ current.

where $g_{K1}$ is the conductance for $I_{K1}$ current. $K1_\infty$ is the activation gate of the current $I_{K1}$ and depends on membrane potential only. $K_{mK1}$ is $K^+$ half-saturation current for $I_{K1}$. This current flows out of the cell during the influx of $Na^+$ ions and during the resting potential period (Fig. 1.15).

#### 1.7.3.3 The rapid component of the delayed rectifier $K^+$ current

The rapid component of the delayed rectifier current is due to the flow of $K^+$ ions during the phase 3 (Fig. 1.1) repolarization of the action potential.

$$I_{Kr} = g_{Kr} R(V) X_{Kr} \sqrt{\frac{[K^+]_e}{4}} (V_m - E_K), \tag{1.50}$$

where $g_{Kr}$ is the conductance of $I_{Kr}$ current and $X_{Kr}$ is the activation gating variable. $E_K$ is the Nernst potential for $K^+$ ions.

#### 1.7.3.4 The slow component of the delayed rectifier $K^+$ current

The slow component of the delayed rectifier current is due to the flow of $K^+$ ions during the phase 3 (Fig. 1.1) repolarization of the action potential.

$$I_{Ks} = g_{Ks} X_{Ks}^2 (V_m - E_K), \tag{1.51}$$

where $g_K$ is the conductance of $I_{Ks}$ current and $X_{Ks}$ is the activation gating variable. $E_{Ks}$ is the Nernst potential for $K^+$ ions.

The exponent of the gating variable $X$ explains that the potassium channel has two arms that can rotate and either block the channel or leave it open for $K^+$ ions to pass

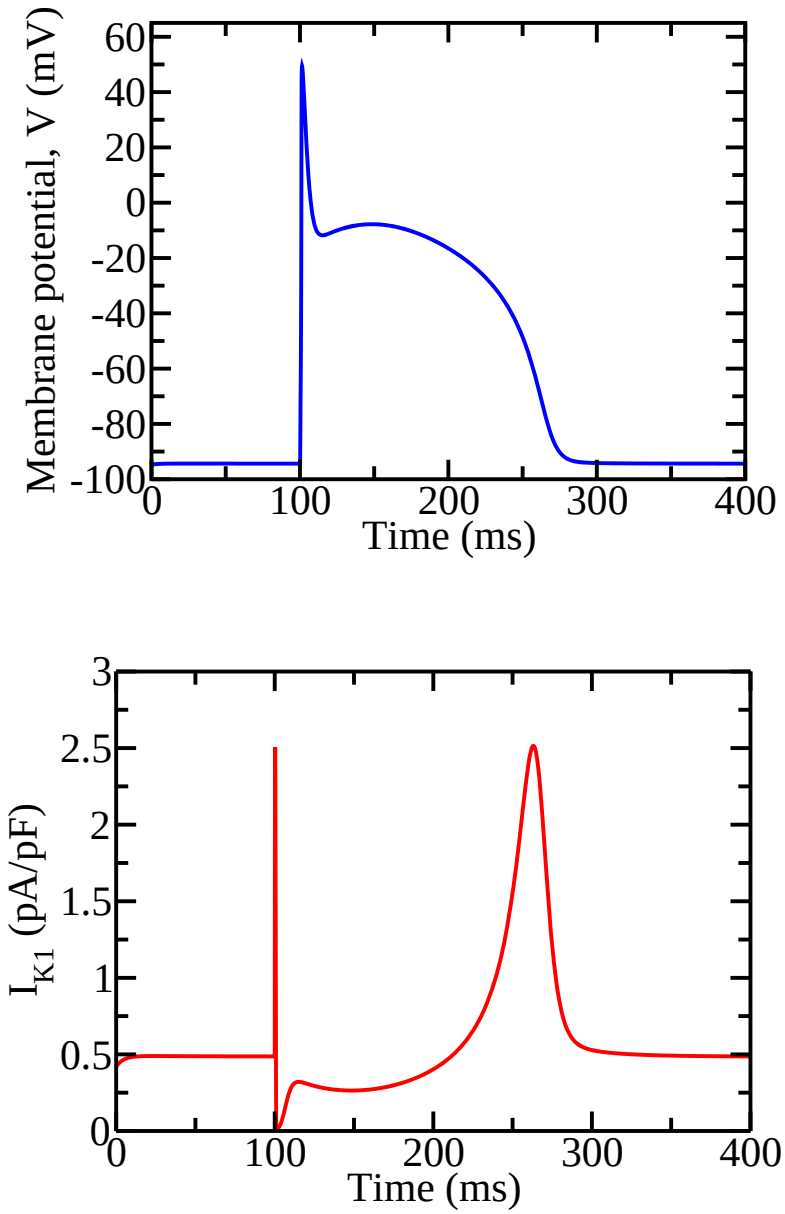


Figure 1.15: (top) Action potential of a ventricular cell, (bottom) the flow of K1 current from the cell.

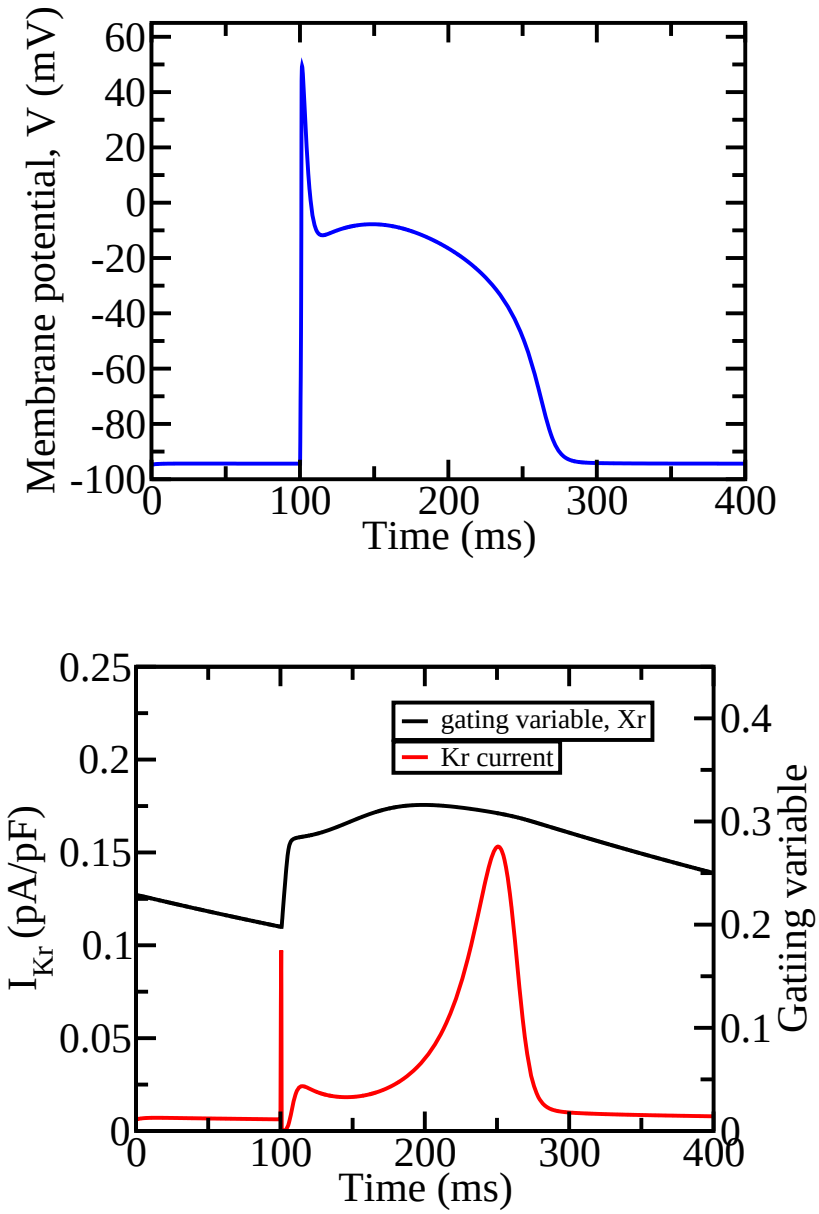


Figure 1.16: (top) Action potential of a ventricular cell, (bottom) gating variable $X_{Kr}$, and the flow of $Kr^+$ current.

through. With the slower opening of the gate $X$, the efflux of $K^+$ ions increases (Fig. 1.17) and thereby increases the potassium current. After reaching a maximum value, the current begins to decrease with the closing of the $X_{Ks}$ gate.

#### 1.7.3.5 The Transient Outward $K^+$ Current

The transient outward current is one of the potassium currents, when the $K^+$ flows out of the cell during phase 1 (Fig. 1.1) repolarization of the action potential.

$$I_{to} = g_{to} X_{to} Y_{to} (V_m - E_{to}). \tag{1.52}$$

This current has two gating variables; $X_{to}$ is the activation variable and $Y_{to}$ is the inactivation variable. $g_{to}$ is the conductance of $I_{to}$ current. $E_{to}$ is the Nernst potential for $I_{to}$ current. As shown in Fig. 1.18, the inactivation gate $to$ is open and the potassium ions flow out of the channels. The $I_{to}$ current reaches a maximum value after which the current decreases with the closing of the gates until the current becomes zero.

#### 1.7.3.6 The Plateau $K^+$ Current

The plateau current is the background outward potassium current which is active during the plateau of the AP.

$$I_{Kp} = g_{Kp} K_{Kp} (V_m - E_K), \tag{1.53}$$

where $g_{Kp}$ is the peak conductance of $I_{Kp}$ current and $K_{Kp}$ is the $I_{Kp}$ activation.

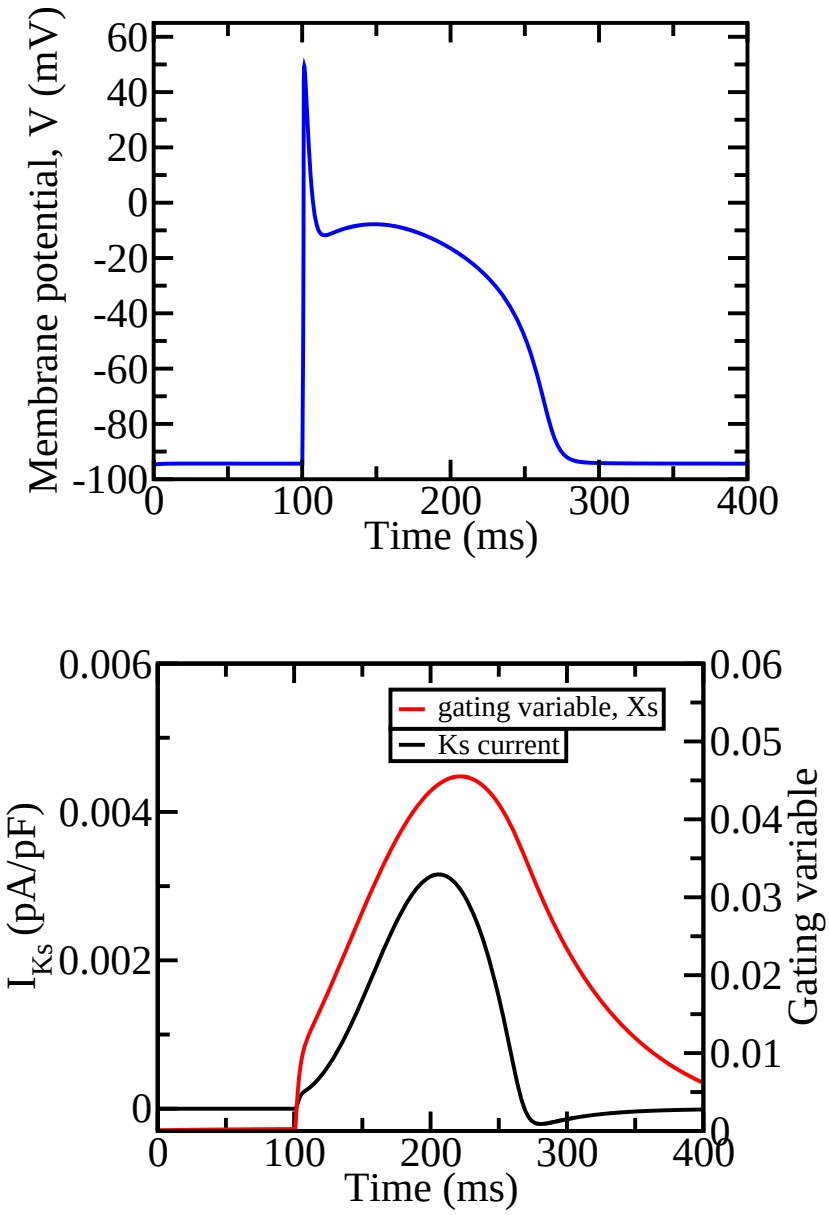


Figure 1.17: (top) Action potential of a ventricular cell, (bottom) gating variable $X_{Ks}$, and the flow of $K^+$ current.

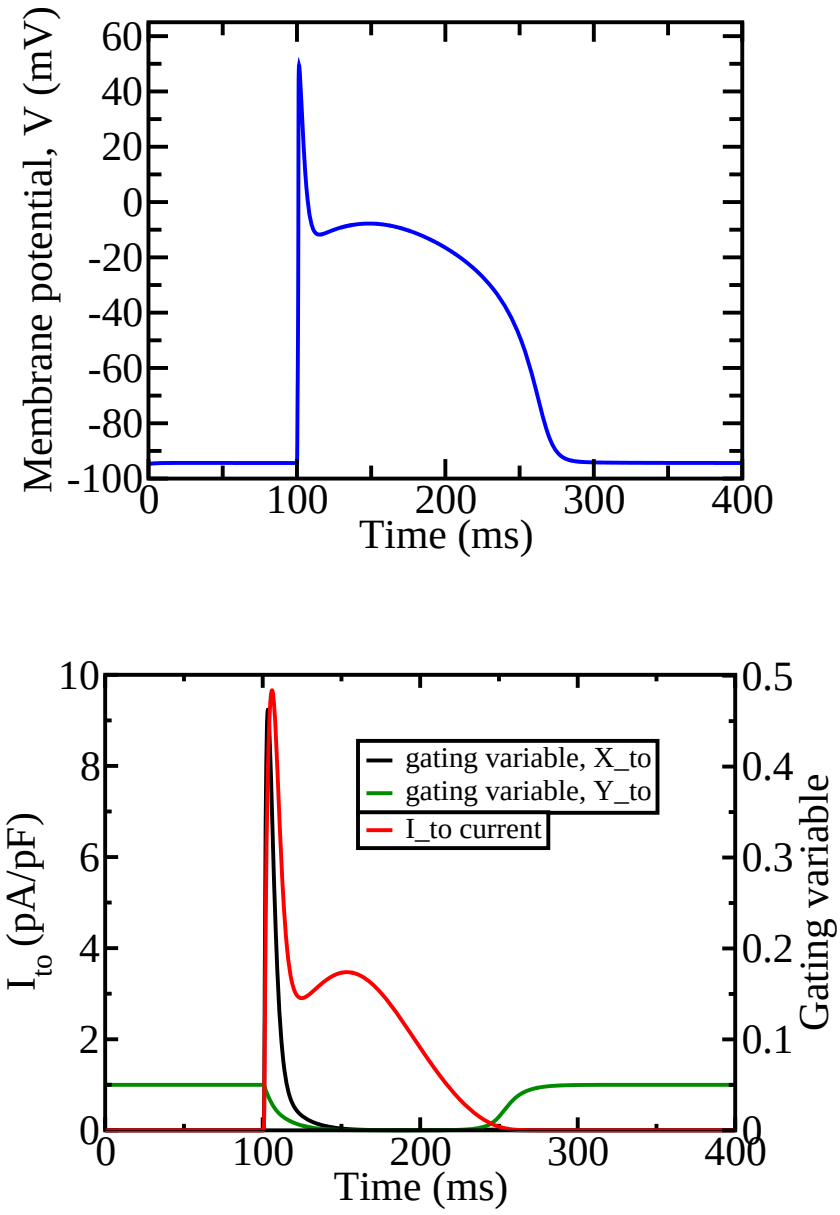


Figure 1.18: (top) Action potential of a ventricular cell, (bottom) activation gating variable $X_{to}$, inactivation gating variable $Y_{to}$ and the flow of transient outward potassium current $I_{to}$.

#### 1.7.3.7 The $Na^+$ - $K^+$ Pump

The activity of the pump is stimulated by extracellular $K^+$ ions and intracellular $Na^+$ ions and depends on the membrane potential. The $Na^+$ - $K^+$ pump allows 3 $Na^+$ ions to exit out of the membrane in exchange for two $K^+$ that enter the cell. The pump works during the various phases of action potential (Fig. 1.10) and allows enough $Na^+$ to get accumulated on the outside of the cell for the next depolarization.

$$I_{NaK} = \bar{I}_{NaK} f_{NaK} \frac{1}{1 + (\frac{K_{mNai}}{[Na^+]}_i)^{1.5}} \frac{[K^+]_e}{[K^+]_e + K_{mKo}}, \tag{1.54}$$

where $g_{NaK}$ is the conductance for $I_{NaK}$ current. $f_{NaK}$ is the voltage dependent parameter of $I_{NaK}$ and $f'_{NaK}$ is the parameter depending upon the fixed ion concentrations of $Na^+$ and $K^+$ ions.

#### 1.7.3.8 The L-type $Ca^{2+}$ Current

The slow calcium current is given by

$$I_{Ca} = \bar{I}_{Ca} f d f_{Ca}, \tag{1.55}$$

where $d$ is the activation variable and $f$ is the inactivation variable. $f_{Ca}$ is a proportional factor independent of $V_m$ and is calculated using

$$f_{Ca} = \frac{1}{1 + ([Ca^{2+}]_i / K_{mf_{Ca}})^3}, \tag{1.56}$$

$$\bar{I}_{Ca} = \frac{\bar{P}_{Ca}}{C_{sc}} \frac{4VF^2}{RT} \frac{[Ca^{2+}]_i \exp(2VF/(RT)) - 0.341[Ca^{2+}]_e}{\exp(2VF/(RT)) - 1}, \tag{1.57}$$

where $g_{Ca}$ is the conductance of $Ca^{2+}$ ions, $f$ is the inactivation variable and $E_{Ca}$ is the Nernst potential for $Ca^{2+}$ ion. $d$ depends on membrane potential only whereas $f$ depends on both membrane voltage and time.

From Fig. 1.19 we see that the inactivation gate $f$ opens and the $Ca^{2+}$ ions enter through the ion channels. The $Ca^{2+}$ current reaches a maximum value and then decreases gradually showing a plateau characteristic of the action potential. The $Ca^{2+}$ current decreases with less ions entering the cell and finally becomes zero, even though the gate remains open.

#### 1.7.3.9 $Na^+$ - $Ca^{2+}$ Exchanger

The $Na^+$- $Ca^{2+}$ exchanger removes a single $Ca^{2+}$ ion in exchange for the import of three $Na^+$ ions into the cell.

$$\begin{aligned} I_{NaCa} = & \frac{k_{NaCa}}{{K^3}_{mNa} + [Na^+]_e^3} \frac{1}{K_{mCa} + [Ca_e^{2+}} \frac{1}{1 + k_{sat} \exp(VF(\eta - 1)/(RT))} \\ & \times [\exp(VF\eta/(RT))[Na^+]_i^3[Ca_e^{2+}] - \exp(VF(\eta - 1)/(RT))[Na^+]_e^3[Ca^{2+}]_i], \end{aligned} \tag{1.58}$$

where $g_{NaCa}$ is the conductance of $I_{NaCa}$ current. $f_{NaCa}$ is the voltage dependent parameter and also depends upon the fixed ion concentrations of $Na^+$ and $Ca^{2+}$ ions.

As shown in Fig. 1.20, the $Na^+$- $Ca^{2+}$ exchanger current flows during various phases of action potential.

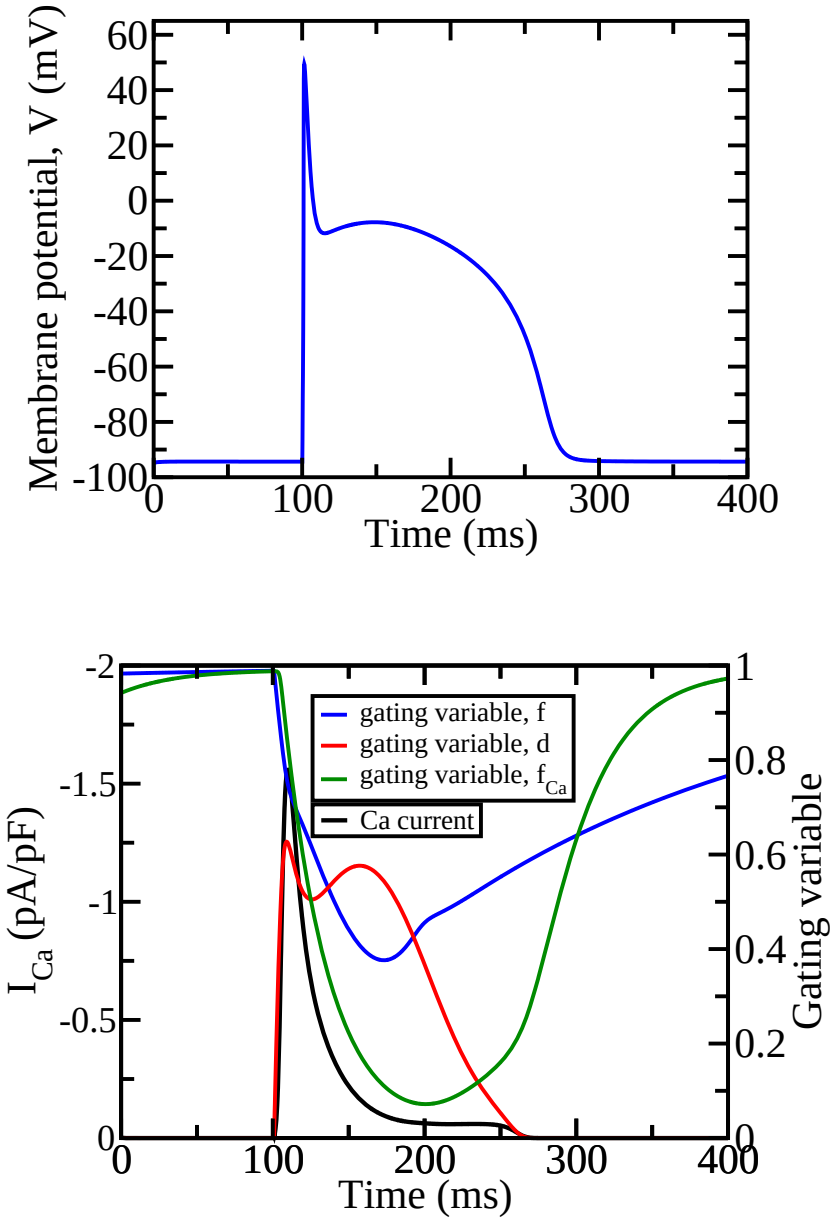


Figure 1.19: (top) Action potential of a ventricular cell, (bottom) gating variable $f$, and the flow of $Ca^{2+}$ current.

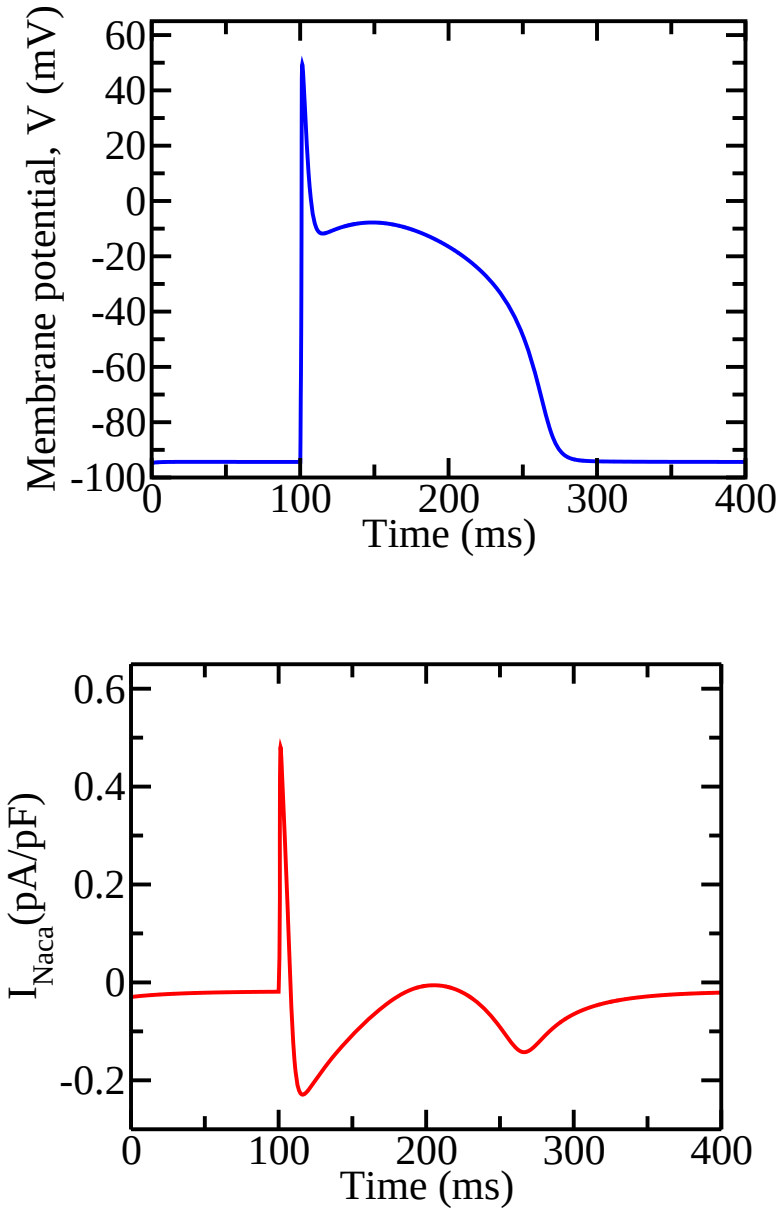


Figure 1.20: (top) Action potential of ventricular cell, (bottom) flow of $NaCa$ current.

#### 1.7.3.10 The Sarcolemmal Pump Current

In addition to the $I_{NaCa}$ exchanger, this pump provides an additional mechanism for the extrusion of $Ca^{2+}$ ions to the exterior region of the cell. This pump maintains the low level of intracellular [$Ca^{2+}$] at rest (107).

$$I_{pCa} = \bar{I}_{pCa} \frac{[Ca^{2+}]_i}{K_{mpCa} + [Ca^{2+}]_i}, \tag{1.59}$$

where $\bar{I}_{pCa}$ is the maximal $I_{pCa}$ and $K_{mpCa}$ is the half-saturation constant for $I_{pCa}$.

#### 1.7.3.11 The $Ca^{2+}$ and $Na^{+}$ background currents

The $Ca^{2+}$ background current $I_{Ca,b}$ is introduced into the model for balancing $Ca^{2+}$ extrusion through $I_{NaCa}$ at resting potential.

$$I_{Ca,b} = g_{Ca,b}(V_m - E_{Ca}), \tag{1.60}$$

where $g_{Ca,b}$ is the conductance of $I_{Ca,b}$ current.

Similarly, $Na^{+}$ background current is introduced for maintaining the resting level of intracellular $Na^{+}$ ions. The $Na^{+}$ ions exit the cell through the pump and entry into the cell through the exchanger maintains the resting level of intracellular $Na^{+}$ ions.

#### 1.7.3.12 The $K^+$ Current through the L-type $Ca^{2+}$ Channel

This current is a modified version of the current used in Luo-Rudy model (102) of pig ventricles.

$$I_{CaK} = \frac{\bar{P}_{CaK}}{C_{sc}} \frac{f df_{Ca}}{1 + \frac{\bar{I}_{Ca}}{I_{Cahalf}}} \frac{1000VF^2}{RT} \frac{[K^+]_i \exp(VF/(RT) - [K^+]_e}{\exp(VF/(RT) - 1}, \tag{1.61}$$

where $\bar{P}_{CaK}$ is the $Ca^{2+}$ channel permeability to $K^+$ ions, $C_{sc}$ is the specific membrane capacity, $\bar{I}_{Ca}$, is the maximal $I_{Ca}$, $I_{Cahalf}$ is the $I_{Ca}$ level which reduces $\bar{P}_{CaK}$ by one-half, R is the ideal gas constant and F is the Faraday constant respectively.

#### 1.7.3.13 Calcium Handling

This model uses the modified form of intracellular calcium dynamics from the rabbit model (105). Sarcoplasmic reticulum (SR) is the intracellular compartment, and is subdivided into two compartments, the junctional SR (JSR) and the network SR (NSR). The rate of change of intracellular ionic concentrations is given by

$$\frac{d[Ca^{2+}]_i}{dt} = \beta_i(J_{rel} + J_{leak} - J_{up} - \frac{A_{Cap}C_{sc}}{2FV_{myo}} \times (I_{Ca} + I_{Cab}I_{pCa} - 2I_{NaCa})), \tag{1.62}$$

where $\beta_i$ is the myoplasmic buffering factor, $J_{rel}$ is release $Ca^{2+}$ flux from the sarcoplasmic reticulum (SR), $J_{leak}$ is the leakage $Ca^{2+}$ flux from the SR, $J_{up}$ is the uptake $Ca^{2+}$ flux from the SR, $A_{Cap}$ is the capacitive membrane area and $V_{myo}$ is the myoplasmic volume.

The rate of change of ionic concentration in the SR is given by

$$\frac{d[Ca^{2+}]_{SR}}{dt} = \beta_{SR}(J_{up} - J_{leak} - J_{rel})\frac{V_{myo}}{V_{SR}}, \tag{1.63}$$

where $\beta_{SR}$ is the sacroplasmic reticulum buffering factor and $V_{SR}$ is the sacroplasmic reticulum volume.

## 1.8 Research Questions

Cardiac arrhythmia is due to the change in the normal sequence of electrical impulses in cardiac cells and causes the heart to beat too fast, too slow or even erratically. This leads to the abnormal heartbeat and the heart cannot pump blood to different parts of the body effectively. As a result, there is a reduction in the heart's ability to work for a prolonged time causing a life-threatening situation. Therefore, the study and prevention of cardiac arrhythmia are very important. Antiarrhythmic drugs are used to treat cardiac arrhythmia. It is found that these drugs also have the capability to aggravate arrhythmia, so proper drug doses are very important in treating arrhythmias.

In our study, we use two different mathematical models of a single cardiac ventricular cell of human (the Bernus Model) and dog (the Fox model) respectively to study the effect of antiarrhythmic drugs on the action potential of these cells. We will simulate the drug effect on APD with the efficacy ranging from zero to the maximum drug efficacy of 1 at normal and fast heart rates, by changing the BCL. We will then answer the following questions with our simulation results.

- How does the action potential of a ventricular cell change with the application of antiarrhythmic drugs?
- How do antiarrhythmic drugs affect the rate dependence of APD?
- How do antiarrhythmic drugs affect hysteresis in cardiace cells?
- How do antiarrhythmic drugs affect the generation of alternating rhythms and alternans in cardiac cells?
- How does the study of restitution curves explain the onset of alternans in our models?
- How does the application of drugs affect the occurrence, enhancement or disappearance of alternans in the Fox model?
- Which class of antiarrhythmic drugs are effective in eliminating alternans?

# Chapter 2

# Methods

This study extends previous work on modeling of antiarrhythmics by giving a detailed assessment of their effect at the cellular level and comparing the effects of three different classes of antiarrhythmic drugs. The use of a mathematical model allows us to study the full range of drug concentrations, from no decrease in ionic current to complete blocking of the current, giving us a full picture of the effect of each drug. In particular, our study will focus on how antiarrhythmics alter rate-dependent responses and susceptibility to arrhythmias in single cells.

We use the Bernus human ventricular epicardial cell model (96) and the Fox canine ventricular cell model (97) to compute the total ionic current through the cell membrane at a given time. While several human ventricular cell models have been proposed and used in other studies (103, 108, 109), we use the Bernus model since it is the simplest model of a human ventricular cell that contains the sodium, potassium, and calcium currents that are required for this study. The simplicity of the model allows for faster numerical computation and avoids the computational instability seen in more complex models (110),

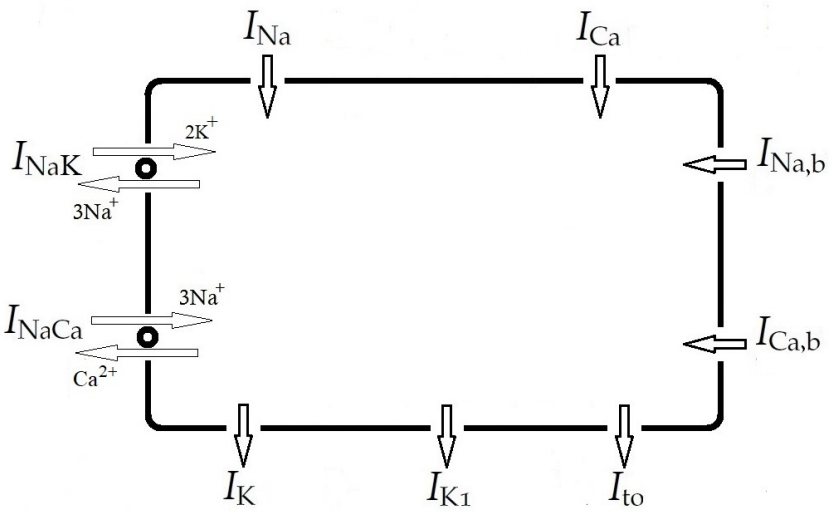


Figure 2.1: Schematic representation of the ionic currents of the Bernus model (96) of a human ventricular cell. It includes a rapid sodium current $I_{Na}$, a slow calcium current $I_{Ca}$, a transient outward current $I_{to}$, a delayed rectifier potassium current $I_K$, an inward rectifier potassium current $I_{K1}$, background sodium current $I_{Na,b}$, background calcium current, $I_{Ca,b}$, a sodium-potassium pump $I_{NaK}$, and a sodium-calcium exchanger $I_{NaCa}$.

particularly when model parameters are varied (111). While it might seem that using such a simple model will lead to inaccurate predictions, a recent study suggests that even simpler models can accurately reproduce a range of electrophysiological phenomena (112). We use the Fox model among the canine models, as this model produces sustained alternans at a certain lower BCL range.

The cell membrane potential $V$ follows an ordinary differential equation,

$$C_m \frac{\mathrm{d}V}{\mathrm{d}t} = -I_{\text{ion}} + I_{\text{stim}}, \tag{2.1}$$

where $I_{\text{stim}}$ is an external stimulus current, $C_m$ is the cell membrane capacitance per unit surface area and $I_{\text{ion}}$ is the sum of all the membrane currents. Our implementation

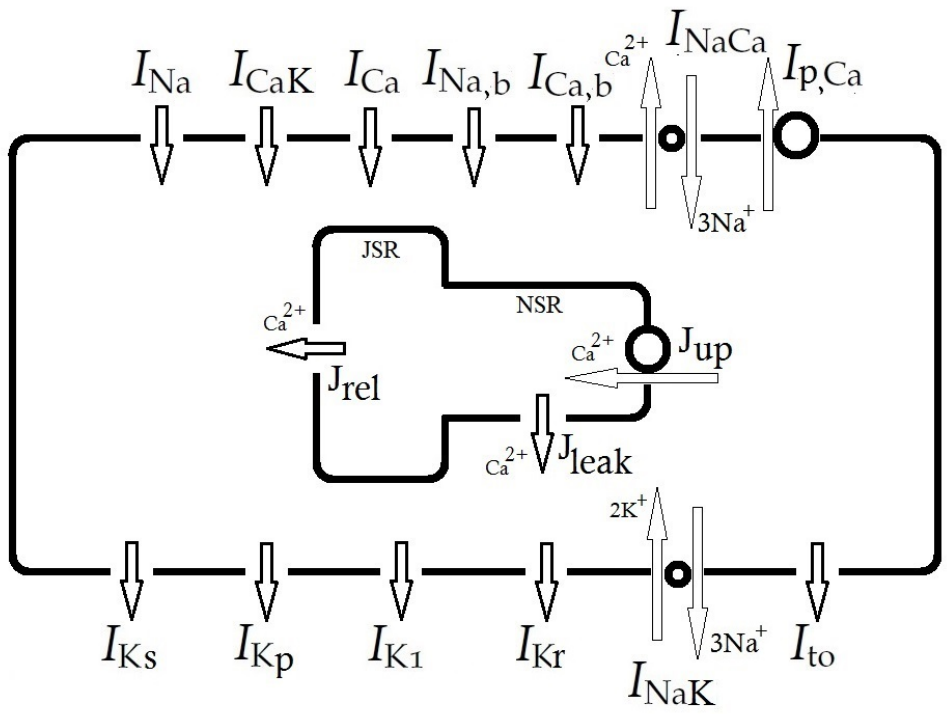


Figure 2.2: Schematic representation of the ionic currents of the Fox model (97) of a canine ventricular cell. It includes a sodium current $I_{Na}$, a L-type calcium current $I_{Ca}$, a transient outward current $I_{to}$, a rapid delayed rectifier potassium current $I_{Kr}$, a slow delayed rectifier potassium current $I_{Kr}$, an inward rectifier potassium current $I_{K1}$, a plateau $I_{Kp}$ current, a sarcolemmal pump current $I_{pCa}$, background sodium current $I_{Na,b}$, background calcium current, $I_{Ca,b}$, a sodium-potassium pump $I_{NaK}$, and a sodium-calcium exchanger $I_{NaCa}$, potassium current $I_{CaK}$ through L-type $Ca^{2+}$ channel.

of the Bernus model and the Fox model use the `Odeint` function from SciPy (open source Python library) to solve the system of ordinary differential equations. `Odeint` dynamically switches from Adams method to the backward differentiation method as needed with a tolerance of $1.5\times10^{-8}$. We use the same values for the various parameters as in the original derivations of each model (96, 97).

The concentrations of intracellular, extracellular ions and the conductance of various ions from the Bernus model are tabulated and are given in Appendix A. Similarly, the concentration and the conductance for various ions and the parameters used in the Fox model are given in Appendix B.

## 2.1 Implementing the Effect of Antiarrhythmics

Since class II drugs, beta blockers, do not directly modify ion channel function (113), we will not consider them in this study. We study the effect of the remaining three classes of antiarrhythmic drugs by multiplying the sodium, potassium or calcium ionic currents by $(1-\varepsilon)$, where $\varepsilon$, which ranges from 0 to 1, in steps of 0.01 is the efficacy of the drug. An efficacy of 0 leaves the current unchanged and corresponds to no drug effect, while an efficacy of 1 reduces the current to 0 and represents the theoretical maximum efficiency of a drug. Ideally, each class of antiarrhythmic drug blocks a specific ion channel, however, many of these drugs are known to have effects on multiple ion channels (5, 114). Since we are not examining a specific drug and are trying to broadly compare the effects of blocking different channels, we will assume that each class of drug blocks only a single ion channel. Note, however, that drugs that block multiple channels can also be modeled

by applying the efficacy to multiple ionic currents. While efficacy may seem like a rather theoretical concept, the efficacy of a drug is determined by the dose of a drug through the $E_{\max}$ model (115).

$$\varepsilon = \frac{\varepsilon_{\max} D}{D + \mathrm{IC}_{50}}, \tag{2.2}$$

where $\varepsilon$ is the efficacy of a drug, $\varepsilon_{\max}$ is the maximum possible effect of the drug, $\mathrm{IC}_{50}$ is the drug concentration needed to achieve half the maximum effect and $D$ is the drug dose. For a given drug, an increase in efficacy corresponds to an increased dose of the drug. This formulation of the drug effect has been used before in modeling of antiarrhythmics (82, 83, 92). Some drugs are known to interact dynamically with the ion channels (116, 117) which would lead to time-dependent changes in the efficacy, a feature that can be included in future studies.

## 2.2 Pacing Protocols

For the Bernus model, action potentials are produced with an external stimulus current of 19.6 pA/pF of 2 ms duration. Action potential durations (APDs) are measured using a threshold membrane potential corresponding to 90% repolarization. For the Fox model, action potentials are produced with an external stimulus current of 80.0 pA/pF of 1 ms duration. APDs are measured using a threshold membrane potential corresponding to 90% repolarization.

## 2.3 Bifurcation Diagrams

Since we are interested in studying how different drugs alter cardiac cell dynamics, we generate bifurcation diagrams using the model with a variety of drug efficacies. Bifurcation diagrams show the relationship between APD and basic cycle length (BCL) (24). The diagram is obtained by recording APD for different values of BCL, first with BCL decreasing (BCL downsweep) to a certain fixed value and then increasing the BCL (BCL upsweep) from its lowest value to its original value. For the Bernus model, without the drug effect, we begin at a BCL of 400 ms and step down to a BCL of 200 ms with a step size of 1 ms, then return to our original BCL using the same step size. We recorded 20 APD for each step of BCL. Note that the Bernus model reaches steady-state within two or three stimuli. For the Fox model, we begin at a BCL of 300 ms and step down to a BCL of 90 ms with a step size of 1 ms, then return to our original BCL using the same step size. The bifurcation process is studied only after 40 stimuli and then recorded the next 20 APD as the Fox model requires at least 30 stimuli to attain the steady state.

## 2.4 Restitution

We study APD restitution in the Bernus and the Fox models, then apply the antiarrhythmic drugs doses to study the change in the slope of the RC. We are interested to see how the steepness of the RCs changes with the application of antiarrhythmic drugs. We will then find the maximum slope of the RC for a given efficacy of the drug in order to test the restitution hypothesis (36). According to the hypothesis, the value of the maximum slope indicates the occurence (maximum slope of RC greater than 1 or equal to 1) or the

disapperance (maximum slope of RC less than 1) of alternans in the bifurcation diagram of APD as a function of BCL. We study two different restitution protocols to generate RCs: the dynamic restitution protocol and the S1-S2 restitution protocol.

### 2.4.1 Dynamic Restitution

For the DRC in the Bernus model, we decrease the BCL from 800 ms to 300 ms in steps of 1 ms and measure steady-state APD and the preceding DI from the last two APs. We measure the APD and DI pairs until the cell transits from a 1:1 response to a 2:1 response to construct the DRC. Similarly, in the Fox model, we decrease the BCL from 400 ms to 90 ms in steps of 1 ms and measure steady-state APD and the preceding DI. We measure the APD and DI pairs until the cell transits from a 1:1 response to a 2:2 response. The RCs are plotted for the entire range of efficacies from 0 to 1 in steps of 0.01 for sodium and calcium channel blockers. We restrict the efficacy for potassium channel blockers to 0.6 as the APD exceeds the BCL at efficacies greater than 0.6. In order to measure the maximum slope of the curve: we measure the difference between two consecutive points on the curve, find their ratios, and find the maximum value. We use linear regression analysis by taking 5 values above and below this maximum, to calculate the maximum value of the slope. After the slope is calculated, we study the variation of the maximum slope of the RC as a function of efficacy so that we can test the restitution hypothesis at each efficacy.

### 2.4.2 S1-S2 Restitution

For the SRC, the cell is paced at a constant S1 BCL of 800 ms in the Bernus model for 20 APs and 400 ms in the Fox model for 40 APs until the steady state is reached. Then it is followed by an extrastimulus S2 with a BCL of 800 ms in the Bernus model and 400 ms in the Fox model. We decrease the length interval between S1 and S2 from 600 ms to 300 ms in the Bernus model and from 400 ms to 100 ms in the Fox model in steps of 1 ms. We measure the APD generated from the extrastimulus S2 and the DI between S1 and S2 to construct the SRC. We obtain SRCs for 3 different values of S1 BCLs and calculate the maximum slope of the RCs corresponding to different S1 BCLs. A similar process is followed as explained in the previous section to study the variation of the maximum slope of the RC as a function of efficacy. The three different S1 values in the Bernus model are 800 ms, 400 ms and 300 ms for sodium and calcium channel blockers and 800 ms, 600 ms and 500 ms for potassium channel blockers. For the Fox model, the three different S1 values are 400 ms, 300 ms and 200 ms for sodium and calcium channel blockers and 500 ms, 400 ms and 300 ms for potassium channel blockers.

# Chapter 3

# Results

## 3.1 The Effect of Antiarrhythmics on Action Potential

A basic element of cardiac electrophysiology is the action potential, so we first use our methodology to contrast and compare the effects of different antiarrhythmics on the action potential. A single stimulus pulse is applied to the Bernus model and the Fox model, and we look at changes to the subsequent action potential as drug efficacy varies.

For the Bernus model, when a drug blocks sodium ion channels (Fig. 3.1, top row, left), our model predicts that the APD does not change for most drug efficacies. At the highest efficacy, the action potential loses its spike and the APD disappears. The figure shows that the APD does not change for a wide range of efficacies ranging from 0 to 0.94. We found that at the efficacy of 0.95 there is a slight increase in APD and as we increased the efficacy from 0.96 to 1, the action potential disappears showing that the cell is not

responding at all. While some experimental studies have observed no change in APD with the application of sodium channel blockers (63–65), the majority of experiments have observed some dose-dependent change (55–62).

For a drug that blocks potassium ion channels (Fig. 3.1, top row, center), our model predicts that the APD increases with an increase in efficacy. At efficacies higher than ∼0.6, the drug is sufficiently strong as to prevent the cell membrane voltage from returning to its original rest state. These model predictions agree with the majority of experiments with potassium channel blockers which show the prolongation of APD (59, 66–74). In the case of calcium ion channel blockers (Fig. 3.1, top row, right), our model predicts that the action potential duration decreases with increase in efficacy. The effect of this drug is to shorten the duration of the plateau phase of the action potential The APD is shortened by almost 20% when the drug efficacy increases from 0 to a maximum efficacy of 1. Even when the calcium channel is completely blocked, there is still an action potential, although it does not have a plateau. This agrees with many experiments which found that various calcium channel blockers shorten APD (59, 62, 76).

We then studied the effects of different antiarrhythmics on the action potential for the Fox model. When a drug blocks sodium ion channels (Fig. 3.1, center row, left), the APD does not change for most drug efficacies and APD decreases at the highest efficacy of the drug. Compared to the Bernus model, the action potential does not disappear completely as we can see there is still a plateau region at the highest drug efficacy. For a drug that blocks potassium ion channels, the increase in APD (Fig. 3.1, center row, center) appears very much similar to the Bernus model, however, there are some changes in the membrane potential during the resting period at the higher doses. The calcium

channel blockers (Fig. 3.1, center row, right) decrease the APD and the pattern pretty much follows the Bernus model. The shape of the APs are different from each other in these models and the APD in the Bernus model is almost twice the duration of the APD in the Fox model. We also see that the maximum membrane potential reaches slightly higher in the Fox model as compared to the Bernus model when no drugs are used. We first use the drug efficacy on the 2 components of the delayed rectifier $K^+$ current; the rapid component $I_{Kr}$ and the slow component, $I_{Ks}$ in the Fox model, (Fig. 3.2) whereas the delayed rectifier $K^+$ current has a single component $I_K$ in the Bernus model. We find that there is a very small change in the APD on $I_{Kr}$, and no change in the APD on $I_{Ks}$ for entire range of the drug efficacy respectively. This makes us choose $I_{K1}$ current in the Fox model, which show a similar response to $I_K$ in the Bernus model to study the changes in the APD with the use of drugs.

Each of the three classes of the drug under study has a distinct effect on APD. These findings are summarized in Fig. 3.1 (bottom left, the Bernus model) and (bottom right, the Fox model) where we have plotted the action potential duration as a function of drug efficacy. These summarizing figures allow us to clearly contrast the effects of the drugs over their full range of effect. Sodium channel blockers have no effect on APD until an efficacy of $\sim$0.94 for both models. With a slightly higher dose of this drug, the APD increases slightly before the action potential is completely blocked in the Bernus model. However, in the Fox model, the APD still exists as the action potential is not completely blocked. The slight increase in APD in the Bernus model is easily missed in studies that examine only a few drug concentrations. The potassium channel blocker causes a quasi-exponential increase in the APD as the efficacy increases, while the calcium channel

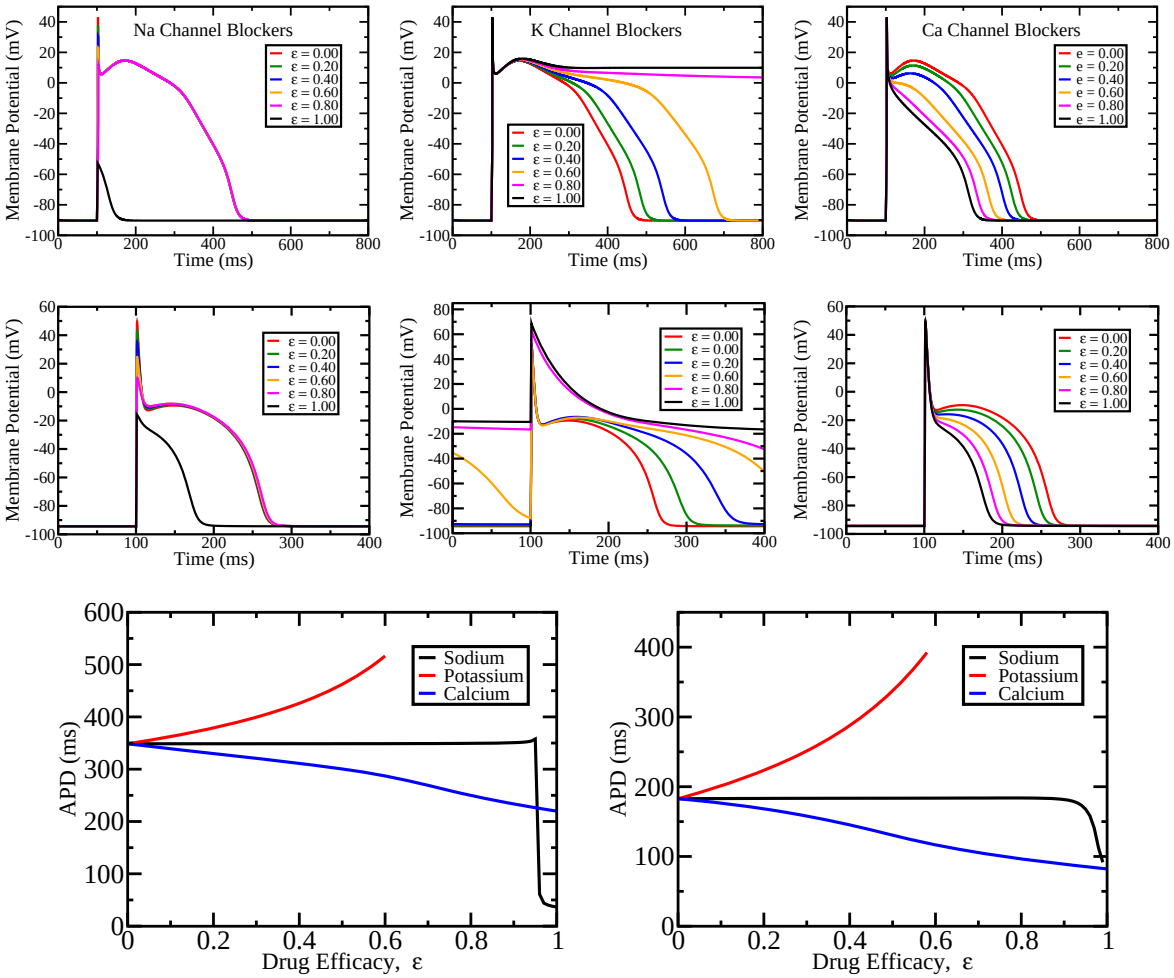


Figure 3.1: Effect of $Na^+$, $K^+$ and $Ca^{2+}$ channel blockers on APs of the Bernus (top) and the Fox model (center). (top and center row, left) For a wide range of $Na^+$ channel blocker efficacies, APD remains almost constant, disappearing only at the highest efficacies. (top and center row, center) For $K^+$ channel blockers, APD increases with efficacy, preventing the transmembrane voltage from returning to the rest state when the efficacy exceeds $\sim$0.6. (top and center row, right) $Ca^{2+}$ channel blockers decrease the APD by decreasing the plateau phase. The effect of $Na^+$, $K^+$, and $Ca^{2+}$ blockers on APD. Bernus (bottom left) and Fox (bottom right). The three classes of drugs have very different effects on APD with $Na^+$ channel blockers (black line) showing little effect, $K^+$ channel blockers (red line) causing quasi-exponential increase in APD, and $Ca^{2+}$ channel blockers (blue line) causing almost linear decrease in APD.

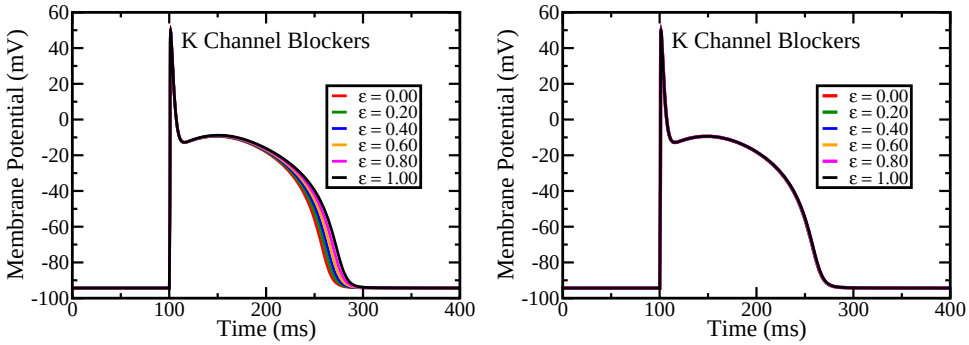


Figure 3.2: Effect of $Na^+$, $K^+$ and $Ca^{2+}$ channel blockers on the 2 component of the delayed rectifier $K^+$ current in the Fox model. (left) The rapid component $I_{Kr}$ and (right) the slow component $I_{Ks}$. There is a very small change in the APD on $I_{Kr}$, and no change in the APD on $I_{Ks}$ for entire range of the drug efficacy respectively.

blocker causes an approximately linear decrease in the APD as the efficacy increases in both models.

## 3.2 Rate-Dependent Changes

One of the characteristic properties of antiarrhythmic drugs is a phenomenon known as rate dependence (118). Rate-dependence refers to a change in the effect of a drug as the pacing rate changes. Potassium channel blockers are characterized by reverse rate dependence (RRD), where the lengthening of APD is greater at longer BCL than at shorter BCL. Reverse rate dependence minimizes the electrophysiological effects of drugs on repolarization during tachyarrhythmias and tends to increase their proarrhythmic potential (77). We examined rate dependence by pacing at a variety of BCLs until a steady steady response. We constrained our study to 1:1 response and for this range of BCLs, the Bernus model reached a steady-state APD within two or three action potentials, as can be seen in the bifurcation diagrams presented later whereas the Fox

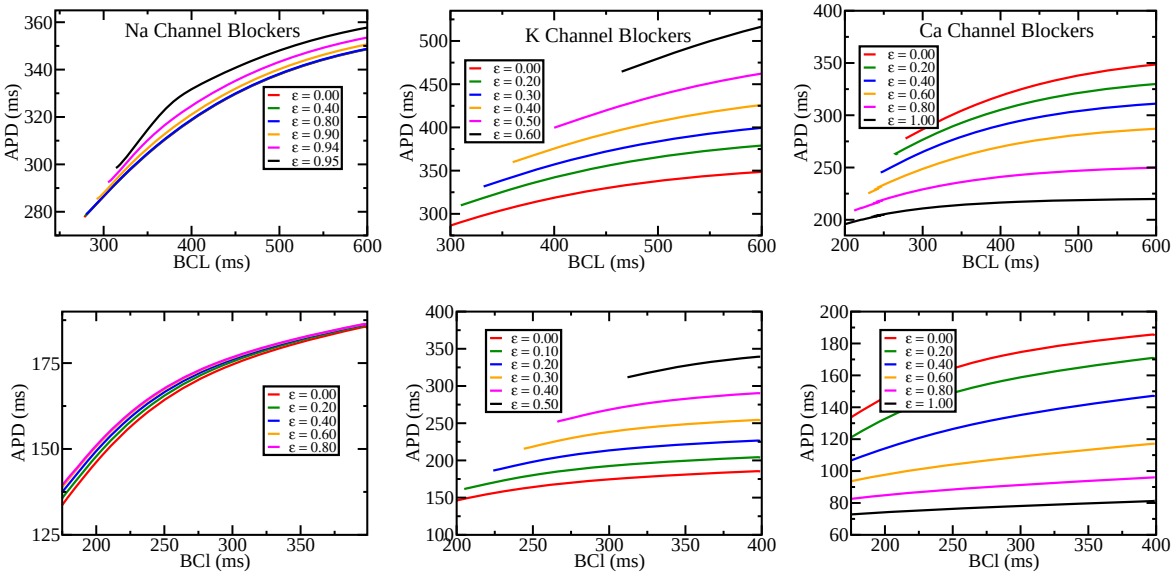


Figure 3.3: BCL dependent change of APD induced by $Na^+$, $K^+$ and $Ca^{2+}$ channel blockers for the Bernus (top) and the Fox model (bottom). (top and bottom row, left) There is little change in APD by $Na^+$ channel blockers at any pacing rate. (top and center row, center). APD is increased by $K^+$ channel blockers. (top and bottom row, right) APD is shortened by $Ca^{2+}$ channel blockers.

model reached a steady state after as many as 40 action potentials. The last action potential was used to calculate the APD for each BCL. The plot of BCL against the steady APD is shown in Fig. 3.3, (top and center row) for several efficacies of each drug for the Bernus and the Fox model respectively.

The lengthening or shortening of APD, $APD_{Diff}$ is calculated by taking the difference between APD in the absence of drug and APD in the presence of drug for a particular BCL. Fig. 3.4, (top and center row) shows the lengthening or shortening of APD as a function of the BCL for several efficacies of each drug for the Bernus and the Fox model respectively. For sodium channel blockers, our models predict that there is no appreciable change in the difference in APD with BCL in the Bernus model, irrespective of drug efficacy. However, we notice an increase of $APD_{Diff}$ in the Fox model at lower BCLs with

an increase in drug efficacy. For potassium channel blockers, the models predict that there is an increase in the change in APD as BCL increases, i.e. the potassium channel blocker has more of an effect at longer BCLs. $APD_{Diff}$ is significantly higher in the Fox model compared to the Bernus model at all drug efficacies. For calcium channel blockers, our models predict a shortening APD, but we again see an increased effect at longer BCLs in both models.

Both potassium and calcium channel blockers show RRD in these models and our simulations show that the strength of this effect depends on the drug efficacy, as can be seen by the changing slopes of the lines. In order to more clearly see the effect of drug efficacy, we plotted the slope of the lines of $APD_{Diff}$ vs. BCL as a function of the drug efficacy. Fig. 3.4 (bottom left, the Bernus model) shows that the slope is almost zero for sodium channel blockers except for a slight positive slope at an efficacy of 0.95, indicating a slight rate-dependent effect, whereas Fig. 3.4 (bottom right, the Fox model), shows that the slope has slight negative slope for most of the efficacies and the slope decreases after drug exceeds an efficacy of 0.95. In both models, potassium channel blockers have a rapidly growing slope while calcium channel blockers have a slope that decreases approximately linearly although the rate of decrease seems to increase abruptly at an efficacy of $\sim$0.6 in the Bernus model and $\sim$0.5 in the Fox model. This analysis suggests that potassium channel blockers will produce a more dramatic rate-dependent effect for a given drug efficacy than calcium channel blockers.

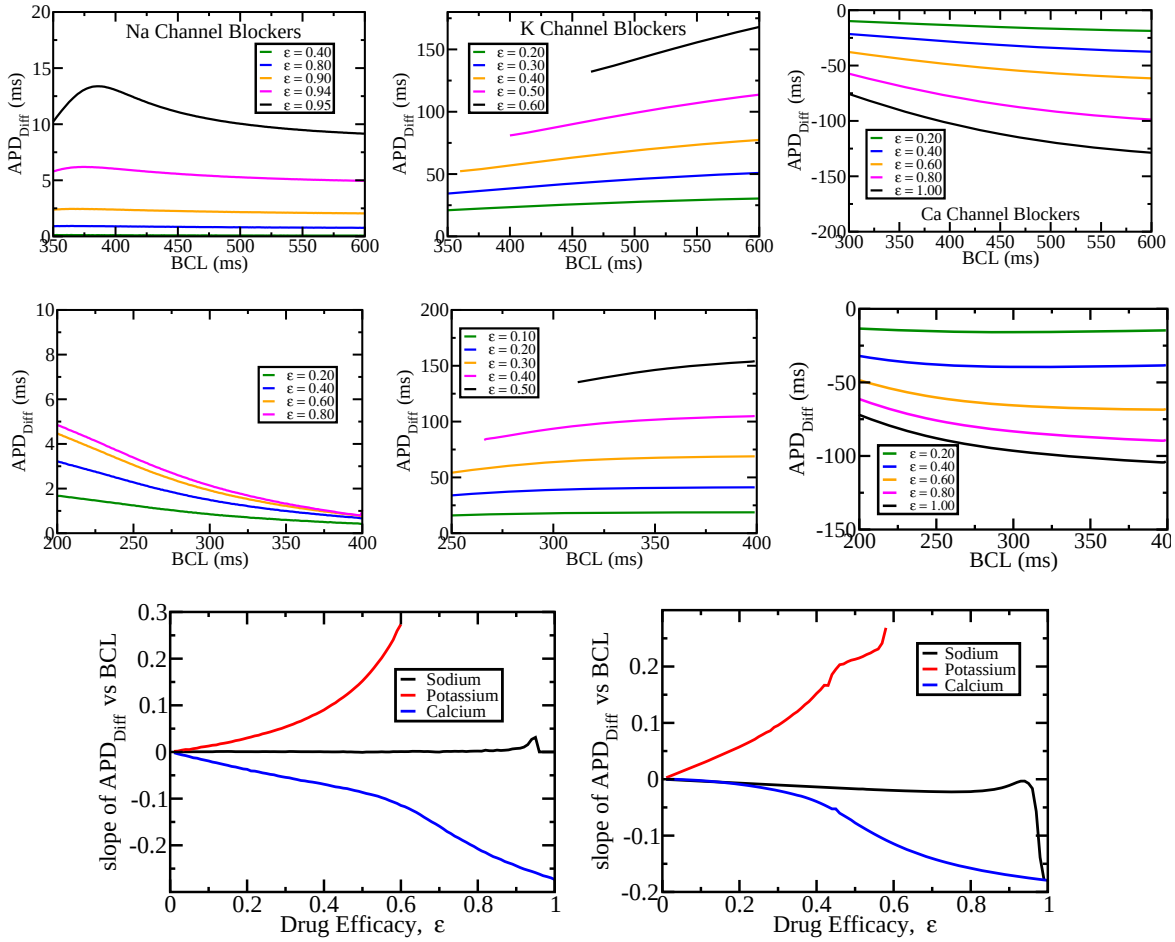


Figure 3.4: Changes in the APD, $APD_{Diff}$ induced by $Na^+$, $K^+$ and $Ca^{2+}$ channel blockers for the Bernus (top) and the Fox model (center). (top and center row, left) There is little change in $APD_{Diff}$ by $Na^+$ channel blockers at any pacing rate. (top and center row, center) APD is lengthened by $K^+$ channel blockers with greater changes at longer BCLs. (top and center row, right) APD is shortened by $Ca^{2+}$ channel blockers with greater changes at longer BCLs. The rate of change of the drug-induced $APD_{Diff}$ with BCL is plotted as a function of the efficacy for $Na^+$, $K^+$ and $Ca^{2+}$ channel blockers: the Bernus model (bottom left) and the Fox model (bottom right). There is little change in the slope for $Na^+$ channel blockers (black line). For $K^+$ channel blockers (red line), the slope grows quasi-exponentially with increase in the efficacy. For $Ca^{2+}$ channel blockers (blue line), the slope decreases linearly at slower rate and then decreases at higher rates with increase in efficacy.

## 3.3 The Effect of Antiarrhythmics on Arrhythmogenesis

### 3.3.1 Bifurcations

Bifurcation diagrams provide a detailed picture of the electrophysiological response of cardiac cells by recording APD at various BCLs. Two features of the bifurcation diagram are thought to be indicators of susceptibility to arrhythmias. Alternans is thought to be a precursor to ventricular fibrillation (25, 27, 34, 35, 119). Bifurcation diagrams also show hysteresis, meaning that the BCL at which the 1:1 response (one action potential for every stimulus) transitions to the 2:1 response (one action potential for every two stimuli) during the downsweep is often not the same BCL at which the reverse transition (2:1 reverting to 1:1) occurs during the upsweep. This hysteresis window has also been linked to arrhythmogenesis (120, 121).

The bifurcation diagram for the Bernus model in the absence of any drugs is shown in Fig. 3.5 (left). During the downsweep, as we decrease the BCL from 400 ms to 200 ms, the APD decreases but remains in a 1:1 pattern. At a BCL of 275 ms, the cell reaches a point at which it cannot recover fast enough to respond to every stimulus. There is an abrupt increase in the APD as the cell transitions to the 2:1 response and remains in the same pattern until the BCL decreases to 200 ms. Then, we begin the BCL upsweep from 200 ms to its original value of 400 ms. The cell remains on the 2:1 branch until BCL=333 ms after which the cell makes an abrupt transition back to 1:1 behavior until the BCL increases to 400 ms again. The transition from 2:1 to 1:1 occurs at a longer BCL

than that at which the transition from 1:1 to 2:1 initially occurs, creating a hysteresis window. The size of the hysteresis window is about 58 ms. Similarly, the bifurcation diagram for the Fox model is shown in Fig. 3.5 (right). The BCL is decreased from 300 ms and remains in a 1:1 pattern until the BCL reaches 200 ms. At this BCL, alternans occurs showing the bifurcation from 1:1 to 2:2 pattern (two action potentials of a different shape for every two stimuli). The cell remains on the 2:2 branch until the BCL reaches 150 ms. The cell returns to 1:1 again and maintains this pattern until the BCL reaches 95 ms. Then there is an abrupt increase in the APD at a BCL of 94 ms as the cell transitions to the 2:1 response and remains in the same pattern until the BCL decreases to 90 ms. Then, we begin the BCL upsweep from 90 ms to its original value of 300 ms. The 2:1 pattern is of a very short duration of only 5 ms. When the BCL is increased from 90 ms, we find that the 2:1 pattern transitions to 1:1 at a BCL of 95 ms. The cell remains in 1:1 pattern until the BCL reaches 150 ms after which the transition from 1:1 to 2:2 again takes place until the BCL exceeds 200 ms. The cell then transitions back to 1:1 and remains in this pattern until the BCL reaches its original value of 300 ms. Compared to the width of the hysteresis window in the Bernus model, the size of the window in the Fox model is very small, with a width of only 1 ms.

Bifurcation diagrams were generated and examined for a variety of efficacies of each of the drug classes for both models. The results for the Bernus model are shown in Fig. 3.6. We adjust the different ranges of BCLs for each of the drugs in order to see the transitions as APD gets lengthened or shortened with the efficacy of different drugs. For all the drugs, we find that there is a transition from 1:1 to 2:1 pattern, and that there is a hysteresis window associated with this transition. For sodium channel blockers, we

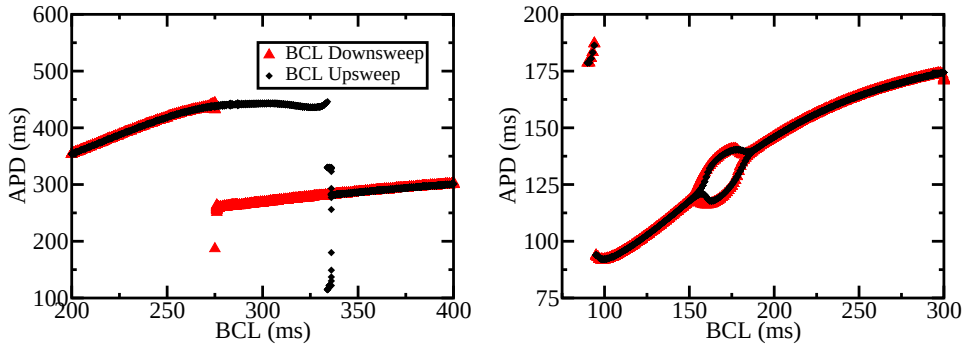


Figure 3.5: Bifurcation diagram for the Bernus model (left) and the Fox model (right) in the absence of any drug effect. The red triangles correspond to APD during BCL downsweep and the black diamonds correspond to APD during BCL upsweep.

can see hysteresis up to an efficacy of 0.95, after which we do not see hysteresis since the action potential vanishes. For potassium channel blockers, we limit the efficacy to 0.6 as the higher values lead to very large APDs. When potassium is used, we see an alternating rhythm appear between BCL≈300–400 ms and move towards longer BCL≈525 ms as the drug efficacy increases. For calcium channel blockers, the transitions shift to lower BCLs due to shortening of the APD.

Bifurcation diagrams for the Fox model are shown in Fig. 3.7. Compared to the Bernus model, we can see a completely different picture in this model. At low efficacies of sodium channel blockers, we can see a very narrow width of hysteresis and it vanishes as the efficacy is increased. There are APD alternans and transitions at lower and intermediate efficacies that vanish with the increase in the efficacy. With potassium channel blockers, APD alternans exist at the lower efficacy of 0.1 and there are higher order transitions at both BCL downsweep and BCL upsweep. Bifurcation diagrams for the calcium channel blockers are quite different compared to the two other channel blockers. There are transitions at lower efficacies of the drug that completely vanish with

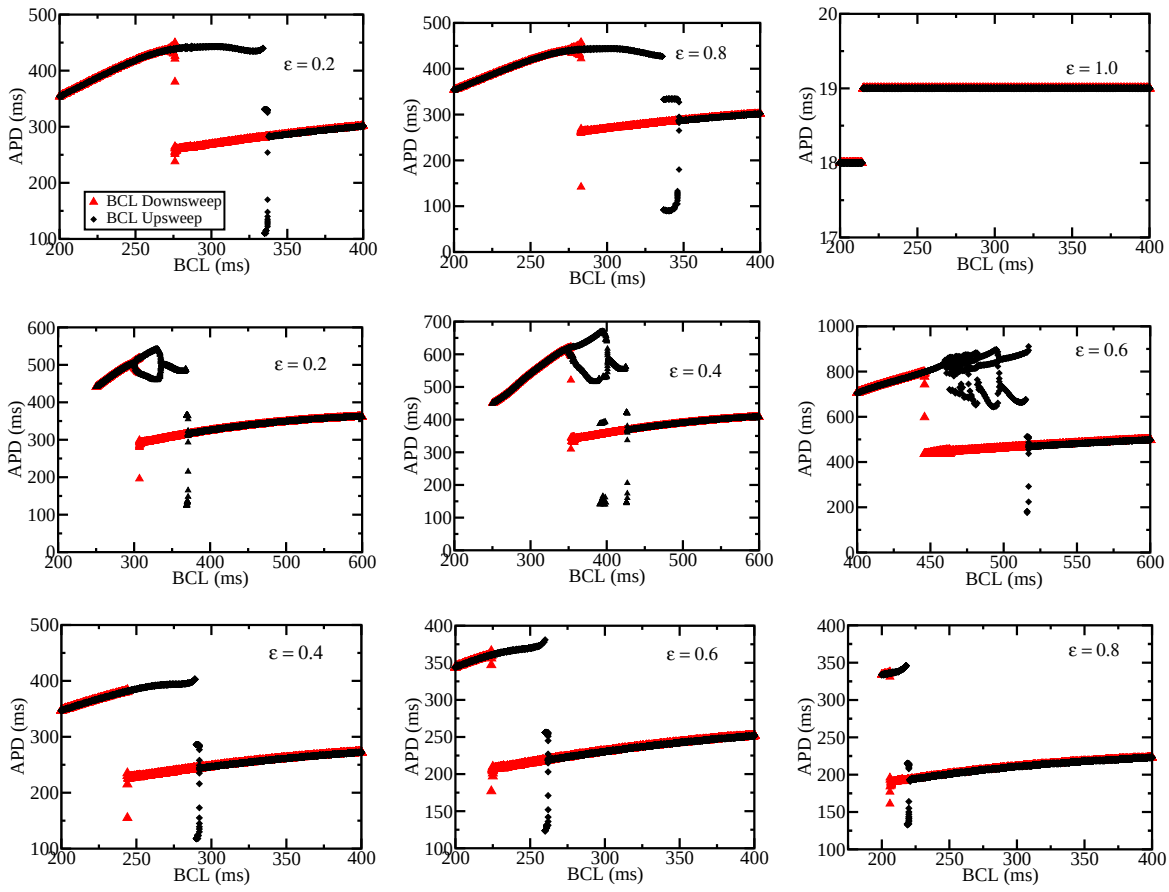


Figure 3.6: The effect of antiarrhythmics on rate-dependent behavior in the Bernus model. Bifurcation diagrams in the presence of various efficacies of $Na^+$ channel blockers (top row), $K^+$ channel blockers (center row) and $Ca^{2+}$ channel blockers (bottom row).

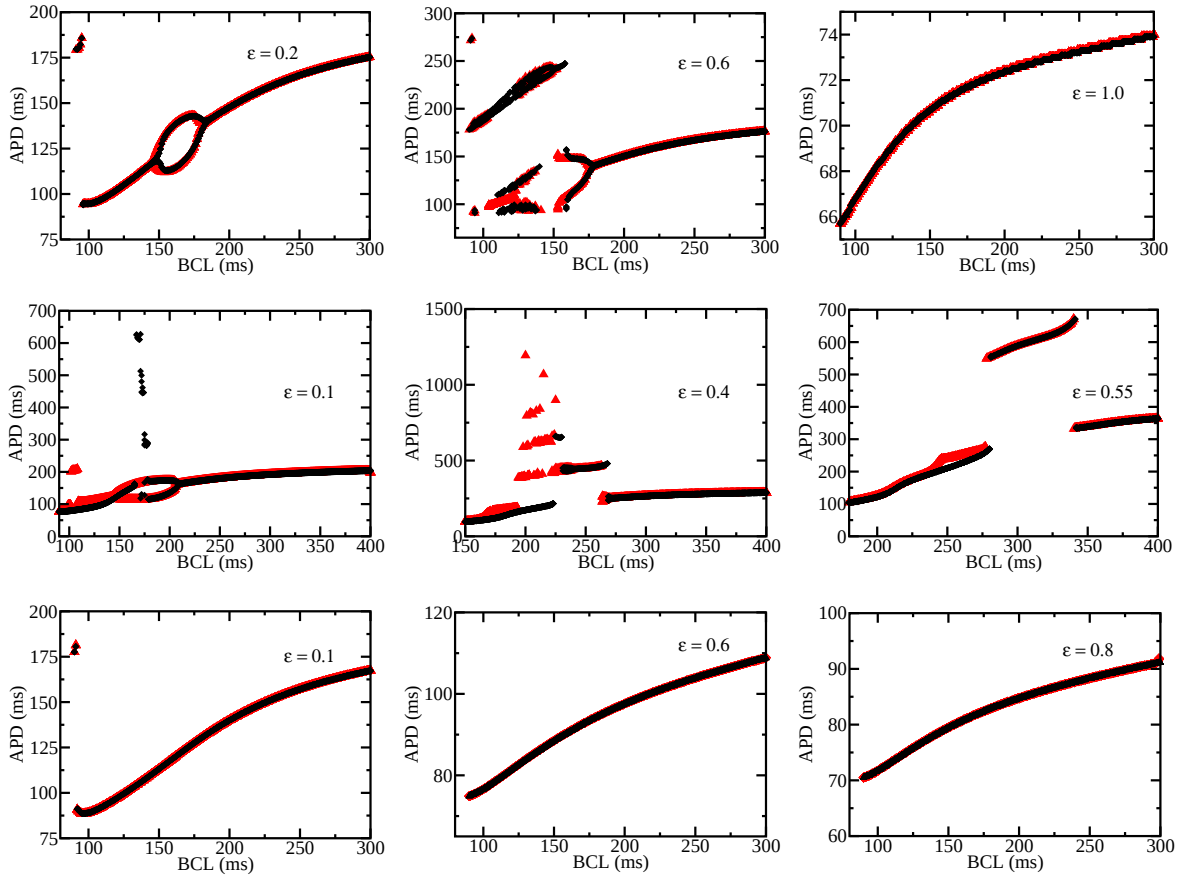


Figure 3.7: The effect of antiarrhythmics on rate-dependent behavior in the Fox model. We show the bifurcation diagrams in the presence of various efficacies of $Na^+$ channel blockers (top row), $K^+$ channel blockers (center row) and $Ca^{2+}$ channel blockers (bottom row).

the increase in the drug efficacy. The APD alternans also disappear at a drug efficacy of 0.06 and greater.

### 3.3.2 Hysteresis

The change in the width of the hysteresis window will only be studied for the Bernus model as the width is very narrow in the Fox model and vanishes at higher drug efficacies. To study how the hysteresis window changes as we apply different doses of the drug, we

define $BCL_{down}$ as the BCL at which we see a transition from 1:1 to 2:1 and $BCL_{up}$ as the BCL at which we see a transition from 2:1 to 1:1. These transition BCLs are plotted as a function of efficacy and the results are shown in Fig. 3.8. For sodium channel blockers, the transitions, both up and down, take place at almost the same BCLs for a wide range of efficacies, only increasing slightly once the efficacy surpasses ∼0.9. For sodium channel blockers, the size of the hysteresis window remains constant at 58 ms for a large range of drug efficacies. For potassium channel blockers, the transitions, both up and down, occur at longer BCLs as the drug efficacy increases. This is a direct consequence of the increase in APD as the drug efficacy increases. $BCL_{up}$ increases smoothly, but $BCL_{down}$ exhibits a sharp discontinuity near $\varepsilon \approx 0.4$, leading to a decrease in the size of the hysteresis window at higher drug efficacies. For calcium channel blockers, the transitions both occur at shorter BCLs as the efficacy increases. $BCL_{up}$ appears to decrease more rapidly than $BCL_{down}$ causing a decrease in the size of the hysteresis window as the efficacy of the drug increases. For calcium channel blockers, the size of the hysteresis window decreases with increasing drug efficacy. The hysteresis window size decreases from 58 ms to 5 ms as the drug efficacy is increased from 0.01 to 0.88 and the window disappears once the efficacy exceeds 0.88.

### 3.3.3 Alternating Rhythms and Alternans

Finally, we examined the effect of drug concentration on the occurrence of alternating rhythms and alternans on both models. We do not observe persistence alternans in the Bernus model, but we do observe other alternating rhythms which are not 2:2 patterns.

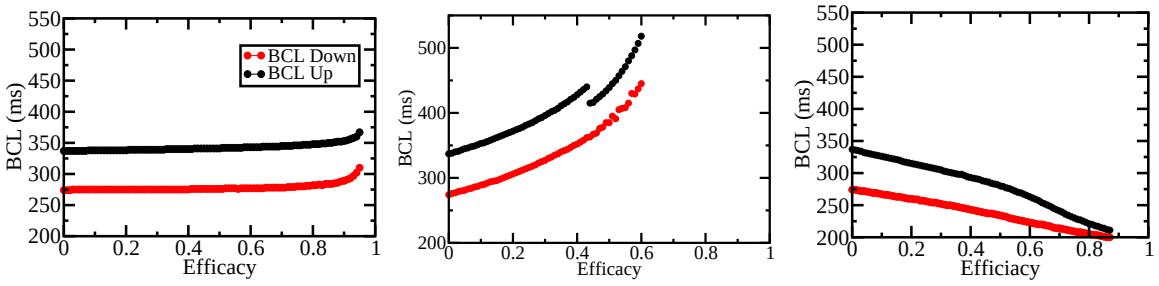


Figure 3.8: The effect of antiarrhythmics on the hysteresis window. For each of the three classes of drug, we plot the BCL at which the dynamics transition from 1:1 to 2:1 behavior ($BCL_{down}$) and the BCL at which the dynamics return from 2:1 to 1:1 behavior ($BCL_{up}$). (left) For sodium channel blockers, the size of the hysteresis window (difference between $BCL_{up}$ and $BCL_{down}$) remains constant for almost the entire range of efficacies of the drug. (center) For class potassium channel blockers, the transitions, both up and down, occur at longer BCLs as the drug efficacy increases. (right) For calcium channel blockers, the transitions both occur at shorter BCLs as the efficacy increases.

In the Bernus model, for each drug efficacy, we counted the number of BCLs at which steady-state alternating rhythms were observed during $BCL_{up}$ and $BCL_{down}$. The results are shown as histograms in Fig. 3.9. For the Bernus model, as shown in Fig. 3.9 (top row, left) when we use sodium channel blockers, the occurrence of alternating rhythms (frequency) increases slightly as the drug efficacy increases. With potassium channel blockers, as shown in Fig. 3.9 (top row, center) the occurrence of alternating rhythms initially increases, reaches a maximum at an efficacy of $\sim$0.35 and then decreases until efficacy reaches 0.6. As shown in Fig. 3.9 (top row, right), the occurrence of alternating rhythms decreases with an increase in efficacy for calcium channel blockers. The alternating rhythms completely vanish when the drug efficacy exceeds 0.88.

As we observe sustained alternans in the Fox model, we are interested in finding the number of alternans at each drug efficacy and the alternans are measured during $BCL_{down}$. As shown in Fig. 3.9 (bottom row, left) there is a slight increase in the number

of alternans at mid efficacies for sodium channel blockers in the Fox model compared to the Bernus model. Fig. 3.9 (bottom row, center) shows the occurrence of alternans increases, reaches a maximum at an efficacy of ∼0.10 and then gradually decreases as the drug efficacy of the potassium channel blockers approaches 0.6. As in Fig. 3.9 (bottom row, right), the occurrence of alternans decreases abruptly with the increase in drug efficacy and then completely vanishes after the drug efficacy exceeds 0.06. The calcium channel blockers show a distinct behavior compared to the sodium and potassium blockers on the Fox model. The calcium channel blockers completely eliminate the alternans at very low efficacies.

## 3.4 Restitution

### 3.4.1 Dynamic Restitution

The dynamic restitution curve (DRC) is determined by steady state APD and DI and is thought to play a role in the stability of the 1:1 response (122).

Once we get the steady-state APD and DI pairs for a range of BCL values, we find the maximum slope of the APD-DI curve for the entire range of drug efficacies. When a drug blocks sodium ion channels (Fig. 3.10, left), both of the models predict that the slope of the DRC does not change for most drug efficacies. The DRCs change when the efficacy jumps to 0.94 and 0.95 showing an increase in the slope of the Bernus model at DI values below 50 ms. In the Fox model, the slope of the DRC is increased at an efficacy of 0.95 and thereafter decreases when the efficacy reaches 1. For a drug that blocks potassium

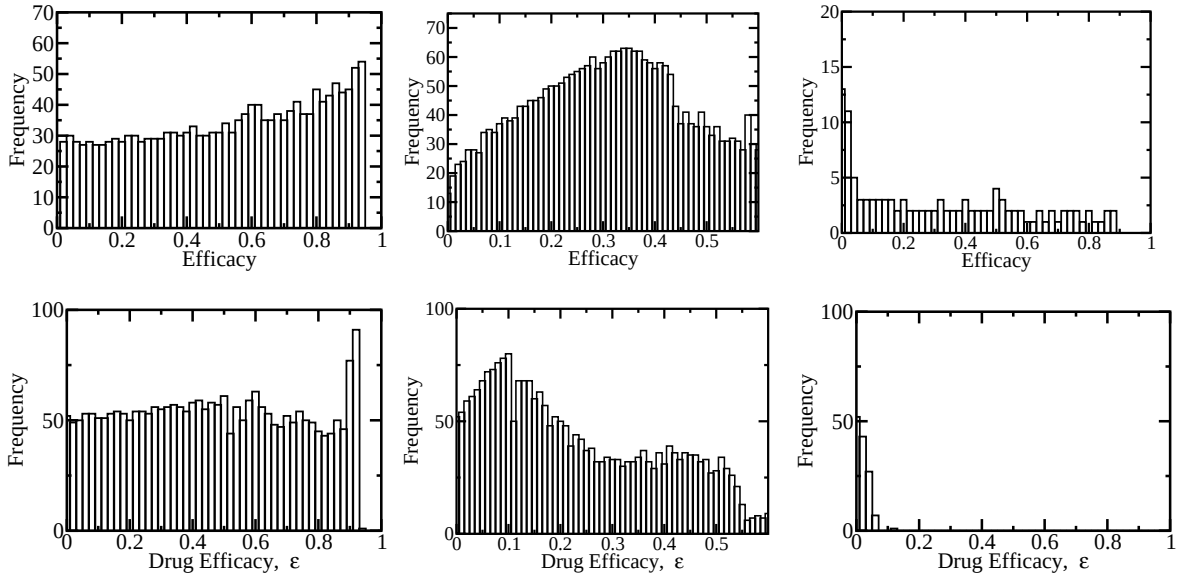


Figure 3.9: The effect of antiarrhythmics on alternating rhythms for the Bernus model (top row) and altenans for the Fox model (bottom row). (top row, left) For sodium channel blockers, the occurrence of alternating rhythms increases slightly as the drug efficacy increases; for potassium channel blockers (top row, center), it increases initially, reaches a maximum at an efficacy of $\sim$0.35 and then decreases until efficacy reaches 0.6 and (top row, right) it decreases with increasing efficacy for calcium channel blockers. For the Fox model (bottom row, left), the occurrence of alternans increases slightly at mid efficacies for the sodium channel blockers. For Class III drugs (bottom row, center), it increases until efficacy reaches 0.1 and then decreases gradually. (bottom row, right) The occurrence of alternating rhythms decreases abruptly with the increase in drug efficacy and completely vanishes after the drug efficacy exceeds 0.06.

ion channels (Fig. 3.10, center), the Bernus model predict that the slope of the RCs remains almost same with the curves pretty much parallel unitl the efficacy of 0.4 and increases slightly thereafter with an increase in efficacy of the drug. Even though the curves appear pretty much parallel, the region where we obtain the maximum slope gives different values with efficacies greater than 0.4 in graph of maximum RC vs. efficacy (Fig. 3.11, left). In the Fox model also, the slope of the RCs remains almost same with the curves pretty much parallel until the efficacy of 0.3 and increases slightly thereafter with an increase in efficacy of the drug. In the case of calcium ion channel blockers (Fig. 3.10, right), our models predict that the slope of the restitution curve decreases with an increase in efficacy of the drug. Fig. 3.10 shows that the slope is steepest at the shortest DI. Variation of the DRC with drug concentration can be determined by finding the maximum slope of the curve and plotting it against the drug efficacy.

Fig. 3.11 shows the maximum slope of the dynamic restitution curve as a function of efficacy for $Na^+$, $K^+$, and $Ca^{2+}$ channel blockers for the Bernus (left) and the Fox model (right). Our measurement shows the maximum slope of the DRC with no drug effect is 0.65 for the Bernus model which is less than 1. So according to the restitution hypothesis, the Bernus model should not have alternans at lower BCLs. The maximum slope of the RC is 1.35 for the Fox model, and we find alternans in the Fox model when the cell is paced at lower BCLs within the range of $150 - 200$ ms. (Fig. 3.5)

In the Bernus model, the maximum slope of the DRC remains the same for most efficacies and increases as the efficacy reaches 0.95 for $Na^+$ channel blockers. The DRC does not exist from the efficacy of 0.96 onwards, so there is no slope. For $K^+$ channel blockers, the slope of the DRC almost remains the same until an efficacy of 0.4 and

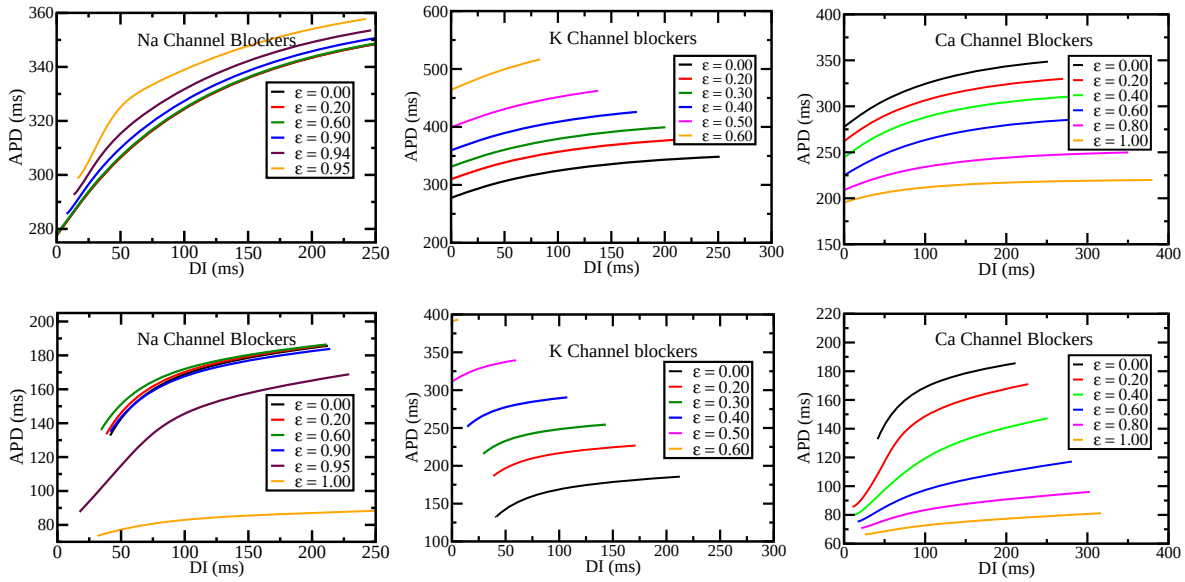


Figure 3.10: Effect of $Na^+$, $K^+$, and $Ca^{2+}$ channel blockers on the dynamic restitution curve for the Bernus (top row) and the Fox model (bottom row). (top and bottom left) The RC remains the same for most of the efficacies, however there are changes when the efficacy exceeds 0.90 for $Na^+$ channel blockers. (top and bottom center) The RC changes as the efficacy of $K^+$ channel blockers is increased. (top and bottom right) The RC changes as the efficacy of $Ca^{2+}$ channel blockers is increased.

thereafter increases with an increase in efficacy. The maximum slope of the DRC is 0.76 at an efficacy of 0.6. For $Ca^{2+}$ channel blockers, the slope of the DRC initially almost remains the same until an efficacy of 0.38 and thereafter decreases with an increase in efficacy. At the highest efficacy of 1.0, the slope decreases to a value of 0.26.

In the Fox model, the maximum slope of DRC continuously decreases very slowly for most efficacies and increases as the efficacy reaches 0.92 for $Na^{+}$ channelblockers and thereafter decreases with increase in efficacy. For $K^{+}$ channel blockers, the change in the slope of the DRC as a function of the drug efficacy is very much different than what we observe in the Bernus model. The slope initially decreases until the efficacy reaches 0.1 and then increases until an efficacy of 0.33. The slope remains nearly the same for a certain range of efficacies and after an efficacy of 0.42, it decreases with a decrease in efficacy. For the $Ca^{2+}$ channel blockers, the plots have a different shape than we observe in the Bernus model. The slope first increases to 1.64 when the drug efficacy reaches 0.02 and thereafter decreases gradually with an increase in efficacy.

Our results show a similar trend with some of the experimental results on the use of the antiarrhythmic drugs on canine ventricles. The $Na^{+}$ channel blocker procainamide did not reduce the slope of the dynamic RC in canine ventricle (44). The $Ca^{2+}$ channel blocker verapamil lowered the slope of DRC and prevented fibrillation in canine ventricle (44). $K^{+}$ channel blocker bretylium also lowered the slope of DRC and prevented fibrillation in pig ventricles (43), however, our study of the Bernus model showed that the slope of the DRC increased with increase in the efficacy of the drug.

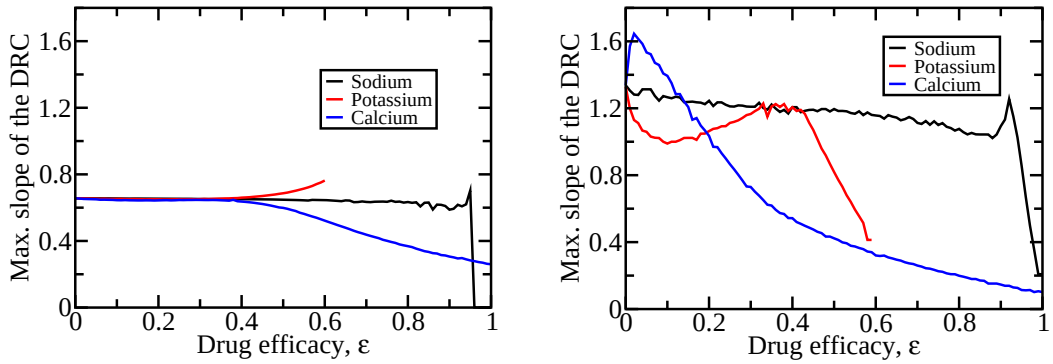


Figure 3.11: The maximum slope of the dynamic RCs vs. efficacy for $Na^+$, $K^+$ and $Ca^{2+}$ channel blockers for the Bernus model (left) and the Fox model (right).

### 3.4.2 S1-S2 Restitution

In the S1-S2 restitution method, we measured the APD and DI for various efficacies of $Na^+$, $K^+$, and $Ca^{2+}$ channel blockers. We plotted the APD against DI and produced a RC curve for each efficacy of the drug for both the Bernus and the Fox model (3.13).

The S1-S2 restitution curves (SRC) for $Na^+$, $K^+$, and $Ca^{2+}$ channel blockers appear similar to the dynamic restitution curves but have different slopes. For the Bernus model, we generated SRCs for three different values of S1=800 ms, S1=500 ms and 400 ms for $Na^+$ and $Ca^{2+}$ channel blockers and S1=800 ms, 600 ms and S1=500 ms for $K^+$ channel blockers (Fig. 3.12). In all the plots of Fig. 3.12, we notice that the slope of the RC continuously increases with decrease in the S1 BCLs and has the maximum value at the lowest BCL for all efficacies of sodium, potassium and calcium channel blockers. However, for all the S1 BCLs, the curves look similar, showing that the slopes of the RCs might be overlapping each other indicating an absence of short-term cardiac memory in Bernus model. The short-term memory arise when the APD depends not only on previous DI,

but also the preceding pairs of APD and DIs.

Similarly, for the Fox model, we generated RCs for three different values of S1=400 ms, S1=300 ms and 200 ms for $Na^+$ and $Ca^{2+}$ channel blockers and S1=500 ms, 400 ms and S1=300 ms for $K^+$ channel blockers (Fig. 3.13). As in the Bernus model, the slope of the RC continuously increases with decrease in the S1 BCLs and has a maximum value at the lowest BCL for all efficacies of sodium, potassium and calcium channel blockers. In contrast to the Bernus model, slopes of the RCs are different at different S1 BCLs for the same efficacies of drugs, showing the presence of short-term cardiac memory in the Fox model.

Fig. 3.14 shows the plot of the maximum slope of the S1-S2 restitution curve as a function of efficacy for $Na^+$, $K^+$, and $Ca^{2+}$ channel blockers for the Bernus (left) and the Fox model (right). Our measurement shows the maximum slope of the SRC with no drug effect is 0.57 for the Bernus model which is less than 1. The maximum slope of the SRC remains the same for most efficacies and increases as the efficacy reaches 0.95 for $Na^+$ channel blockers. The SRC does not exist from the efficacy of 0.96 onwards, so there is no slope. For $K^+$ channel blockers, the slope of the SRC almost remains the same until an efficacy of 0.35 and thereafter increases with an increase in efficacy. The maximum slope of the SRC is 0.71 at an efficacy of 0.6. For $Ca^{2+}$ channel blockers, the slope of the SRC initially almost remains the same until an efficacy of 0.2 and then increases within increase in efficacy. The slope becomes maximum at an efficacy of 0.45 and then decreases continuously and reaches a value of 0.15 at the highest efficacy of 1.0.

The maximum slope of the SRC is 1.64 for the Fox model in the absence of any drugs, and we find alternans in the Fox model when the cell is paced at lower BCLs in the range

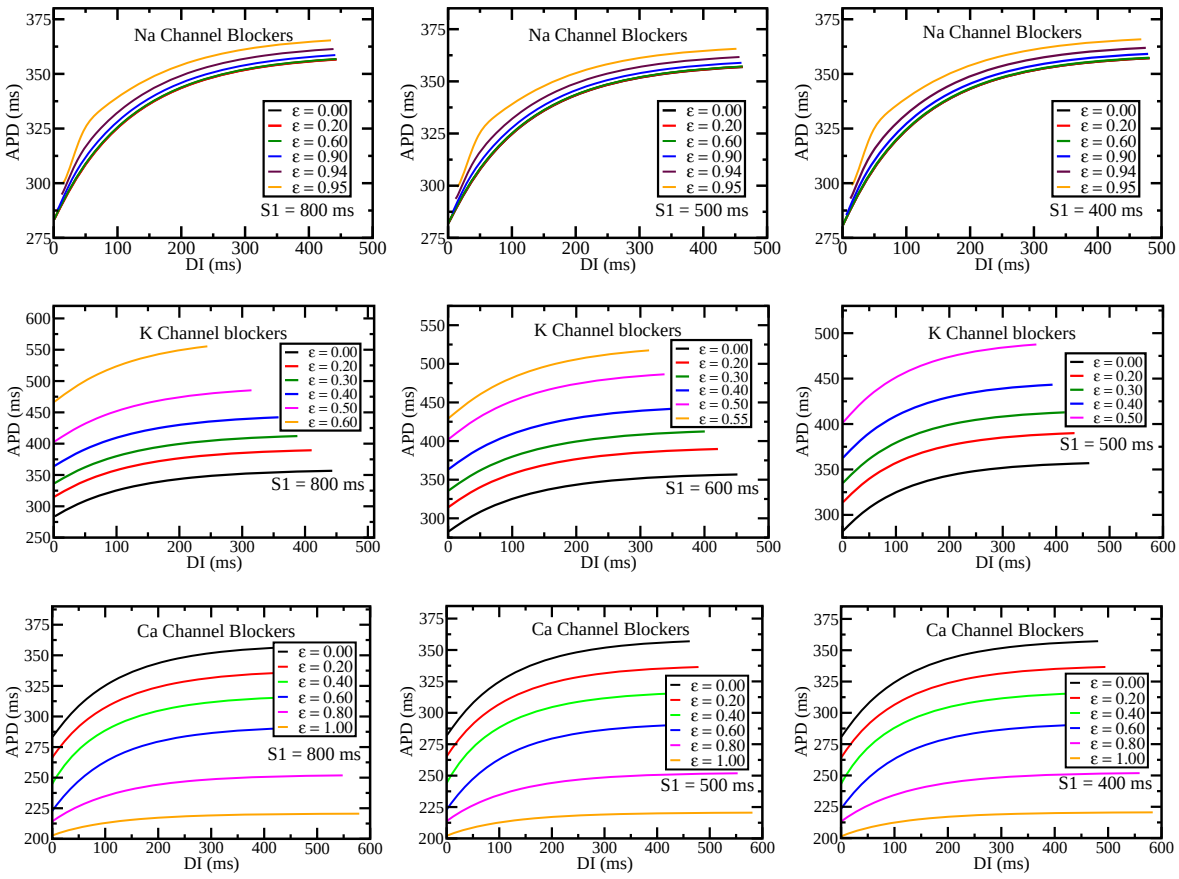


Figure 3.12: Effect of $Na^+$, $K^+$, and $Ca^{2+}$ channel blockers on S1-S2 restitution curve for the Bernus model at various S1 values. The SRC remains the same for most of the efficacies and changes at an efficacy of 0.94 and above for $Na^+$ channel blockers (top row). The SRC changes with increase in the APD as the efficacy of $K^+$ channel blockers is increased (center row). The SRC changes with decrease in the APD as the efficacy of $Ca^{2+}$ channel blockers is increased (bottom row).

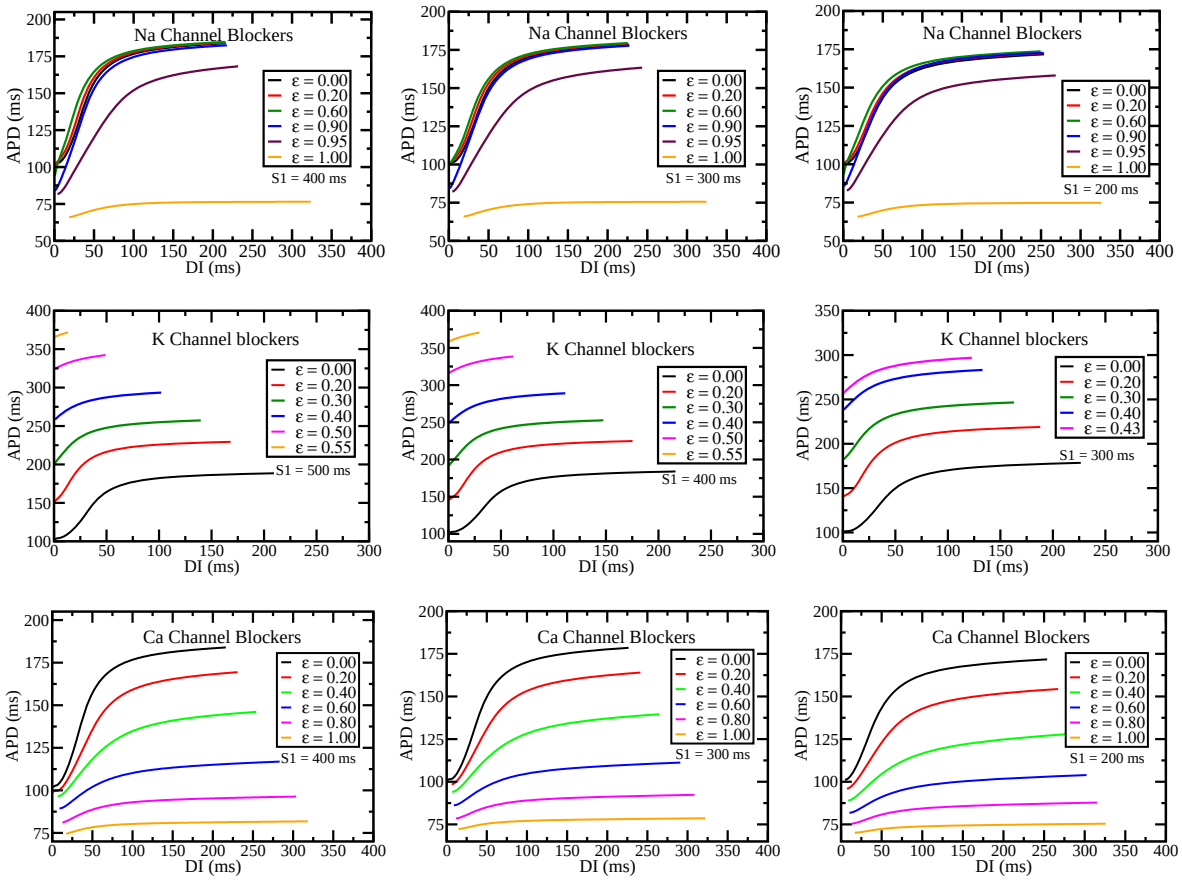


Figure 3.13: Effect of $Na^+$, $K^+$, and $Ca^{2+}$ channel blockers on S1-S2 restitution curve for the Fox model at various S1 values. The SRC remains the same for most of the efficacies and changes at an efficacy of 0.95 and above for $Na^+$ channel blockers (top row). The SRC changes with increase in efficacy of $K^+$ channel blockers (center row row). The SRC changes with decrease in the APD as the efficacy of $Ca^{2+}$ channel blockers is increased (bottom row).

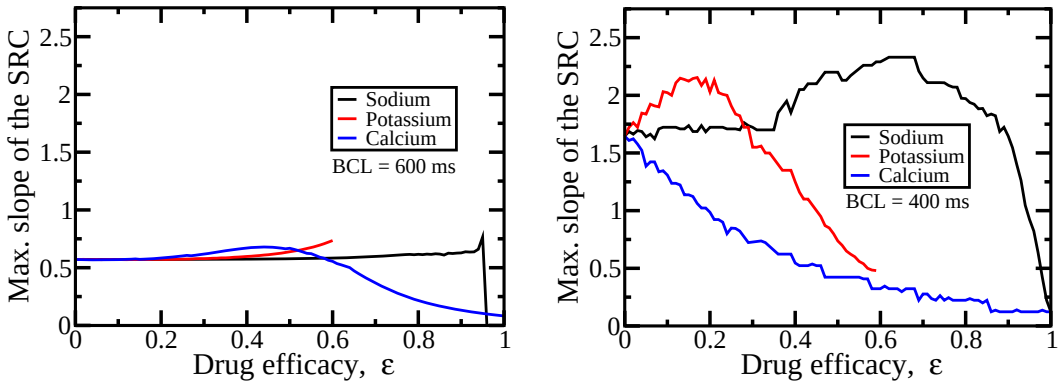


Figure 3.14: The maximum slope of the SRCs is plotted as a function of the efficacy for $Na^+$, $K^+$ and $Ca^{2+}$ channel blockers at S1=600 ms for the Bernus model (left) and at S1=400 ms for the Fox model (right).

of $150 - 200$ ms. In the Fox model for $Na^+$ channel blockers, the maximum slope of SRC has the same value until an efficacy of 0.37 and thereafter increases gradually and becomes maximum with a value of 2.2 at drug efficacy of 0.70. The slope then decreases gradually until it reaches a value of 0.122 at an efficacy of 1. The maximum slope decreases below 1 at an efficacy of 0.95 and onwards corresponding to the disapperance of alternans in the bifurcation diagram. For $K^+$ channel blockers, the change in the slope of the SRC as a function of the drug efficacy is very different than what we observe in the Bernus model. The slope initially increases and reaches a value of 2.14 at an efficacy of 0.15 and then starts to decrease with a decrease in efficacy and attains a value of 0.47 at the highest efficacy of 0.6. The slope decreases below 1 at an efficacy of 0.46 and onwards. For the $Ca^{2+}$ channel blockers, the slope continuously decreases from its maximum value at an efficacy of 0 and reaches 0.12 at the highest drug efficacy of 1. The value of the slope decreases below 1 at an efficacy of 0.2 and onwards.

The plots of SRCs for different values of S1 BCLs at a particular value of efficacy are

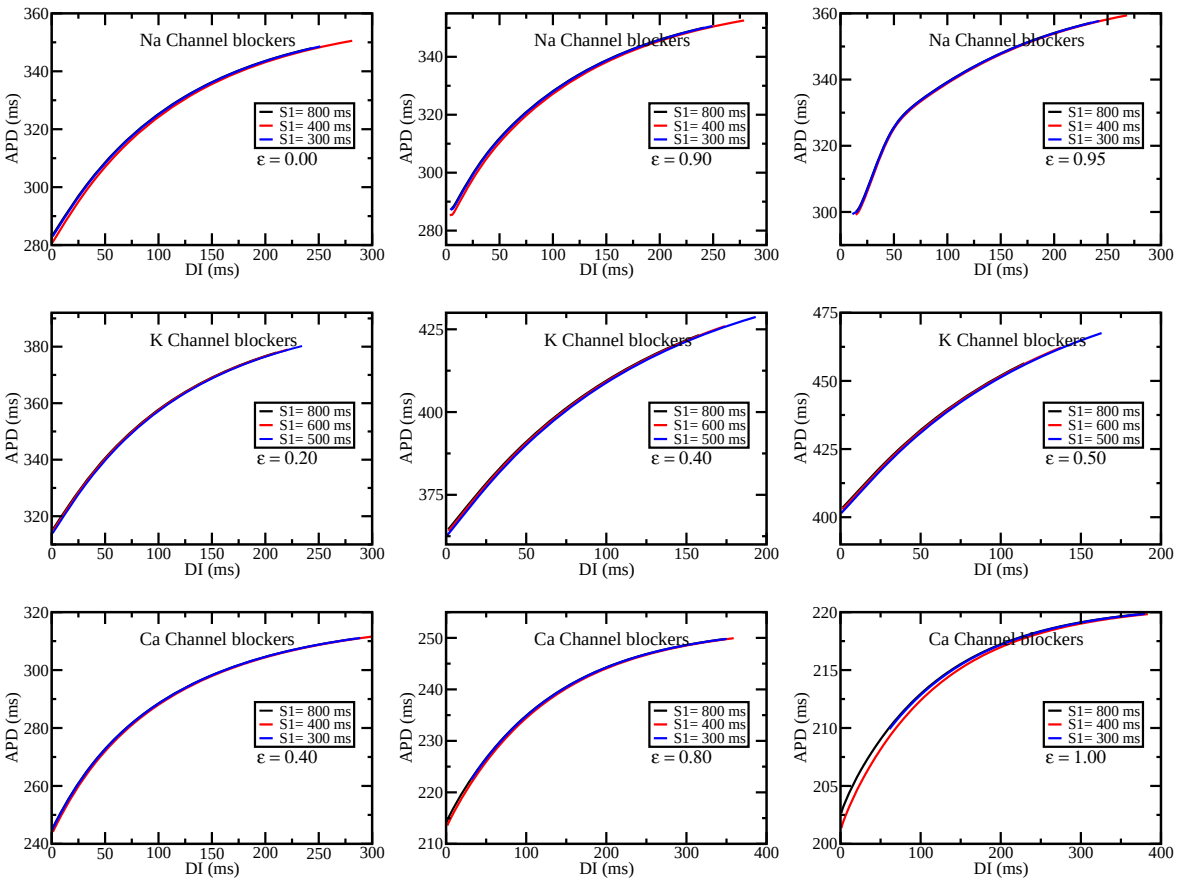


Figure 3.15: Effect of $Na^+$ channel blockers (top row), $K^+$ channel blockers (center row), and $Ca^{2+}$ channel blockers (bottom row) of given efficacy on S1-S2 restitution curve for the Bernus model at various S1 values.

shown in Fig. 3.15. The S1 BCLs are 800 ms, 400 ms and 300 ms respectively for $Na^+$ channel blockers, and $Ca^{2+}$ channel blockers. For $K^+$ channel blockers, the S1 BCLs are 800 ms, 500 ms and 400 ms respectively.

We see that the RCs almost overlap at all the S1 BCLs for given efficacy of drugs, showing that the cardiac memory is absent in the Bernus model. The reason the Bernus model attains a steady state after the very first AP is because of the lack of memory.

Fig. 3.16 shows the maximum slope of the S1-S2 RCs curves plotted as a function of efficacy for $Na^+$, $K^+$ and $Ca^{2+}$ channel blockers for three different values of S1 for the

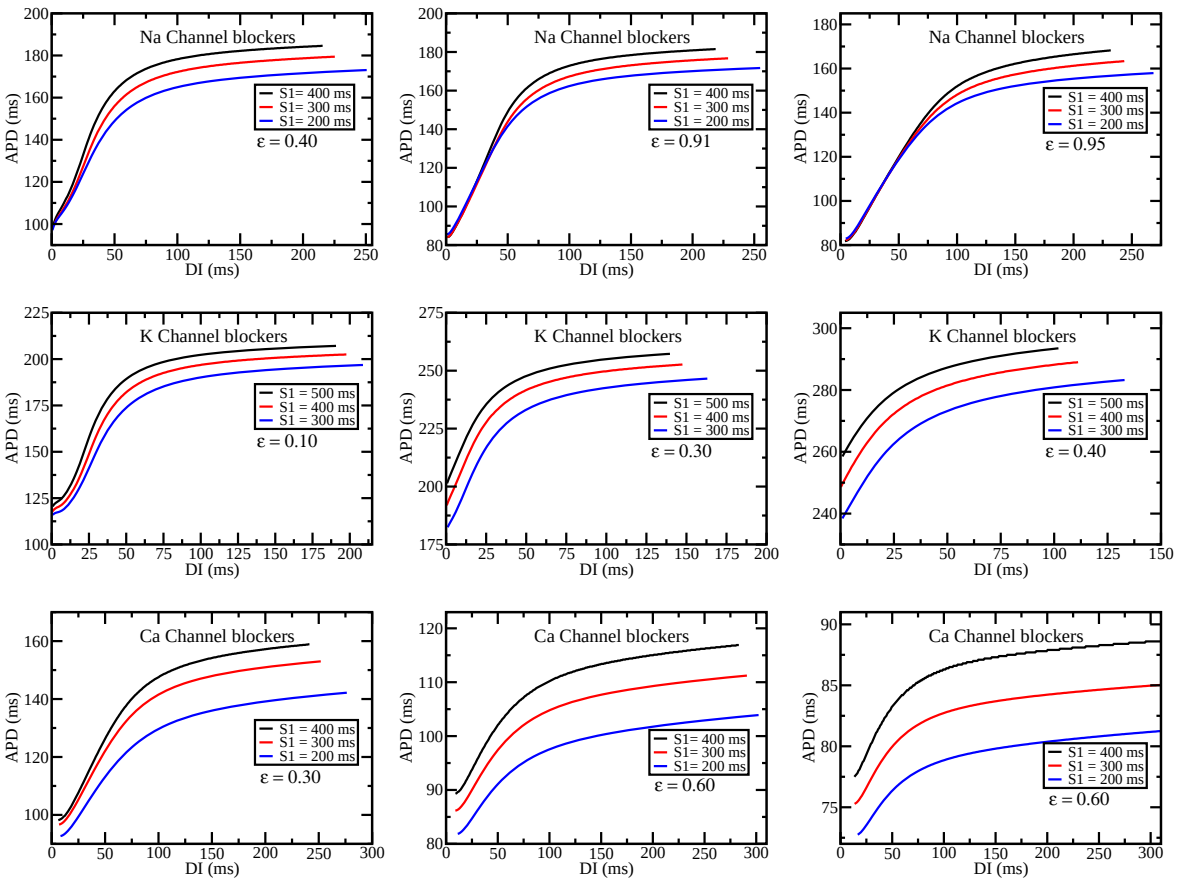


Figure 3.16: Effect of $Na^+$ channel blockers (top row), $K^+$ channel blockers (center row), and $Ca^{2+}$ channel blockers (bottom row) of given efficacy on S1-S2 restitution curve for the Fox model at various S1 values.

Fox model. The plots show that there are different RCs for different values of the S1 BCLs. This shows that cardiac memory is present in the Fox model. The steady state is attained after a very large number of APs in the Fox model as compared to a single AP in the Bernus model.

Fig. 3.17 and Fig. 3.18 show the plots of the maximum slope of the SRC as a function of drug efficacy for 3 different values of S1 BCLs for the Bernus model and the Fox model respectively. The slope overlaps for all the S1 BCLs in the Bernus model. However, the slopes are distinct for each value of S1 BCL in the Fox model. In the Fox model, the

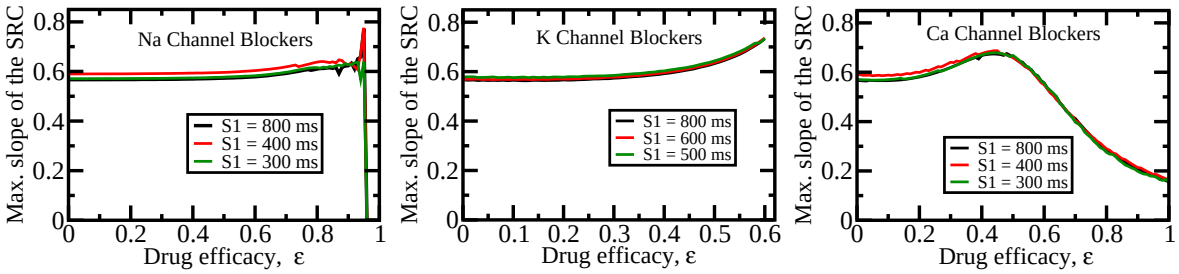


Figure 3.17: The maximum slope of the S1-S2 RCs is plotted as a function of efficacy for $Na^+$ channel blockers (left), $K^+$ channel blockers (middle) and $Ca^{2+}$ channel blockers (right) for three different values of S1 BCLs for the Bernus model.

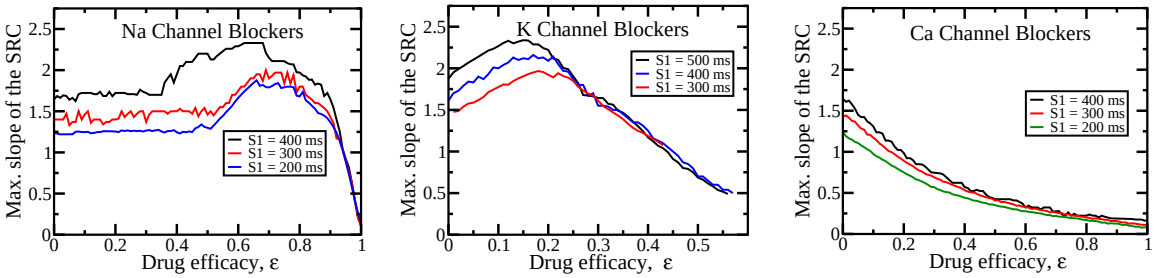


Figure 3.18: The maximum slope of the S1-S2 RCs is plotted as a function of efficacy for $Na^+$ channel blockers (left), $K^+$ channel blockers (middle) and $Ca^{2+}$ channel blockers (right) for three different values of S1 BCLs for the Fox model.

slopes of the RCs decrease as S1 BCL is lowered, as APD shortens for a same range of DIs for each lower S1 BCL. At efficacies of 0.95 and higher for $Na^+$ channel blockers, the slope seems to overlap for all the S1 BCLs. Similar results can be seen for $K^+$ channel blockers at an efficacy of 0.25 and higher and for $Ca^{2+}$ channel blockers, overlapping begins at an efficacy of 0.5 and higher. Beyond these efficacies, the drug effect saturates and the changes in DIs cause the same changes in APDs for all the given SI BCLs.

# Chapter 4

# Discussion

Mathematical modeling and computer simulation are powerful tools to investigate the electrical dynamics of cardiac cells. We employed mathematical modeling of ventricular cells of two different species to study how antiarrhythmic drugs could influence the various ionic currents and the shape of the AP of a cardiac cell. We studied the application of three different classes of antiarrhythmic drugs to these models, using the concept of efficacy, $\epsilon$, to study the action potential of ventricular cells. The use of drug efficacy in these models provide us with a technique to block the various ionic currents flowing into the cell and coming out of the cell through the cell membrane. Both Bernus and Fox model has a single sodium current and calcium current entering into the cell through the cell membrane, whereas there are several potassium currents exiting the cell. For the potassium currents, we used efficacy for a particular potassium current which changed AP the most. We used efficacy in various potassium currents and found that $I_K$ current in the Bernus model and $I_{K1}$ in the Fox model showed the largest change in the shape of the AP, thus bringing a change in the APD. We neglected the effect of efficacy on other

potassium currents as the APs showed very little change in shape in some and no change at all in others.

First of all, we used the drug efficacy of three classes of antiarrhythmic drugs to study the change in the APs produced with an external stimulus current in both models. The time of simulation was 800 ms in the Bernus model and 400 ms in the Fox model. We found that the three classes of antiarrhythmic drugs examined had very different effects on the AP with sodium channel blockers exhibiting no effect, potassium channel blockers increasing the APD, and calcium channel blockers decreasing the APD on both models.

We studied the rate-dependent effects of the three classes of antiarrhythmic drugs by decreasing the BCL to value just before the cell transit from 1:1 state in the Bernus model and to 2:2 state in the Fox model and found that both models predicted reverse rate dependency (RRD) in potassium channel blockers and calcium channel blockers. We also studied the rate of APD change with pacing rate as a function of drug efficacy, and the results showed differences between the three classes of antiarrhythmic drugs. For potassium channel blockers, the prolongation of the APD is most pronounced at lower BCL in comparison to higher BCL. Our results suggested that RRD was less severe for calcium channel blockers, potentially making them a more effective choice for reducing cardiac arrhythmias.

We studied the bifurcation of APD on both models. We observed the variation of APDs during the BCL downsweep and BCL upsweep. During BCL downsweep, we saw cell transition from 1:1 to 2:1 state in the Bernus model, from 1:1 to 2:2, 2:2 to 1:1, and 1:1 to 2:1 in the Fox model. During BCL upsweep, the cell response made an abrupt transition back to 1:1 state at a different BCL indicating the presence of hysteresis. For

the Fox model during the BCL downsweep, the 2:2 state continued for a certain range of BCL after which the cell returned to 1:1 state again. The cell transitioned to 2:1 state for a very short period of time at the lower DIs. During BCL upsweep, we saw a very small hysteresis, which is insignificant in our study as we were more interested to study the alternans in the Fox model. The Fox model (97) is the only canine model demonstrating alternans of APD when they are paced rapidly among the other existing models (101, 102, 104, 105), thus making this model a favorite among researchers in studying the alternans.

Two restitution protocols were used to study the restitution on both models with the use of antiarrhythmic drugs. Dynamic restitution protocol measures the steady-state response of the cell when the BCL is varied, providing a unique restitution curve (RC) for a given cell. This study can be related to the fast beating heart of a running athlete where the APD and DI are changing with the fast heart rate corresponding to the decreasing BCL. S1-S2 restitution protocol measures the immediate response to a change in S1 BCL such that the RCs are different for various S1 BCL values. Similarly, this can be related to the sudden change in heart rate when a person is startled. The restitution condition by Nolan and Dalesco predicted the generation of alternans when the maximum slope of the RC was greater than 1 and the disappearance of alternans when the slope of the RC was less than 1. The Bernus model did not produce alternans and the maximum slope of the RCs was always less than 1 for all three classes of drugs and therefore the restitution hypothesis could not be tested in the Bernus model. Since alternans were generated in the Fox model, the restitution hypothesis can be tested in this model. Our study found that alternans were present when the maximum slope of the RC was less than 1 with

potassium channel blockers, and greater than 1 when alternans were absent with calcium channel blockers. Our study of restitution on the Fox model supported some experiments (24, 40, 49, 50) in which the restitution condition was proved inaccurate and that the prediction of alternans based on the restitution condition was not true. Therefore, the maximum slope of the RCs in the Fox model is not an accurate predictor of the alternans. We found that the occurrence of alternans at a certain range of lower BCLs during BCL downsweep. Fig. 3.9 (bottom row) shows the number of occurrences of alternans as a function of drug efficacies of sodium channel blockers, potassium channel blockers, and calcium channel blockers. The occurrence of alternans was not reduced by sodium channel blockers and showed a biphasic pattern with potassium channel blockers. However, the alternans were completely eliminated by calcium channel blockers as efficacy exceeded 0.06. Our results indicated that alternans can be eliminated by the use of the desired drug efficacy of calcium channel blockers and may help in the development of antiarrhythmic drugs with correct drug doses.

Still, there is a question on why alternans are generated in the Fox model and not in the Bernus model. The answer lies in the presence of the sarcoplasmic reticulum (SR) in the cell. Bernus model does not incorporate SR in the cell, so it does not produce alternans. SR is a reservoir for $Ca^{2+}$ ions. During contraction of the cell, SR releases the calcium ions into the cytoplasm increasing $Ca^{2+}$ contents into the intracellular region and absorbs them during relaxation of the cell. Experiment on rats (123), human atrial cells (124), and a study of the single cell mapping model of calcium cycling (125) found that alternans arises due to changes in SR $Ca^{2+}$ contents.

The following section will help explain the outcomes of simulations of both models.

## 4.1 Questions Answered

With the simulation of the mathematical model of the Bernus model and the Fox model, and the application of sodium channel blockers, potassium channel blockers, and calcium channel blockers on these models we are now able to answer the questions that were raised in the introduction of this paper.

- *How does the action potential of a ventricular cell change with the application of antiarrhythmic drugs?*

Using the efficacy of sodium channel blockers, and varying from 0 to 1, we have found that APD does not change for a wide range of efficacies in both models. A slight increase in the APD is found when the efficacy is 0.95; thereafter, the AP vanishes as efficacy reaches 1 in the Bernus model. At an efficacy of 1, the drug blocks all the sodium channels, at which point and we do not have depolarization. However, the action potential does not vanish completely in the Fox model.

For potassium channel blockers, the APD lengthens with an increase in the efficacy of the drug in both models. These drugs bring a large increase in the APD for a small increase in the efficacy of the drug, such that the APD exceeds the time of simulation when the drug efficacy is above 0.6.

With the use of calcium channel blockers, the APD decreases with an increase in the efficacy of the drug in both models. We know that the influx of calcium ions produces a characteristic plateau phase. The calcium blocker shortens this plateau phase, thus decreasing the APD. At the highest efficacy of 1, the calcium ion channels are completely blocked, such that the plateau phase completely vanishes, but there still is an AP.

- *How do antiarrhythmic drugs affect the rate dependence of APD?*

Our simulation of both models predicted there was little change in APD by sodium channel blockers at any BCL. Potassium channel blockers increased APD and calcium channel blockers drugs decreased APD with increasing drug efficacies. We found that APD is lengthened by potassium channel blockers with greater changes at longer BCLs and that APD is shortened by calcium channel blockers with greater changes at longer BCLs. We found that the potassium channel blockers produce a more dramatic rate-dependent effect for a given drug dose than calcium channel blockers. Fig. 3.4 shows that the change in APD, $APD_{Diff}$ is less at lower BCL (below 400 ms in the Bernus model and below 300 ms in the Fox model), and greater at higher BCL (at 600 ms in the Bernus model and at 400 ms in the Fox model), with increasing drug efficacies of potassium and calcium channel blockers. There is no significant change in $APD_{Diff}$ for the Bernus model with sodium channel blockers. However, in the Fox model, we see that $APD_{Diff}$ decreases with increasing BCL, with increasing drug efficacies.

Our mathematical models allowed us to also study the rate of APD change with BCL as a function of drug efficacy. We found that there is no change in the rate of change of APD with the efficacy of sodium channel blockers. For potassium channel blockers, the rate of APD change increases non-linearly with drug efficacy; and for calcium channel blockers, the rate of APD change decreases quasi-linearly with an increase in drug efficacy. Our models do not agree with observations of rate dependence with sodium channel blockers such as lidocaine (78), tetrodotoxin and mexiletine (80). The use of sodium channel blockers tetrodotoxin and mexiletine showed RRD in the papillary muscles from

human heart (80) and canine ventricular preparation (78). In both models under study, sodium channel blockers do not show RRD.

We were able to produce results similar to the experiments in which potassium channel blockers are used on canine ventricular preparations (77, 126), guinea pigs (71, 72), and papillary muscles from human heart (80), to determine the change in APD with drug usage. The predictions of our model are also in agreement with the majority of experiments which observed RRD in potassium channel blockers (66–69, 71–73, 76–79). We observed RRD for both potassium channel blockers and calcium channel blockers, although it was less severe for calcium channel blockers, potentially making calcium channel blockers a more effective choice for reducing arrhythmias.

- *How do antiarrhythmic drugs affect hysteresis in cardiac cells?*

From our bifurcation plot, we are able to determine the size of the hysteresis window with no drug effect as well as for various efficacies of sodium channel blockers, potassium channel blockers, and calcium channel blockers for the Bernus model. For sodium blockers, the size of the hysteresis window remains constant at 58 ms for a large range of drug efficacies. For potassium channel blockers, we find that the size of the hysteresis window does not change until an efficacy of 0.4 and thereafter there is an abrupt decrease in the size after the efficacy of 0.4. For calcium channel blockers, the size of the hysteresis window decreases with increasing drug efficacy. In the Fox model, the hysteresis is irrelevant in our study, as it occurs at a very low BCL which is electrophysiologically unimportant. Furthermore, we are interested in studying the generation and the prevention of alternans in this model.

- *How do antiarrhythmic drugs affect the generation of alternating rhythms in cardiac cells?*

We studied the occurrence of alternating rhythms by plotting the number of BCLs at which alternating rhythms were observed as a function of drug efficacy (Fig. 3.9). We notice alternating rhythms in the Bernus model, both during BCL downsweep and BCL upsweep, but they are not alternans (Fig. 3.6). The alternating rhythms in the Fox model during BCL dowsweep are alternans (Fig. 3.7). The occurrence of alternating rhythms increases at higher concentrations of sodium channel blockers in both models; however, the occurrence shows biphasic behavior in the Fox model. With potassium channel blockers, the occurrence of alternating rhythms shows biphasic behavior in both models. Finally, with calcium channel blockers, the occurrence of alternating rhythms decreases with increasing efficacy of the drugs. The alternating rhythms completely vanish in the Fox model when the efficacy exceeds 0.06. These results serve to highlight the different effects of each of the three classes of the drug on the electrophysiology of single cells.

- *How does the study of restitution curves (RCs) explain the onset of alternans in our models?*

The restitution hypothesis suggests that the maximum slope of the RC predicts the onset of alternans. According to the hypothesis, alternans are induced when the maximum slope of the RC is equal to or greater than 1, alternans disappears when the maximum slope of the RC is less than 1.

We studied the RCs for both models. The study of dynamic restitution curves (DRCs) and S1-S2 restitution curves (SRCs) shows that the maximum slope of the restitution

curve is always less than 1 in the Bernus model for the entire range of drug efficacies of sodium, potassium, and calcium channel blockers. Alternans are not generated in this model at fast pacing. Potassium channel blockers tend to increase the slope of the RC as efficacy increases but the maximum slope of the RC does not approach 1 at the highest efficacy of 0.6.

The Fox model generates alternans for a range of BCLs at fast pacing in the bifurcation diagram. In the RCs, the maximum slope of the DRCs and SRCs is found to be greater than 1 without any drugs. However, the value of maximum slope changes with the application of drugs. The maximum slope of the RCs remains above 1 for sodium channel blockers for almost the entire range of efficacies. The maximum slope of the RC shows biphasic behavior for increasing potassium channel blockers in both restitution protocols with the value of RC above and below 1. The maximum slope of the RCs in both protocols decreases below 1 as the efficacy of calcium channel blockers exceeds a certain value. Our results showed that alternans are present even though the maximum slope of the RC is less than 1, and the absence of alternans when the maximum slope of the RC is greater than 1. Therefore, we conclude that the maximum slope of the RCs cannot predict the onset of alternans in the Fox model.

- *How does the application of drugs affect the occurrence, enhancement or disappearance of alternans in the Fox model?*

We studied how alternans occur, enhance or disappear when the drugs are applied using DRC. For most efficacies of sodium channel blockers, alternans are present and are enhanced at all these efficacies (Fig. 3.9). However, the alternans vanishes as the drug

efficacy exceed 0.95. Potassium channel blockers gradually increase the occurrence of alternans until the efficacy of 0.1 and then gradually decreases when the efficacy of drug exceeds 0.1. There is a sudden decrease in the occurrence of alternans when the drug efficacy exceeds 0.5. With calcium channel blockers, the occurrence of alternans decreases with an increase in efficacy. The alternans completely disappears when the drug efficacy exceeds 0.06. We found that sodium channel blockers got rid of alternans at higher efficacies of the drug, potassium channel blocker increased and decreased depending upon the efficacy and calcium channel blockers eliminated the alternans completely when the drug efficacy exceeded 0.06. in the Fox model.

- *Which class of antiarrhythmic drugs are effective in eliminating alternans?*

From our simulation results on the Fox model, we plotted a graph of the number of alternans as a function of drug efficacy (Fig. 3.9). In this graph, we observe sustained alternans within a range of BCL when the BCL is lowered. Sodium channel blockers did not eliminate alternans for a very large range of drug efficacies. Additionally, potassium channel blockers showed some effectiveness in reducing the alternans at some specific range of efficacies of the drug. Furthermore, calcium channel blockers eliminated the alternans as the drug efficacy exceeded a certain value. Comparing these results, we see that calcium channel blockers are effective in eliminating alternans, compared to sodium and potassium channel blockers.

The extension of our study to the tissue in 3-dimensional modeling help present whole heart modeling approach and will contribute to the understanding of the functioning of the heart. The computational modeling of the heart can be applied to heart physiology

and the models can be used in diagnosis and treatment of heart disease. In our study, we only studied the electrical behavior in a cardiac cell and did not study the mechanical properties of the cardiac cell. The modeling of mechanical properties of cardiac tissue along with the electrical properties can provide a realistic picture of the actual heart. Our research will be helpful clinically so as to ascertain mathematically the required dose of various classes of antiarrhythmic drugs needed to treat arrhythmias.

The model structure and model parameters used within the structure contribute to predictions made by the mathematical models (127). The model structure provides us to choose the functions and equations used to represent various biological processes. For cardiac cells, this structure is driven by measurements of different ionic currents experimentally from cells of different species. Our modeling studies which implemented the term drug efficacy would help assess the effect of model structure on predicted behavior of antiarrhythmic drugs.

## 4.2 Limitations

We qualitatively compared our results with the experiments most of which were performed on non-human mammalian cardiac preparations, except for one experiment (80), on human papillary muscle tissue. Our results showed a similar trend with some experiments; however, there are some experimental results, which did not agree with our results. We speculate that variation in some of the results between our models and the experimental studies could be due to differences in how antiarrhythmics affect different species of cells (55, 59, 61, 70, 78, 80, 128, 129). Furthermore, we used potassium channel

blockers to block only one type of potassium current ($I_K$ in the Bernus model and $I_{K1}$ in the Fox model) which is in contrast with experiments where the drug blocked different potassium currents.

Most of the experiments are performed on tissue rather than a single cell; and in tissue, it is possible for electrotonic effects to suppress alternans (38). In tissue, the ionic charges spread from one cell to another through the gap junction in the absence of action potentials. This spread of electrical activity through the tissue give rise to a current, called electrotonic current. The potential difference is generated across the ends of a tissue is the electrotronic potential. Therefore, electrotonic current can play a major role in the action potentials and alternans in a tissue (38, 53) which is absent in the study of a single cell.

We considered only the simplistic view of the effect of antiarrhythmics, a class of drug blocking only one type of ion channel. As newer antiarrhythmics drugs are known to affect more than one ion channel (5, 114, 130–133), our measurements of APD will be different, as various currents are affected while using class I, II or IV drugs. This limitation could be overcome by combination therapy using multiple efficacies, each affecting a different ion channel, to more accurately model specific antiarrhythmic drugs. This would definitely be an important step for creating an accurate model of the effects of antiarrhythmics.

There are electrophysiological differences among epicardial, endocardial cells, and midmyocardial cells (134–136) in the ventricle walls and our study is limited to an epicardial cell in the Bernus model, and midmyocardial cell in the Fox model. The shape of the action potentials in the epicardial, endocardial cells, and midmyocardial cells are different (134, 135, 137) with the midmyocardial cells showing the higher APDs com-

pared to epicardial and endocardial cells. Therefore, this deficiency can be addressed by performing simulations on a model of all three types of cells and compare the results.

# Chapter 5

# Conclusion

We have been able to compare thoroughly the effect of ion channel blocking antiarrhythmic drugs using mathematical models of a human ventricular cell and a canine ventricular cell. By using the Bernus model and the Fox model, and then implementing the theoretical concept of the efficacy of the antiarrhythmic drugs in the model, we have seen distinctly different changes in APD, rate-dependent behavior, and bistability in the presence of sodium channel blockers, potassium channel blockers, and calcium channel blockers. In our simulations, we block various ions crossing the cell membrane by implementing accurate doses of drugs bringing a change in the cardiac behavior of ventricular cells. The application of three classes of drugs with various efficacies showed how the occurrence of alternans could be minimized, enhanced or eliminated. The $Na^+$ channel blockers enhance alternans until the efficacy approaches 0.95 and then completely eliminates when the efficacy exceeds 0.95. The $K^+$ channel blockers enhance alternans until the efficacy of 0.40 and thereafter minimize the alternans, but it never attains the level that is seen at efficacy of 0. We found that the $Ca^{2+}$ channel blockers only can eliminate

alternans even at a very low efficacy value of 0.06 and onwards. From Eq. (2.2), using the $\varepsilon_{\max}$ and $IC_{50}$ values of various drugs, we can change the efficacy to the correct drug dose in treating ventricular arrhythmia.

The fact that alternans is not generated in the Bernus model, and the maximum slope of the RC does not exceed 1 for all the drug efficacies, restitution hypothesis cannot be applied in the Bernus model. Since alternans is generated for a certain range of BCLs in the bifurcation diagram of the Fox model, we tested the hypothesis. Alternans is present even though the maximum slope of the RC is less than 1 (K channel blockers) and alternans does not appear when the maximum slope of the RC is greater than 1 ($Ca^{2+}$ channel blockers) for certain range of efficacies of drugs. This shows that the restitution hypothesis fails in the Fox model.

Presently, there are a large number of computational cardiac cell models of a variety of cardiac cells from different species (138–140). These models have different equations for different types of currents. The technique of implementation of drug efficacy in these models would help us to study the predictive behavior of antiarrhythmics. While we have used an ionic model of the human ventricular cell which contains only 6 variables and uses 9 different ionic currents, we have also implemented the drug effect in a model of a canine ventricular cell with 13 variables and 13 different ionic currents in order to study alternans, which are absent in the human model. The increased number of variables and currents results in more differential equations and requires more simulation time.

Our study on rate dependence of drugs on the cardiac cell as well as the results from dynamic and S1-S2 restitution curves suggest calcium channel blockers as the most effective antiarrhythmic drug for the fast-paced cardiac cell. From Fig. 3.9 where we plotted

the occurrence of alternans as a function of efficacy, the alternans disappeared with $Ca^{2+}$ channel blockers efficacy exceeding a small efficacy value of 0.06 while we required a higher efficacy of 0.95 and above for $Na^{+}$ channel blockers to eliminate alternans. In Fig. 3.11 and Fig. 3.14, the plot of maximum slope of the RC as a function of drug efficacy also showed how $Ca^{2+}$ channel blockers reduced the value of the slope continuously with increase in drug efficacy, which was not shown by $Na^{+}$ and $K^{+}$ channel blockers. The lower values of the slope will maintain 1 stimulus:1 response state that will keep the heartbeat normal.

We used a canine ventricular cell model to study alternans as our human ventricular cell model lacks that mechanism. In order to study alternans in a human ventricular cell, we can only predict that the animal model can be applied to human and tests must be evaluated to determine how it confirms to human response.

Our research will be helpful clinically so as to ascertain mathematically the required dose of various classes of antiarrhythmic drugs needed to treat arrhythmias.

## 5.1 Future Works

In this paper, our results are based on the fact that one class of drug blocks only one type of an ion channel. There are drugs available that block more than one type of ion channel. There have been some limited studies of combining antiarrhythmic medications (141–144). However, the implementation of combination therapy may face some difficulties in finding an optimal dose combination of the two different drugs (145). Modern computers with their extremely fast processing speed can simulate hundreds of different

dose combinations. Thus, we can reduce the number of possibilities that need to be investigated in the laboratory or in clinical trials. This will definitely help to improve the safety of patients.

In order to incorporate those drugs blocking more than one type of ion channel, we can modify our simulations to take account of these drug effects using combination therapy. We can use three classes of drugs of different efficacies $\epsilon_1$, $\epsilon_2$, and $\epsilon_3$ with various proportions, and multiply the current of interest by $(1-\epsilon_1)$, $(1-\epsilon_2)$, and $(1-\epsilon_3)$ respectively and again start the simulations. We expect a different result in the action potential duration as we can show that our models can be modified for modeling of new drugs belonging to more than one class of the drug classification. This result might be interesting to see how APD changes, as three drugs have a different effect on APD.

We will extend our simulations to cardiac tissue where the cells are coupled diffusively. A group of cells aligned, make up a tissue and in turn tissues make up organs. Hence it is more interesting for us to extend our simulation to tissues which are the building blocks of vital organs in a body so that we can then directly relate our antiarrhythmic drugs effect on an organ as a whole.

For cardiac cells in one-dimensional tissue, Eq. (1.31), should be modified as

$$I = I_C + I_{ions} + D\frac{\delta^2 V_m}{\delta^2 x}, \tag{5.1}$$

where D is the diffusion coefficient in the $x$ direction. D can be expressed in terms of $\rho_x$, the cellular resistivity in the $x$ direction and $S_x$, the surface to volume ratio in the $x$

direction.

$$D = \frac{1}{\rho_x S_x} \tag{5.2}$$

The above equation can be modified to two-dimensional modeling by adding diffusively coupled cells in $y$ direction as follows.

$$I = I_C + I_{ions} + \frac{1}{\rho_x S_x}\frac{\delta^2 V_m}{\delta^2 x} + \frac{1}{\rho_y S_y}\frac{\delta^2 V_m}{\delta^2 y} \tag{5.3}$$

where $\rho_x$, $\rho_y$ are the cellular resistivity and $S_x$ and $S_y$ are the surface to volume ratio in the $x$ direction and $y$ direction respectively.

# Bibliography


[1] Zipes DP, Wellens HJJ. Sudden Cardiac Death. Circulation. 1998;98:2334–2351.

[2] Gaeta SA, Christini DJ. Non-linear dynamics of cardiac alternans: Subcellular to tissue-level mechanisms of arrhythmia. Frontiers in Physiology. 2012;3(157):1–13.

[3] Kogan BJ. Introduction to Computational Cardiology: Mathematical Modeling and Computer Simulation. New York: Springer; 2009.

[4] Williams V. The experimental basis for the choice of an anti-arrhythmic drug. Advances in cardiology. 1970;86:62–77.

[5] Roden DM. Antiarrhythmic drugs: from mechanisms to clinical practice. Heart. 2000;84:339–346.

[6] Huang Y, He Q, Yang M, Zhan L. Antiarrhythmia drugs for cardiac arrest:a systemic review and meta-analysis. Critical Care. 2013;17(4):R173. doi:10.1186/cc12852.

[7] Thireau J, Pasquie JL, Martel E, Le Guennec JY, Richard S. New drugs vs. old concepts: A fresh look at antiarrhythmics. Pharmacology and Therapeutics. 2011;132(2):125–145. doi:10.1016/j.pharmthera.2011.03.003.

[8] Lafuente-Lafuente C, Valembois L, Bergmann JF, Belmin J. Antiarrhythmics for maintaining sinus rhythm after cardioversion of atrial fibrillation. Cochrane Database of Systematic Reviews. 2015;3:CD005049. doi:10.1002/14651858.CD005049.pub4.

[9] Lazzara R. From first class to third class: Recent upheaval in antiarrhythmic therapy - Lessons from clinical trials. American Journal of Cardiology. 1996;78(4A):28–33. doi:10.1016/S0002-9149(96)00450-X.

[10] Katz AM. Selectivity and toxicity of antiarrhythmic drugs: Molecular interactions with ion channels. American Journal of Medicine. 1998;104(2):179–195. doi:10.1016/S0002-9343(97)00388-4.

[11] Herbette LG. Membrane Pathways for Drug Ion-Channel Interactions — Molecular-Basis for Pharmacokinetic Properties. Drug Development Research. 1994;33(3):214–224. doi:10.1002/ddr.430330305.

[12] Rekka E, Mannhold R, Bast A, Timmerman H. Molecular Pharmacological Aspects of Antiarrhythmic Activity. 1. — Class-I and Class-III Compounds and Lipid-Peroxidation. Biochemical Pharmacology. 1990;39(1):95–100. doi:10.1016/0006-2952(90)90652-2.

[13] Herbette LG, Chester DW, Rhodes DG. Structural Aanalysis of Drug Molecules in Biological Membranes. Biophysical Journal. 1986;49(1):91–94.

[14] Nattel S. Experimental evidence for proarrhythmic mechanisms of antiarrhythmic drugs. Cardiovascular Research. 1998;97:567–577.

[15] Zipes DP. Proarrhythmic effects of antiarrhythmic drugs. American Journal of Cardiology. 1987;59.

[16] Creamer JE, Nathan AW, Camm AJ. The proarrhythmic effects of antiarrhythmic drugs. American Heart Journal. 1987;114:397–406.

[17] Podrid PJ. Proarrhythmia, a serious complication of antiarrhythmic drugs. Current Cardiology Reports. 1999;1:289–296.

[18] Kidwell GA, Gonzalez MD. Effects of flecainide and D-sotalol on myocardial conduction and refractoriness: relation to antiarrhythmic and proarrhythmic drug effect. Journal of Cardiovascular Pharmacology. 1993;21:621–632.

[19] Hohnloser SH, Singh BN. Proarrhythmia with class III antiarrhythmic drugs: definition, electrophysiologic mechanisms, incidence, predisposing factors, and clinical implications. Journal of Cardiovascular Electrophysiology. 1995;6(10):920–936.

[20] Hohnloser SH, Singh BN. Proarrhythmia with class III antiarrhythmic drugs: types, risks, and management. American Journal of Cardiology. 1997;80(8A):82G–89G.

[21] Bassett AL, Chakko S, Epstein M. Are calcium antagonists proarrhythmics? Journal of Hypertension. 1997;9:915–923.

[22] Krough-Madsen T, Christini DJ. Non linear dynamics in Cardiology. Annual Review of Biomedical Engineering. 2012;14:179–203.

[23] Strogatz SH. Nonlinear Dynamics and Chaos: With Applications to Physics, Biology, Chemistry, and Engineering. Cambridge, MA: Perseus Books Publishing, LLC; 1994.

[24] Hall GM, Bahar S, Gauthier DJ. Prevalence of rate–dependent behaviors in cardiac muscle. Physical Review Letters. 1999;82(14):2995–2998.

[25] Pastore JM, Girouard SD, Laurita KR, Akar FG, Rosenbaum DS. Mechanism linking T–wave alternans to the genesis of cardiac fibrillation. Circulation. 1999;99:1385–94.

[26] Weiss J, Nivala M, Garfinkel A, Qu Z. Alternans and Arrhythmias: From Cell to Heart. Circulation Research. 2011;108:98–112.

[27] Qu Z. Controlling cardiac alternans. Heart Rhythm. 2013;10:573–574.

[28] Tolkacheva E, Schaeffer D, Gauthier D, Krassowska W. Condition for alternans and stability of the 1:1 response pattern in a 'memory' model of paced cardiac dynamics. Physical Review E. 2003;67:031904.

[29] Karma A. Electrical alternans and spiral wave breakup in cardiac tissue. Chaos. 1994;4:461–472.

[30] Watanabe M, Otani N, Gilmour R. Biphasic restitution of action potential duration and complex dynamics in ventricular myocardium. Circulation Research. 1995;76(5):915–21.

[31] Gilmour RF, Chialvo DR. Editorial: Electrical restitution, critical mass and the riddle of fibrillation. Journal of Cardiovascular Electrophysiology. 1999;10:1087–1089.

[32] Qu Z, Weiss J, Garfinkel A. Cardiac electrical restitution properties and stability of reentrant spiral waves: a simulation study. American Journal of Physiology — Heart and Circulatory Physiology. 1999;276:H269–H283.

[33] Shiferaw Y, Karma A. Turing instability mediated by voltage and calcium diffusion in paced cardiac cells. Proceedings of the National Academy of Sciences USA. 2006;103(15):5670–5.

[34] Smith JM, Clancy SM, Valeri R, Ruskin JN, Cohen RJ. Electrical alternans and cardiac electrical instability. Circulation. 1988;77:110–21.

[35] Rosenbaum DS, Jackson LE, Smith JM, Garan H, Ruskin JN, Cohen RJ. Electrical Alternans and Vulnerability to Ventricular Arrhythmias. The New England Journal of Medicine. 1994;330(4):235–241.

[36] Nolasco JW, Dahlen RW. A graphic method for the study of alternation in cardiac action potentials. Journal of Applied Physiology. 1968;25:191–6.

[37] Guevara M, Wars G, Shrier A, Glass L. Electrical alternans and period doubling bifurcations. Computers in Cardiology. 1984; p. 167.

[38] Cherry EM, Fenton FH. Suppression of alternans and conduction blocks despite APD restitution: electrotonic, memory and conduction velocity effects. American Journal of Physiology–Heart and Circulatory Physiology. 2004;286:H2332–H2341.

[39] Koller M, Riccio M, Gilmour R. Dynamic restitution of action potential duration during electrical alternans and ventricular fibrillation. American Journal of Physiology. 1998;275:H1635–1642.

[40] Kalb S, Dobrovolny HM, Tolkacheva EG, Idriss SF, Krassowska W, Gauthier DJ. The Restitution Portrait: A new method of investigating rate–dependent restitution. Journal of Cardiovascular Electrophysiology. 2004;15:698–709.

[41] Otani NF, Gilmour RF. Memory models for the electrical properties of local cardiac systems. Journal of Theoretical Biology. 1997;187:409–36.

[42] Tolkacheva EG, Anumonwa JMB, Jalife J. Action Potential Duration Restitution Portraits of Mammalian Ventricular Myocytes: Role of Calcium Current. Biophysical Journal. 2006;91:2735–2745.

[43] Garfinkel A, Kim YH, Voroshilovsky O, Qu Z, Kil JR, Lee MH, et al. Preventing ventricular fibrillation by flattening cardiac restitution. Proceedings of the National Academy of Sciences USA. 2000;97(11):6061–6.

[44] Riccio ML, Koller ML, Gilmour RF. Electrical restitution and spatiotemporal organization during ventricular fibrillation. Circulation Research. 1999;84:955–963.

[45] Courtemanche M. Electrical alternans and spiral wave breakup in cardiac tissue. Chaos. 1996;6:579–600.

[46] Gilmour RF. A novel approach to identifying antiarrhythmic drug target. Drug Discovery Today. 2003;8:162–167.

[47] Weiss JN, Garfinkel A, Karagueuzian HS, Qu Z, Chen PS. Chaos and transition to ventricular fibrillation: A new approach to antiarrhythmic drugs evaluation. Clinical Medicine Insights: Cardiology. 2016;10:2819–2826.

[48] Shattock MJ, Park KC, Yang HY, Lee AWC, Nieder S, MacLeod KT, et al. Restitution slope is principally determined by steady-state action potential duration. Cardiovascular Research. 2017;0:1–12.

[49] Banville I, Gray RA. Effect of action potential duration and conduction velocity restitution and their spatial dispersion on alternans and the stability of arrhythmias. Journal of Cardiovascular Electrocardiology. 2002;13:1141–1149.

[50] Gilmour RF, Otani NF, Watanabe MA. Memory and complex dynamics in cardiac Purkinje fibers. American Journal of Physiology. 1997;272:H1826–H1832.

[51] Boyett R, Jewell BR. Analysis of the Effects of Changes in Rate and Rhythm Upon Electrical-Activity in the Heart. Progress in Biophysics and Molecular Biology. 1980;36:1–52.

[52] Elharrar V, Surawicz B. Cycle Length Effects on Restitution of Action Potential Duration in Dog Cardiac Fibers. American Journal of Physiology. 1983;244:H782–H792.

[53] Cherry EM, Fenton FH. A tale of two dogs: analyzing two models of canine ventricular electrophysiology. American Journal of Physiology–Heart and Circulatory Physiology. 2007;292:H43–H55.

[54] Fenton FH, Evans HMHSJ. Memory in an Excitable Medium: A Mechanism for Spiral Wave Breakup in the Low Excitability limit. Physical Review Letters. 1999;83:3964–3967.

[55] Anyukhovsky EP, Rosen MR. Electrophysiologic Effects of Alprafenone on Canine Cardiac Tissue. Journal of Cardiovascular Pharmacology. 1994;24(3):411–419. doi:10.1097/00005344-199409000-00009.

[56] Wyse KR, Ye V, Campbell TJ. Action-Potential Prolongation Exhibits Simple Dose-Dependence for Sotalol, but Reverse Dose-Dependence for Quinidine and Disopyramide — Implications for Proarrhythmia due to Triggered Activity. Journal of Cardiovascular Pharmacology. 1993;21(2):316–322.

[57] Yang XS, Yu TW, Kesteloot H. Clinical and Electrophysiologic Studies of R61748 (Transcainide) — a new Class Ic Antiarrhythmic Drug. Acta Cardiologica. 1992;47(1):43–56.

[58] Campbell TJ, Wyse KR, Pallandi R. Differential effects on action potential duration of class Ia, b and c antiarrhythmic drugs: modulation by stimulation rate and extracellular $K^+$ concentration. Clinical and Experimental Pharmacology and Physiology. 1991;18:533–541.

[59] Gibson JK, Yue Y, Bronson J, Palmer C, Numann R. Human stem cell-derived cardiomyocytes detect drug-mediated changes in action potentials and ion currents. Journal of Pharmacological and Toxicological Methods. 2014;70(3):255–267. doi:10.1016/j.vascn.2014.09.005.

[60] Sager PT, Behboodikhah M. Frequency-Dependent Electrophysiologic Effects of d,l-Sotalol and Quinidine and Modulation by Beta-Adrenergic Stimulation. Journal of Cardiovascular Pharmacology. 1995;25(6):1006–1011. doi:10.1097/00005344-199506000-00022.

[61] Sosunov EA, Anyukhovsky EP, Rosen MR. Effects of Quinidine on Repolarization in Canine Epicardium, Midmyocardium, and Endocardium. Circulation. 1997;96:4011–4018. doi:10.1161/01.CIR.96.11.4011.

[62] Noguchi K, Kase J, Saitoh M, Masumiya H, Saitoh M, Nakazawa T, et al. Effects of HNS-32, a Novel Antiarrhythmic Agent, on Guinea-Pig Myocardium. Pharmacology. 2002;64(1):36–42.

[63] Orth PMR, Hesketh JC, Mak CKH, Yang Y, Lin S, Beatch GN, et al. RSD1235 blocks late $I_{Na}$ and suppresses early afterdepolarizations and *torsades de pointes* induced by class III agents. Cardiovascular Research. 2006;70:486–496. doi:10.1016/j.cardiores.2006.01.026.

[64] Fukuda K, Watanabe J, Yagi T, Wakayama Y, Nakano M, Kondo M, et al. A Sodium Channel Blocker, Pilsicainide, Produces Atrial Post-Repolarization Refractoriness through the Reduction of Sodium Channel Availability. Tohoku Journal of Experimental Medicine. 2011;225(1):35–42. doi:10.1620/tjem.225.35.

[65] Duff HJ, Sheldon RS, Cannon NJ. Tetrodotoxin: Sodium channel specific antiarrhythmic activity. Cardiovascular Research. 1988;22:800–807.

[66] Takacs J, Iost N, Lengyel C, Virag L, Nesic M, Varro A, et al. Multiple cellular electrophysiological effects of azimilide in canine cardiac preparations. European Journal of Pharmacology. 2003;470(3):163–170. doi:10.1016/S0014-2999(03)01792-8.

[67] Qi XQ, Newman D, Dorian P. The class III effect of azimilide is not associated with reverse use-dependence in open-chest dogs. Journal of Cardiovascular Pharmacology. 1999;34(6):898–903. doi:10.1097/00005344-199912000-00019.

[68] Gintant GA. Azimilide Causes Reverse Rate-Dependent Block While Reducing Both Components of Delayed-Rectifier Current in Canine Ventricular Myocytes. Journal of Cardiovascular Pharmacology. 1998;31(6):945–953.

[69] Beatch GN, Davis DR, Laganiere S, Williams BA. Rate-dependent effects of sematilide on ventricular monophasic action potential duration and delayed rectifier $K^+$ current in rabbits. Journal of Cardiovascular Pharmacology. 1996;28(5):618–630. doi:10.1097/00005344-199611000-00003.

[70] Kodama I, Kamiya K, Toyama J. Cellular electropharmacology of amiodarone. Cardiovascular Research. 1997;35:13–29.

[71] Jurkiewicz NK, Sanguinetti MC. Rate-dependent prolongation of cardiac action potentials by a methanesulfonanilide class III antiarrhythmic agent. Specific block of rapidly activating delayed rectifier $K^+$ current by dofetilide. Circulation Research. 1993;72(1):75–83. doi:10.1161/01.RES.72.1.75.

[72] Williams BA, Dickenson DR, Beatch GN. Kinetics of rate-dependent shortening of action potential duration in guinea-pig ventricle; effects of $I_{K1}$ and $I_{Kr}$ blockade. British Journal of Pharmacology. 1999;126:1426–1436.

[73] Pickoff AS, Stolfi A. Comparison of the rate dependent effects of dofetilide and ibutilide in the newborn heart. PACE. 2001;24:816–823.

[74] Wang ZG, Fermini B, Nattel S. Mechanism of Flecainides Rate-Dependent Actions on Action-Potential Duration in Canine Atrial Tissue. Journal of Pharmacology and Experimental Therapeutics. 1993;267(2):575–581.

[75] Fermini B, Jurkiewicz NK, Jow B, Guinosso PJ, Baskin EP, Lynch JJ, et al. Use-Dependent Effects of the Class-III Antiarrhythmic Agent NE-10064 (azimilide) on Cardiac Repolarization — Block of Delayed Rectifier Potassium and L-Type Calcium Currents. Journal of Cardiovascular Pharmacology. 1995;26(2):259–271. doi:10.1097/00005344-199508000-00012.

[76] Chiang CE, Luk HN, Wang TM, Ding PYA. Effects of sildenafil on cardiac repolarization. Cardiovascular Research. 2002;255:290–299.

[77] Banyasz T, Horvath B, Virag L, Barandi L, Szentandrassy N, Harmati G, et al. Reverse rate dependency is an intrinsic property of canine cardiac preparations. Cardiovascular Research. 2009;84:237–244.

[78] Bányász T, Bárándi L, Harmati G, Virág L, Szentandrássy N, Márton I, et al. Mechanism of Reverse Rate-Dependent Action of Cardioactive Agents. Current Medicinal Chemistry. 2011;18:3597–3606.

[79] Marschang H, Beyer T, Karolyi L, Kubler W, Brachmann J. Differential rate and potassium dependent effects of class III agents d-sotalol and dofetilide on guinea pig papillary muscle. Cardiovascular Drugs and Therapy. 1998;12(6):573–583. doi:10.1023/A:1007743521932.

[80] Bárándi L, Virág L, Jost N, Horváth Z, Koncz I, Papp R, et al. Reverse rate-dependent changes are determined by baseline action potential duration in mammalian and human ventricular preparations. Basic Research in Cardiology. 2010;105:315–323. doi:10.1007/s00395-009-0082-7.

[81] Koller M, Riccio M, Gilmour R. Effects of $[K^+]_o$ on electrical restitution and spatiotemporal organization during ventricular fibrillation. American Journal of Physiology. 2000;279:H2665–2672.

[82] Trenor B, Gomis-Tena J, Cardona K, Romero L, Rajamani S, Belardinelli L, et al. In silico assessment of drug safety in human heart applied to late sodium current blockers. Channels. 2013;7(4):249–262. doi:10.4161/chan.24905.

[83] Mirams GR, Cui Y, Sher A, Fink M, Cooper J, Heath BM, et al. Simulation of multiple ion channel block provides improved early prediction of compounds clinical torsadogenic risk. Cardiovascular Research. 2011;91:53–61. doi:10.1093/cvr/cvr044.

[84] Chay TR. Proarrhythmic and antiarrhythmic actions of ion channel blockers on arrhythmias in the heart: Model study. American Journal of Physiology–Heart and Circulatory Physiology. 1996;271(1):H329–H356.

[85] Chay TR. Why are some antiarrhythmic drugs proarrhythmic? Cardiac arrhythmia study by bifurcation analysis. Journal of Electrocardiology. 1995;28(S):191–197. doi:10.1016/S0022-0736(95)80055-7.

[86] Tsumoto K, Ashihara T, Haraguchi R, Nakazawa K, Kurachi Y. Ischemia-Related Subcellular Redistribution of Sodium Channels Enhances the Proarrhythmic Effect of Class I Antiarrhythmic Drugs: A Simulation Study. Plos One. 2014;9(10):e109271. doi:10.1371/journal.pone.0109271.

[87] Xia H, Zhao X, Bains J, Wortham DC. Influence of Channel Blockers on Cardiac Alternans. In: Proceedings of the 31st Annual International Conference of the IEEE EMBS; 2009. p. 2823–2826.

[88] Trénor B, José M Ferrero J, Rodríguez B, Montilla F. Effects of Pinacidil on Reentrant Arrhythmias Generated During Acute Regional Ischemia: A Simulation Study. Annals of Biomedical Engineering. 2005;33(7):897–906. doi:10.1007/s10439-005-3554-4.

[89] Courtemanche M, Ramirez RJ, Nattel S. Ionic targets for drug therapy and atrial fibrillation-induced electrical remodeling: insights from a mathematical model. Cardiovascular Research. 1999;42(2):477–489. doi:10.1016/S0008-6363(99)00034-6.

[90] Paci M, Hyttinen J, Rodriguez B, Severi S. Human induced pluripotent stem cell-derived versus adult cardiomyocytes: an in silico electrophysiological study on effects of ionic current block. British Journal of Pharmacology. 2015;172(21):5147–5160. doi:10.1111/bph.13282.

[91] O'Hara T, Virag L, Varro A, Rudy Y. Simulation of the Undiseased Human Cardiac Ventricular Action Potential: Model Formulation and Experimental Validation. PLOS Computational Biology. 2011;7:e1002061.

[92] Brennan T, Fink M, Rodriguez B. Multiscale modeling of drug-induced effects on cardiac electrophysiological activity. European Journal of Pharmaceutical Sciences. 2009;36(1):62–77. doi:10.1016/j.ejps.2008.09.013.

[93] Brennan TP, Stokeley D, Fink M, Rodriguez B, Tarassenko L. Modelling Effects of Sotalol on T-wave Morphology. Computer Cardiology. 1998;34:249–252.

[94] ten Tusscher KH, Panfilov AV. Alternans and spiral breakup in human ventricular tissue model. American Journal of Physiology-Heart and Circulatory Physiology. 2006;286:1573–1589.

[95] Huikuri HV, Yli-Mayry. Frequency dependent effects of d-sotalol and amiodarone on the action potential duration of the human right ventricle. Pacing and Clinical Electrophysiology. 1992;15:2103–2107.

[96] Bernus O, Wilder R, Zemlin CW, Verschelde H, Panfilov AV. A computationally efficient electrophysiological model of human ventricular cells. American Journal of Physiology-Heart and Circulatory Physiology. 2002;282:2296–2308.

[97] Fox JJ, McHarg JL, Gilmour RF. Ionic mechanism of electrical alternans. American Journal of Physiology – Heart and Circulatory Physiology. 2002;282:H516–H530.

[98] Hodgkin AL, Huxley AF. A quantitative description of membrane current and its application to conduction and excitation in nerve. The Journal of Physiology. 1952;117:500–544.

[99] Noble D. A modification of the Hodgkin–Huxley equations applicable to Purkinje fibre action and pace-maker potentials. The Journal of Physiology. 1962;160:317–352.

[100] Beeler GW, Reuter H. Reconstruction of the action potential of ventricular myocardial fibers. Journal of Physiology. 1977;268:177–210.

[101] Luo CH, Rudy Y. A model of the ventricular Cardiac action potential. Depolarization, Repolarization, and Their Interaction. Circulation Research. 1991;68(6):1501–1526.

[102] Luo CH, Rudy Y. A dynamic model of the cardiac ventricular action potential. I. Simulations of ionic currents and concentration changes. Circulation Research. 1994;74(6):1071–1096.

[103] Priebe L, Beuckelmann DJ. Simulation study of cellular electric properties in heart failure. Circulation Research. 1998;82:1206–1223.

[104] Winslow RL, Rice J, Jafri S, Marban E, O'Rourke B. Mechanisms of altered excitation-contraction coupling in canine tachycardia-induced heart failure, II: model studies. Circulation Research. 1999;84:571–586.

[105] Chudlin E, Goldhaber J, Weiss J, Kogan B. Intracellular $K^+$ dynamics and the stability of ventricular tachycardia. Biophysics Journal. 1999;77:2930–2941.

[106] Freeman LC, Pacioretty LM, Moss NSKRS, Gilmour RF. Decreased density of $I_{to}$ in the left ventricular myocytes from German shepherd dogs with inherited arrhythmias. Journal of Cardiovascular Electrophysiology. 1997;8:872–883.

[107] Rasmusson RL, Clark JW, Clark WR, Shibata EF, Campbell DL. A mathematical model of electrophysiological activity in a bullfrog atrial cell. American Journal of Physiology — Heart and Circulatory Physiology. 1990;259.

[108] ten Tusscher KH, Noble D, Noble PJ, Panfilov AV. A model for human ventricular tissue. American Journal of Physiology-Heart and Circulatory Physiology. 2004;291:H1088–H1100.

[109] Iyer V, Mazhari R, Windslow RL. Simulation study of cellular electric properties in heart failure. Biophysics Journal. 2004;87:1507–1525.

[110] Wilhelms M, Hettmann H, Maleckar MM, Koivumâki JT, Dössel O, Seemann G. Benchmarking electrophysiological models of human atrial myocytes. Frontiers in Physiology. 2013;3:487. doi:10.3389/fphys.2012.00487.

[111] Livshitz L, Rudy Y. Uniqueness and Stability of Action Potential Models during Rest, Pacing, and Conduction Using Problem-Solving Environment. Biophysical Journal. 2009;97(5):1265–1276. doi:10.1016/j.bpj.2009.05.062.

[112] Lombardo DM, Fenton FH, Narayan SM, Rappel WJ. Comparison of Detailed and Simplified Models of Human Atrial Myocytes to Recapitulate Patient Specific Properties. PLoS Computational Biology. 2016;12(8):e1005060. doi:10.1371/journal.pcbi.1005060.

[113] Zicha S, Tduji Y, Shirishita-Takeshita A, Nattel S. Beta-blockers as antiarrhythmic agents. Handbook of Experimental Pharmacology. 1998;171:235–266.

[114] Klabunde RE. Cardiovascular Physiological Concepts. Philadelphia: Lippincott Williams & Wilkins; 2011.

[115] Ting N, editor. Dose Finding in Drug Development. New York: Springer Sciences; 2006.

[116] Carmliet E, Mubagwa K. Antiarrhythmic drugs and cardiac ion channels: mechanisms of action. Progress in Biophysics and Molecular Biology. 1998;70:1–72.

[117] Melichercik J, Brachmann J, Schöls W, Hilbel T, Beyer T, Kübler W. Rate and Time Dependent Effects of D-Sotalol on the Monophasic Action Potential After Sudden increase of the Heart Rate. Pacing and Clinical Electrophysiology. 1999;22:65–72.

[118] Weirich J, Antoni H. Rate-dependence of antiarrhythmic and proarrhythmic properties of class I and class III antiarrhythmic drugs. Basic Research in Cardiology. 1998;93:1–15.

[119] Narayan S. T–wave alternans and the susceptibility to ventricular arrhythmias. Journal of the American College of Cardiology. 2006;47:269–281.

[120] Oliver RA, Hall GM, Bahar S, Krassowska W, Wolf PD, Dixon-Tulloch EG, et al. Existence of bistability and correlation with arrhythmogenesis in paced sheep atria. Journal of Cardiovascular Electrophysiology. 2000;11(7):797–805. doi:10.1111/j.1540-8167.2000.tb00051.x.

[121] Oliver RA, Henriquez CS, Krassowska W. Bistability and correlation with arrhythmogenesis in a model of the right atrium. Annals of Biomedical Engineering. 2005;33:577–589.

[122] Dobrovolny H. Spatial variation of cardiac restitution and the onset of alternans. Duke University, Durham, NC; 2008.

[123] Diaz ME, O'Neill CS, Eisner DA. Sarcoplasmic Reticulum Calcium Content Fluctuation Is the Key to Cardiac Alternans. Circulation Research. 2004;94:650–656.

[124] Llach A, Molins CE, Fernandes J, Padró J, Cinca J, Hove-Madsen L. Sarcoplasmic reticulum and L-type Ca2+ channel activity regulate the beat-to-beat stability of calcium handling in human atrial myocytes. Journal of Physiology. 2011;589:3247–3262.

[125] Weinberg SH. Impaired Sarcoplasmic Reticulum Calcium Uptake and Release Promote Electromechanically and Spatially Discordant Alternans: A Computational Study. Circulation. 1999;99:2819–2826.

[126] Peralta AO, John RM, Gaasch WH, Taggert PI, Martin DT, Venditti FJ. The class III antiarrhythmic effect of sotalol exerts a reverse use-dependent positive inotropic effect in the intact canine heart. Journal of the American College of Cardiology. 2000;36(4):1404–1410.

[127] Niederer SA, Fink M, Noble D, Smith NP. A meta-analysis of cardiac electrophysiology computational models. Experimental Physiology. 2009;94(5):486–495. doi:10.1113/expphysiol.2008.044610.

[128] Pankusci C, Banyasz T, Magyar J, Gyonos I, Kovacs A, Varro A, et al. Electrophysiological effects of EGIS-7229, a new antiarrhythmic agent, in isolated mammalian and human cardiac tissues. Naunyn-Schmiedeberg's Archive of Pharmacology. 1997;355:398–405.

[129] Lu HR, Vlaminckx E, Teisman A, Gallacher DJ. Choice of cardiac tissue plays an important role in the evaluation of drug-induced prolongation of the QT interval in vitro in rabbit. Journal of Pharmacological and Toxicological Methods. 2005;52(1):90–105. doi:10.1016/j.vascn.2005.04.007.

[130] Jacobson I, Duker G, Florentzson M, Linhardt G, Lindhardt E, Nordkam AK, et al. Experimental Study Electrophysiological Characterization and Antiarrhythmic Efficacy of the Mixed Potassium Channel-Blocking Antiarrhythmic Agent AZ13395438 In Vitro and In Vivo. Journal of Cardiovascular Pharmacology and Therapeutics. 2013;1(3):290–300. doi:0.1177/1074248412470512.

[131] Dai DZ, Yu F, Li HT, qun Tang Y, An LF, Huang WL, et al. Blockade on Sodium, Potassium, and Calcium Channels by a New Antiarrhythmic Agent CPU 86017. Drug Development Research. 1996;39:138–146.

[132] Su MJ, Chang GJ, Wu MH, Kuo SC. Electrophysiological basis for the antiarrhythmic action and positive inotropy of HA-7, a furoquinoline alkaloid derivative, in rat heart. British Journal of Pharmacology. 1997;122:1285–1298.

[133] Bai DL, Chen WZ, Bo YX, Dong YL, Kang AL, Sun WK, et al. Discovery of N-(3,5-bis(1-pyrrolidylmethyl)-4-hydroxy-benzyl)-4-methoxybenzenesulfamide (sulcardine) as a novel anti-arrhythmic agent. Acta Pharmacologica Sinica. 2012;33:1176–1186. doi:10.1038/aps.2012.119.

[134] Anyukhovsky EP, Sosunov EA, Rosen MR. Regional Differences in Electrophysiological Properties of Epicardium, Midmyocardium, and Endocardium. Circulation. 1996;94:1981–1988.

[135] Lukas A. Electrophysiology of Myocardial Cells in the Epicardial, Midmyocardial, and Endocardial Layers of the Ventricle. Journal of Cardiovascular Pharmacology and Therapeutics. 1997;2(1):61–72.

[136] Liu DW, Gintant GA, Antzelevitch C. Ionic bases for electrophysiological distinctions among epicardial, midmyocardial, and endocardial myocytes from the free wall of the canine left ventricle. Circulation Research. 1993;72(3):671–687.

[137] Elshrif MM, Cherry EM. A Quantitative Comparison of the Behavior of Human Ventricular Cardiac Electrophysiology Models in Tissue. PLoS ONE. 2013;9:e84401.

[138] Baláti B, Varró A, Papp JG. Comparison of the cellular electrophysiologicalcharacteristics of canine left ventricular epicardium, M cells, endocardium and Purkinje fibres. Acta Physiologica Scandinavica. 1998;164:181–190.

[139] Cooper J, Corrias A, Gavaghan D, Noble D. Considerations for the use of cellular electrophysiology models within cardiac tissue simulations. Progress in Biophysics and Molecular Biology. 2011;107(1):74–80. doi:10.1016/j.pbiomolbio.2011.06.002.

[140] Clayton RH, Bernus O, Cherry EM, Dierckx H, Fenton FH, Mirabella L, et al. Models of cardiac tissue electrophysiology: Progress, challenges and open questions. Progress in Biophysics and Molecular Biology. 2011;104(1–3):22–48. doi:10.1016/j.pbiomolbio.2010.05.008.

[141] Almotrefi AA, Bukhari IA, Alhumayyd MS. Investigation of the antifibrillatory drug interactions between Amiodarone and Ibutilide in isolated, perfused Rabbit hearts. Fundamental & Clinical Pharmacology. 2015;29(6):553–557. doi:10.1111/fcp.12141.

[142] Varró A, Lathrop DA. Sotalol and mexiletine: Combination of rate-dependent electrophysiological effects. Journal of Cardiovascular Pharmacology. 1990;16(4):557–567.

[143] Jin Q, Chen X, Smith WM, Ideker RE, Huang J. Effects of procainamide and sotalol on restitution properties, dispersion of refractoriness, and ventricular fibrillation activation patterns in pigs. Journal of Cardiovascular Pharmacology. 2008;19(10):1090–1097. doi:10.1111/j.1540-8167.2008.01200.x.

[144] Verrier RL, Pagotto VPF, Kanas AF, Sobrado MF, Nearing BD, Zeng D, et al. Low doses of ranolazine and dronedarone in combination exert potent protection against atrial fibrillation and vulnerability to ventricular arrhythmias during acute myocardial ischemia. Heart Rhythm. 2013;10(1):121–127. doi:10.1016/j.hrthm.2012.09.015.

[145] Singh BN. Augmenting Maintenance of Sinus Rhythm in the Control of Atrial Fibrillation by Antiarrhythmic Drug Combinations. Journal of Cardiovascular Pharmacology and Therapeutics. 2010;15(4):31S–35S. doi:10.1177/1074248410377617.

# Appendix A

# Model Equations-The Bernus model

The Nernst potentials are

$$E_{Na} = \frac{RT}{F} \ln \left( \frac{[Na^+]_e}{[Na^+]_i} \right) \tag{A.1}$$

$$E_{Ca} = \frac{RT}{2F} \ln \left( \frac{[Ca^{2+}]_e}{[Ca^{2+}]_i} \right) \tag{A.2}$$

$$E_{to} = \frac{RT}{F} \ln \left( \frac{0.043[Na^+]_e + [K^+]_e}{0.043[Na^+]_i + [K^+]_i} \right) \tag{A.3}$$

$$E_K = \frac{RT}{F} \ln \left( \frac{[K^+]_e}{[K^+]_i} \right) \tag{A.4}$$

where $R$ is the ideal gas constant, $T$ is the absolute temperature, $F$ is the Faraday constant. $[Na^+]_e$, $[Ca^{2+}]_e$, $[K^+]_e$ are the extracellular $Na^+$, $Ca^{2+}$, and $K^+$ ions concentration respectively, and $[Na^+]_i$, $[Ca^{2+}]_i$, $[K^+]_i$ ions are the intracellular $Na^+$, $Ca^{2+}$, and $K^+$ concentration respectively.

**Inward Currents:**
**Fast $Na^+$ current**

$$
\begin{aligned}
I_{Na} &= g_{Na} m^3 v^2 (V_m - E_{Na}) \\
m_\infty &= \frac{\alpha_m}{\alpha_m + \beta_m} \\
\alpha_m &= \frac{0.32(V_m + 47.13)}{1 - \exp[-0.1(V_m + 47.13)]} \\
\beta_m &= 0.08 \exp\left(\frac{-V_m}{11}\right) \\
\tau_m &= \frac{1.0}{\alpha_m + \beta_m} \\
v_\infty &= \frac{1}{2}[1 - \tanh(7.74 + 0.12 V_m)] \\
\tau_v &= 0.25 + 2.24 \frac{1 - \tanh(7.74 + 0.12 V_m)}{1 - \tanh[0.07(V_m + 92.4)]}
\end{aligned}
\tag{A.5}
$$

There are no $\alpha_v$ and $\beta_v$, and the gating variables $m$ and $v$ are computed from their steady state values and time constants.

**Slow $Ca^{2+}$ current**

$$I_{Ca} = g_{Ca} d_\infty f f_{Ca} (V_m - E_{Ca})$$

$$d_\infty = \frac{\alpha_d}{\alpha_d + \beta_d}$$

$$\alpha_d = \frac{14.98 \exp[-0.5 \left[\frac{V_m - 22.26}{16.68}\right]^2]}{16.68\sqrt{2\pi}}$$

$$\beta_d = 0.1471 - \frac{5.3 \exp[-0.5[(V_m - 6.27)/14.93]^2}{14.93\sqrt{2\pi}}$$

$$f_\infty = \frac{\alpha_f}{\alpha_f + \beta_f} \tag{A.6}$$

$$\alpha_f = \frac{6.87 * 10^{-3}}{1 + \exp[-(6.1546 - V_m)/6.12]}$$

$$\beta_f = \frac{0.069 \exp[-0.11(V_m + 9.825)] + 0.011}{1 + \exp[-0.278(V_m + 9.825)]} + 5.75 * 10^{-4}$$

$$f_{Ca} = \frac{1}{1 + [Ca^{2+}]_i / 0.0006}$$

$$\tau_f = \frac{1.0}{\alpha_f + \beta_f}$$

The gating variable $f$ is computed from its steady-state value and time constant, which are in turn computed from $\alpha_f$ and $\beta_f$.

**Outward Currents:**

**Transient outward current**

This current has two gating variables: the activation variable $r$ and the inactivation variable $to$.

$$
\begin{aligned}
I_{to} &= g_{to} r_{\infty} to (V_m - E_{to}) \\
r_{\infty} &= \frac{\alpha_r}{\alpha_r + \beta_r} \\
\alpha_r &= \frac{0.5266 \exp[-0.0166(V_m - 42.2912)]}{1 + \exp[-0.0943(V_m - 42.2912)]} \\
\beta_r &= \frac{5.186 * 10^{-5} V_m + 0.5149 \exp[-0.1344(V_m - 5.0027)]}{1 + \exp([-(0.1348(V_m - 5.186 * 10^{-5}])} \\
\alpha_{to} &= \frac{5.612 * 10^{-5} V_m + 0.721 \exp[-0.173(V_m + 34.2531)]}{1 + \exp[-0.1732(V + 34.2531)]} \\
\beta_{to} &= \frac{1.215 * 10^{-4} V_m + 0.0767 \exp[-1.66 * 10^{-9}(V_m + 34.0235)]}{1 + \exp[-0.1604(V_m + 34.0235)]} \\
\tau_{to}(V_m) &= \frac{1}{p\alpha_{to} + p\beta_{to}} \\
to_{\infty}(V_m) &= \frac{\alpha_{to}(V_m - V_{shift})}{\alpha_{to}(V_m - V_{shift}) + \beta_{to}(V_m - V_{shift})}
\end{aligned}
\tag{A.7}
$$

**Delayed rectifier $K^+$ current**

For endocardial and epicardial cells

$$
\begin{aligned}
I_K &= g_K X^2 (V_m - E_K) \\
X_{\infty} &= \frac{0.988}{1 + \exp(-0.861 - 0.0620 V_m)} \\
\tau_X &= 240 \exp\left[\frac{-(25.5 + V_m)^2}{156}\right] + 182[1 + \tanh(0.154 + 0.0116 V_m)] + \tau'_X \\
\tau'_X &= 40[1 - \tanh(160 + 2V_m)]
\end{aligned}
\tag{A.8}
$$

**Inward rectifier $K^+$ current**
This current has no direct time dependence and its dynamic behavior depends only on the membrane potential.

$$
\begin{aligned}
I_{K1} &= g_{K1} K1_\infty (V_m - E_K) \\
K1_\infty &= \frac{\alpha_{K1}}{\alpha_{K1} + \beta_{K1}} \\
\alpha_{K1} &= \frac{0.1}{1 + \exp[0.06(V_m - E_K - 200)]} \\
\beta_{K1} &= \frac{3\exp[2 * 10^{-4}(V_m - E_K + 100)] + \exp[0.1(V_m - E_K - 10)]}{1 + \exp[-0.5(V_m - E_K)]}
\end{aligned}
\tag{A.9}
$$

**Background Currents:**
**$Na^+$ background current**

$$
I_{Na,b} = g_{Na,b}(V_m - E_{Na}) \tag{A.10}
$$

**$Ca^{2+}$ background current**

$$
I_{Ca,b} = g_{Ca,b}(V_m - E_{Ca}) \tag{A.11}
$$

**Pump and Exchanger Currents:**
**$Na^+$-$K^+$ pump**
This curent involves two factors, one depending on $V_m$, the other on the ion concentrations.

$$
\begin{aligned}
I_{NaK} &= g_{NaK} f_{NaK} f'_{NaK} \\
f_{NaK} &= \frac{1}{1 + 0.1245\exp(-0.0037V_m) + 0.0365\sigma\exp(-0.037V_m)} \\
f'_{NaK} &= \frac{1}{1 + \left(\frac{10}{[Na^+]_i)^{1.5}}\right)} \left(\frac{[K^+]_e}{[K^+]_e + 1.5}\right) \\
\sigma &= \frac{1}{7}[\exp\left(\frac{[Na^+]_e}{67.3} - 1\right)
\end{aligned}
\tag{A.12}
$$

**$Na^+/Ca^{2+}$ exchanger**

$$
\begin{aligned}
I_{NaCa} &= g_{NaCa} f_{NaCa} \\
f_{NaCa} &= \frac{([Na^+]_i^3[Ca^{2+}]_e \exp(0.013V_m) - ([Na^+]_e^3[Ca^{2+}]_e \exp(0.024V_m)}{(87.5^3 + [Na^+]_e^3)(1.38 + [Ca^{2+}]_i)[1 + 0.1\exp(-0.024V_m)]}
\end{aligned}
\tag{A.13}
$$

Table A.1: Intracellular and extracellular ion concentrations for the Bernus model.

| **Ions** | **Concentrations**(mM) |
|---|---|
| $[Ca^{2+}]_i$ | 0.0004 |
| $[Ca^{2+}]_e$ | 4 |
| $[Na^+]_i$ | 10 |
| $[Na^+]_e$ | 138 |
| $[K^+]_i$ | 140 |
| $[K^+]_e$ | 4 |

Table A.2: Conductances of currents in the Bernus model.

| **Conductances** | nS/pF |
|---|---|
| $g_{Na}$ | 16.0 |
| $g_{Ca}$ | 0.064 |
| $g_{to}$ | 0.4 |
| $g_{K}$ | 0.019 |
| $g_{K1}$ | 3.9 |
| $g_{Na,b}$ | 0.00085 |
| $g_{Ca,b}$ | 0.001 |
| $g_{NaK}$ | 1.3 |
| $g_{NaCa}$ | 1000.0 |

## A.1 Glossary

| | |
|---|---|
| $m$ | $I_{Na}$ activation gate |
| $v$ | $I_{Ca}$ inactivation gate |
| $\alpha_m$ | Voltage-dependent $m$ gate parameter for $I_{Ca}$ |
| $\beta_m$ | Voltage-dependent $m$ gate parameter for $I_{Ca}$ |
| $v_\infty$ | Steady-state $I_{Na}$ activation |
| $\tau_m$ | $I_{Na}$ activation time constant |
| $\tau_v$ | $I_{Na}$ inactivation time constant |
| $\alpha_d$ | Voltage-dependent activation $d$ parameter for $I_{Ca}$ |
| $\beta_d$ | Voltage-dependent activation $d$ parameter for $I_{Ca}$ |
| $\alpha_f$ | Voltage-dependent inactivation $f$ gate parameter for $I_{Ca}$ |
| $\beta_f$ | Voltage-dependent inactivation $f$ gate parameter for $I_{Ca}$ |
| $f_{Ca}$ | $Ca^{2+}$-dependent $I_{Ca}$ inactivation parameter |
| $\tau_f$ | $Ca^{2+}$-dependent $I_{Ca}$ inactivation time constant |
| $\alpha_r$ | Voltage-dependent fast activation $r$ parameter |
| $\beta_r$ | Voltage-dependent fast activation $r$ parameter |
| $\alpha_{to}$ | Voltage-dependent inactivation $to$ gate parameter for $I_{to}$ |
| $\beta_{to}$ | Voltage-dependent inactivation $to$ gate parameter for $I_{to}$ |
| $\tau_{to}$ | $I_{to}$ inactivation time constant |

| | |
|---|---|
| $X$ | $I_K$ activation gate |
| $\tau_X$ | $I_K$ activation time constant |
| $\tau_X^{'}$ | $I_K$ activation time constant |
| $\alpha_{K1}$ | Voltage-dependent activation $K1$ gate parameter |
| $\beta_{K1}$ | Voltage-dependent activation $K1$ gate parameter |
| $\sigma$ | Extracellular $Na^+$ $I_{NaK}$ factor |
| $[Na^+]_i$ | Intracellular $Na^+$ concentration |
| $[Na^+]_e$ | Extracellular $Na^+$ concentration |
| $[K^+]_i$ | Intracellular $K^+$ concentration |
| $[K^+]_e$ | Extracellular $K^+$ concentration |
| $[Ca^{2+}]_i$ | Intracellular $Ca^{2+}$ concentration |
| $[Ca^{2+}]_e$ | Extracellular $Ca^{2+}$ concentration |
| $d_\infty$ | Steady-state $I_{Ca}$ activation |
| $E_{Ca}$ | $Ca^{2+}$ equilibrium potential |
| $E_K$ | $K^+$ equilibrium potential |
| $E_{Na}$ | $Na^+$ equilibrium potential |

| | |
|---|---|
| $f$ | $I_{Ca}$ inactivation gate |
| $f_\infty$ | Steady-state $I_{Ca}$ inactivation |
| $f_{NaK}$ | Voltage-dependent $I_{NaK}$ factor |
| $g_{Na}$ | Peak $I_{Na}$ conductance |
| $g_K$ | Peak $I_K$ conductance |
| $g_{Ca}$ | Peak $I_{Cab}$ conductance |
| $g_{K1}$ | Peak $I_{K1}$ conductance |
| $g_{to}$ | Peak $I_{to}$ conductance |
| $g_{NaK}$ | Peak $I_{Nab}$ conductance |
| $g_{Nab}$ | Peak $I_{Nab}$ conductance |
| $g_{Cab}$ | Peak $I_{Cab}$ conductance |
| $d_{NaK}$ | Peak $I_{Nab}$ conductance |
| $f'_{NaK}$ | Peak $I_{Nab}$ conductance |
| $I_{Na}$ | $Na^+$ current |
| $I_K$ | Inward rectifier $K^+$ current |
| $I_{Ca}$ | $Ca^{2+}$ current |
| $I_{K1}$ | Inward rectifier $K^+$ current |
| $I_{to}$ | Transient outward $K^+$ current |

| | |
|---|---|
| $I_{Nab}$ | $Na^+$ background current |
| $I_{Cab}$ | $Ca^+$ background current |
| $I_{NaCa}$ | $Na^+/Ca^{2+}$ exchange current |
| $I_{NaK}$ | $Na^+$-$K^+$ pump current |
| $I_{stim}$ | Stimulus current |
| $F$ | Faraday constant |
| $R$ | Ideal gas constant |
| $T$ | Temperature |
| $V_m$ | Membrane Voltage |

# Appendix B

# Model Equations-The Fox model

The Nernst potentials are

$$E_{Na} = \frac{RT}{F} \ln \left( \frac{[Na^+]_e}{[Na^+]_i} \right) \tag{B.1}$$

$$E_{Ca} = \frac{RT}{2F} \ln \left( \frac{[Ca^{2+}]_e}{[Ca^{2+}]_i} \right) \tag{B.2}$$

$$E_K = \frac{RT}{F} \ln \left( \frac{[K^+]_e}{[K^+]_i} \right) \tag{B.3}$$

$$E_{Ks} = \frac{RT}{F} \ln \left( \frac{[K^+]_e + 0.01833[Na^+]_e}{[K^+]_i + 0.01833[Na^+]_i} \right) \tag{B.4}$$

where $R$ is the ideal gas constant, $T$ is the absolute temperature, $F$ is the Faraday constant. $[Na^+]_e$, $[Ca^{2+}]_e$, $[K^+]_e$ are the extracellular $Na^+$, $Ca^{2+}$, and $K^+$ ions concentration respectively, and $[Na^+]_i$, $[Ca^{2+}]_i$, $[K^+]_i$ are the intracellular $Na^+$, $Ca^{2+}$, and $K^+$ ions concentration respectively.

**Fast $Na^+$ current**

$$
\begin{aligned}
I_{Na} &= g_{Na} m^3 h j (V_m - E_{Na}) & \alpha_m &= \frac{0.32(V_m + 47.13)}{1 - \exp[-0.1(V_m + 47.13)]} \\
\frac{dm}{dt} &= \alpha_m(1 - m) - \beta_m & \beta_m &= 0.08 \exp\left(\frac{-V_m}{11}\right) \\
\frac{dh}{dt} &= \alpha_h(1 - m) - \beta_h & \alpha_h &= 0.135 \exp(V_m + 80)/ - 6.8 \\
\frac{dj}{dt} &= \alpha_j(1 - m) - \beta_j & \beta_h &= \frac{7.5}{1 + \exp[-0.1(V_m + 11)]} \\
& & \alpha_j &= \frac{0.175 \exp(V_m + 100)/ - 2.3}{1 + \exp[-0.15(V_m + 79)]} \\
& & \beta_j &= \frac{0.3}{1 + \exp[-0.1(V_m + 32)]}
\end{aligned}
\tag{B.5}
$$

**Transient outward current**

This current has two gating variables: the activation variable $r$ and the inactivation variable $to$.

$$
\begin{aligned}
I_{to} &= g_{to} X_{to} Y_{to} (V_m - E_{to}) & \alpha_{X_{to}} &= 0.04516 \exp[-0.03577 V_m] \\
& & \beta_{X_{to}} &= 0.0989 \exp[-0.06237 V_m] \\
\frac{dX_{to}}{dt} &= \alpha_{X_{to}}(1 - X_{to}) - \beta_{X_{to}} X_{to} & \alpha_{Y_{to}} &= \frac{0.005415 \exp[-0.173(V_m + 33.5)/ - 5]}{1 + 0.051335 \exp[V_m + 33.5)/ - 5]} \\
\frac{dY_{to}}{dt} &= \alpha_{Y_{to}}(1 - Y_{to}) - \beta_{Y_{to}} Y_{to} & \beta_{Y_{to}} &= \frac{0.005415 \exp[-0.173(V_m + 33.5)/5]}{1 + 0.051335 \exp[V_m + 33.5)/5]}
\end{aligned}
\tag{B.6}
$$

**Inward rectifier $K^+$ current**

This curent has no direct time dependence and its dynamic behavior depends only

on the membrane potential.

$$I_{K1} = g_{K1} K1_\infty \frac{[K^+]_e}{[K^+]_e + K_{mK1}} (V_m - E_K)$$
$$K1_\infty = \frac{1}{2 + \exp[1.62F/(RT)(V_m - E_K)]} \tag{B.7}$$

**Rapid component of the delayed rectifier $K^+$ current**

$$I_{Kr} = g_{Kr} R(V) X_{Kr} \sqrt{\frac{[K^+]_e}{4}} (V_m - E_K)$$

$$\frac{dX_{Kr}}{dt} = \frac{X_{Kr}^\infty - X_{Kr}}{\tau_{Kr}}$$

$$\tau_{Kr} = 43 + \frac{1}{\exp[-5.495 + 0.1691 V_m] + \exp[-7.677 - 0.0128 V_m]} \tag{B.8}$$

$$R(V) = \frac{1}{1 + \exp[2.182 - 0.1819 V_m]}$$

$$X_{Kr}^\infty = \frac{1}{1 + 2.5 \exp[0.1(V_m + 28)]}$$

**Slow component of the delayed rectifier $K^+$ current**

$$I_{Ks} = g_{Ks} X_{Ks}^2 (V_m - E_K)$$

$$\frac{dX_{Ks}}{dt} = \frac{X_{Ks}^\infty - X_{Ks}}{\tau_{Ks}}$$

$$\tau_{Ks} = \frac{1}{\frac{0.0000719(V_m - 10)}{1 - \exp[-0.148(V_m - 10)]} + \frac{0.0000719(V_m - 10)}{\exp[-0.148(V_m - 10) - 1]}} \tag{B.9}$$

$$X_{Ks}^\infty = \frac{1}{1 + 2.5 \exp[(V_m - 16)/-13.6]}$$

**Plateau $K^+$ current**

$$I_{Kp} = g_{Kp} K_{Kp} (V_m - E_K)$$
$$K_{Kp} = \frac{1}{1 + \exp[(7.488 - V_m)/5.98]} \tag{B.10}$$

**Pump and Exchanger Currents:**
**$Na^+$-$K^+$ pump current**

$$I_{NaK} = \bar{I}_{NaK} f_{NaK} \frac{1}{1 + \left(\frac{K_{mNai}}{[Na^+]_i}\right)^{1.5}} \frac{[K^+]_e}{[K^+]_e + K_{mKo}}$$
$$f_{NaK} = \frac{1}{1 + 0.1245 \exp[-0.1 V_m F/(RT)] + 0.365\sigma \exp[-V_m F/(RT)]} \tag{B.11}$$
$$\sigma = 1/7(\exp \frac{[Na^+]_e}{67.3} - 1)$$

**Sarcolemmal pump current**

$$I_{pCa} = \bar{i}_{pCa} \frac{[Ca^{2+}]_i}{K_{mpCa} + [Ca^{2+}]_i} \tag{B.12}$$

**$Na^+$-$Ca^{2+}$ exchange current**

$$I_{NaCa} = \frac{k_{NaCa}}{K^3{}_{mNa} + [Na^+]_e^3} \frac{1}{K_{mCa} + [Ca_e^{2+}} \frac{1}{1 + k_{sat} \exp(V_m F(\eta - 1)/(RT))} \tag{B.13}$$
$$\times [\exp(V_m F \eta/(RT))[Na^+]_i^3 [Ca^{2+}]_e - \exp(V_m F(\eta - 1)/(RT))[Na^+]_e^3 [Ca^{2+}]_i]$$

**Background Currents:**

**$Na^+$ background current**

$$I_{Na,b} = g_{Na,b}(V_m - E_{Na}) \tag{B.14}$$

**$Ca^{2+}$ background current**

$$I_{Ca,b} = g_{Ca,b}(V_m - E_{Ca}) \tag{B.15}$$

**L-type $Ca^{2+}$ channel current**

$$\bar{I}_{Ca} = \frac{\bar{P}_{Ca}}{C_{sc}} \frac{4V_m F^2}{RT} \frac{[Ca^{2+}]_i \exp(2V_m F/(RT)) - 0.341[Ca^{2+}]_e}{\exp(2V_m F/(RT)) - 1}$$

$$f^{\infty} = \frac{1}{1 + \exp[(V_m + 12.5)/5]}$$

$$\tau_f = 30 + \frac{200}{1 + \exp[(V_m + 20)/9.5]}$$

$$d^{\infty} = \frac{1}{1 + \exp[(V_m + 10)/-6.24]}$$

$$\tau_d = \frac{1}{\frac{0.25\exp[-0.01V_m]}{1+\exp[-0.07V_m]} + \frac{0.07\exp[-0.05(V_m+40)]}{1+\exp[0.05(V_m+40)]}}$$

$$f_{Ca}^{\infty} = \frac{1}{1 + \left(\frac{[Ca^{2+}]_i}{K_{mf_{Ca}}}\right)^3}$$

$$\tau_{f_{Ca}} = 30$$

$$I_{Ca} = \bar{I}_{Ca} f d f_{Ca}$$

$$\frac{df}{dt} = \frac{f^{\infty} - f}{\tau_f}$$

$$\frac{dd}{dt} = \frac{d^{\infty} - f}{\tau_d}$$

$$\frac{df_{Ca}}{dt} = \frac{f_{Ca}^{\infty} - f_{Ca}}{\tau_{f_{Ca}}} \tag{B.16}$$

**The $K^+$ current through the L-type $Ca^{2+}$ current**

$$I_{CaK} = \frac{\bar{P}_{CaK}}{C_{sc}} \frac{f d f_{Ca}}{1 + \frac{\bar{I}_{Ca}}{I_{Cahalf}}} \frac{1000 V_m F^2}{RT} \frac{[K^+]_i \exp(V_m F/(RT) - [K^+]_e}{\exp(V_m F/(RT) - 1} \tag{B.17}$$

**Calcium handling**

$$
\begin{aligned}
\frac{d[Ca^{2+}]_i}{dt} &= \beta_i \left( J_{rel} + J_{leak} - J_{up} - \frac{A_{Cap} C_{sc}}{2 F V_{myo}} \times (I_{Ca} + I_{Cab} I_{pCa} - 2 I_{NaCa}) \right) \\
\beta_i &= \left( 1 + \frac{[CMDN]_{tot} K_m^{CMDN}}{(K_m^{CMDN} + [Ca^{2+}]_i)^2} \right)^{-1} \\
J_{rel} &= \bar{P}_{rel} f df_{Ca} \frac{\gamma [Ca^{2+}]_{SR} - [Ca^{2+}]_i}{1 + 1.65 \exp[V_m/20]} \\
J_{up} &= \frac{V_{up}}{1 + \left( \frac{K_{m_{up}}}{[Ca^{2+}]_i} \right)^2} \\
J_{leak} &= \bar{P}_{leak} \left( [Ca^{2+}]_{SR} - [Ca^{2+}]_i \right) \\
\gamma &= \frac{1}{1 + \left( \frac{2000}{[Ca^{2+}]_{SR}} \right)^2} \\
\frac{d[Ca^{2+}]_{SR}}{dt} &= \beta_{SR} (J_{up} - J_{leak} - J_{rel}) \frac{V_{myo}}{V_{SR}} \\
\beta_{SR} &= \left( 1 + \frac{[CSQN]_{tot} K_m^{CSQN}}{(K_m^{CSQN} + [Ca^{2+}]_{SR})^2} \right)^{-1}
\end{aligned}
\tag{B.18}
$$

Table B.1: Parameters and initial conditions.

| **Parameters** | **Values** |
|---|---|
| $g_{Na}$ | 12.8 mS/μF |
| $g_{K1}$ | 2.8 mS/μF |
| $g_{Kr}$ | 0.0136 mS/μF |
| $g_{Ks}$ | 0.0245 mS/μF |
| $g_{Kp}$ | 0.00216 mS/μF |
| $g_{to}$ | 0.23815 mS/μF |
| $g_{Na,b}$ | 0.0031 mS/μF |
| $g_{Ca,b}$ | 0.0003842 mS/μF |
| $\bar{P}_{Ca}$ | 0.0003842 cm/ms |
| $\bar{P}_{CaK}$ | $5.7 \times 10^{-7}$ cm/ms |
| $\bar{P}_{rel}$ | 6 m/s |
| $\bar{P}_{leak}$ | 0.000001 m/s |
| $\bar{I}_{NaK}$ | 0.693 μA/μF |
| $\bar{I}_{pahalf}$ | $-0.265$ μA/μF |
| $\bar{I}_{pCa}$ | 0.05 μA/μF |
| $R$ | 8.314 J/mol K |
| $T$ | 310 Kelvins |
| $F$ | 96.5 coulomb/mol K |
| $A_{cap}$ | $1.534 \times 10^{-4}$ cm$^2$ |
| $C_{sc}$ | 0.00216 μF/cm$^2$ |
| $\eta$ | 0.35 |
| $k_{sat}$ | 0.2 |

contd.

| Parameters | Values |
|---|---|
| $k_{NaCa}$ | 0.0003842 μA/μF |
| $\bar{P}_{Ca}$ | 0.0003842 cm/ms |
| $K_{mf_{Ca}}$ | 0.18 μM |
| $K_{mK1}$ | 13 mM |
| $K_{mNa}$ | 87.5 mM |
| $K_{mCa}$ | 1380 μM |
| $K_{mNa_i}$ | 10 mM |
| $K_{mpKo}$ | 1.5 mM |
| $K_{mpCa}$ | 0.05 μM |
| $[CMDN]_{tot}$ | 0.32 μM |
| $[CSQN]_{tot}$ | 10000 μM |
| $K_m^{CMDN}$ | 2 μM |
| $K_m^{CSQN}$ | 600 μM |
| $V_{up}$ | 0.1 μM/ms |
| $V_{myo}$ | $25.84 \times 10^{-6}$ μL |
| $V_{SR}$ | $2 \times 10^{-6}$ μL |
| $[Na^+]_i$ | 10 mM |
| $[K^+]_i$ | 149.5 mM |
| $[Na^+]_i$ | 138 mM |
| $[K^+]_e$ | 4 mM |
| $[Ca^{2+}]_i$ | 2000 μM |

Table B.2: Initial Conditions

| **Parameters** | **Values** |
|---|---|
| Initial Conditions | |
| $t$ | 0.0 ms |
| $V_i$ | $-94.7$ μV |
| $[Ca^{2+}]_i$ | 0.0472 μmol |
| $[Ca^{2+}]_{SR}$ | 320 μmol |
| $f$ | 0.983 |
| $d$ | 0.0001 μM |
| $m$ | $2.4 \times 10^{-4}$ |
| $h$ | 0.99869 |
| $j$ | 0.99857 |
| $f_{Ca}$ | 0.942 μM |
| $X_{Kr}$ | 0.229 mM |
| $X_{Ks}$ | 0.0001 mM |
| $X_{to}$ | $3.742 \times 10^{-5}$ mM |
| $Y_{to}$ | 1 μM |

## B.1 Glossary

| | |
|---|---|
| $\alpha_h$ | Voltage-dependent $h$ gate parameter |
| $\alpha_j$ | Voltage-dependent $j$ gate parameter |
| $\alpha_m$ | Voltage-dependent $m$ gate parameter |
| $\alpha_{X_{to}}$ | Voltage-dependent $X_{to}$ gate parameter |
| $\beta_h$ | Voltage-dependent $h$ gate parameter |
| $\beta_i$ | Myoplasmic buffering factor |
| $\beta_j$ | Voltage-dependent $j$ gate parameter |
| $\beta_m$ | Voltage-dependent $m$ gate parameter |
| $\beta_{SR}$ | Sarcoplasmic reticulum buffering factor |
| $\beta_{X_{to}}$ | Voltage-dependent $X_{to}$ gate parameter |
| $\gamma$ | Sarcoplasmic reticulum $Ca^{2+}$dependent $J_{rel}$ factor |
| $\eta$ | Controls voltage dependence of $I_{NaCa}$ |
| $\sigma$ | Extracellular $Na^+$ $I_{NaK}$ factor |
| $\tau_d$ | $I_{Ca}$ activation time constant |
| $\tau_f$ | $I_{Ca}$ inactivation time constant |
| $\tau_{f_{Ca}}$ | $Ca^{2+}$-dependent $I_{Ca}$ inactivation time constant |
| $\tau_{Kr}$ | $I_{Kr}$ activation time constant |
| $\tau_{Ks}$ | $I_{Ks}$ activation time constant |
| $A_{cap}$ | Capacitive membrane area |

| | |
|---|---|
| $C_{sc}$ | Specific membrane capacity |
| $\Delta Ca_{max}$ | Maximum change in $Ca^{2+}$ |
| $\Delta Ca_{min}$ | Minimum change in $Ca^{2+}$ |
| $[Ca^{2+}]_i$ | Intracellular $Ca^{2+}$ concentration |
| $[Ca^{2+}]_e$ | Extracellular $Ca^{2+}$ concentration |
| $[Ca^{2+}]_{SR}$ | Sarcoplasmic reticulum $Ca^{2+}$ concentration |
| $[CMDN]_{tot}$ | Total calmodulin concentration |
| $[CSQN]_{tot}$ | Total calsequestrin concentration |
| $d$ | $I_{Ca}$ activation gate |
| $d^{\infty}$ | Steady-state $I_{Ca}$ activation |
| $E_{Ca}$ | $Ca^{2+}$ equilibrium potential |
| $E_K$ | $K^+$ equilibrium potential |
| $E_{Ks}$ | $I_{Ks}$ equilibrium potential |
| $E_{Na}$ | $Na^+$ equilibrium potential |
| $f$ | $I_{Ca}$ inactivation gate |

| | |
|---|---|
| $f^{\infty}$ | Steady-state $I_{Ca}$ inactivation |
| $f_{Ca}^{\infty}$ | Steady-state $Ca^{2+}$-dependent $I_{Ca}$ inactivation |
| $f_{Ca}$ | $Ca^{2+}$-dependent $I_{Ca}$ inactivation gate |
| $f_{NaK}$ | Voltage-dependent $I_{NaK}$ factor |
| $F$ | Faraday constant |
| $g_{Cab}$ | Peak $I_{Cab}$ conductance |
| $g_{K1}$ | Peak $I_{K1}$ conductance |
| $g_{Kp}$ | Peak $I_{Kp}$ conductance |
| $g_{Kr}$ | Peak $I_{Kr}$ conductance |
| $g_{Ks}$ | Peak $I_{Ks}$ conductance |
| $g_{Na}$ | Peak $I_{Na}$ conductance |
| $g_{to}$ | Peak $I_{to}$ conductance |
| $h$ | Fast $I_{Na}$ inactivation gate |
| $I_{Ca}$ | L-type $Ca^{2+}$ channel current |
| $\bar{I}_{Ca}$ | Maximal $I_{Ca}$ |
| $I_{Cab}$ | $Ca^{2+}$ background current |
| $I_{Cahalf}$ | $\bar{I}_{Ca}$ level that reduces $\bar{P}_{CaK}$ by one-half |
| $I_{CaK}$ | $K^{+}$ current through the L-type $Ca^{2+}$ channel |
| $I_{K1}$ | Inward rectifier $K^{+}$ current |

| | |
|---|---|
| $I_{Kp}$ | Plateau $K^+$ current |
| $I_{Kr}$ | Rapid component of the delayed rectifier $K^+$ current |
| $I_{Ks}$ | Slow component of the delayed rectifier $K^+$ current |
| $I_{Na}$ | $Na^+$ current |
| $I_{Nab}$ | $Na^+$ background current |
| $I_{NaCa}$ | $Na^+/Ca^{2+}$ exchange current |
| $I_{NaK}$ | $Na^+$-$K^+$ pump current |
| $\bar{I}_{NaK}$ | Maximal $I_{NaK}$ |
| $I_{pCa}$ | Sarcolemmal $Ca^{2+}$ pump current |
| $I_{pCa}$ | Maximal $I_{pCa}$ |
| $I_{stim}$ | Stimulus current |
| $I_{to}$ | Transient outward $K^+$ current |
| $j$ | Slow $I_{Na}$ inactivation gate |
| $J_{leak}$ | Leakage $Ca^{2+}$ flux from the sarcoplasmic reticulum |
| $J_{rel}$ | Release $Ca^{2+}$ flux from the sarcoplasmic reticulum |
| $J_{up}$ | Uptake $Ca^{2+}$ flux to the sarcoplasmic reticulum |
| $J_{SR}$ | Junctional sarcoplasmic reticulum |
| $k_{NaCa}$ | Scaling factor for $I_{NaCa}$ |
| $k_{sat}$ | $I_{NaCa}$ saturation factor for $I_{NaCa}$ |

| | |
|---|---|
| $K_1^\infty$ | Steady-state $I_{K1}$ activation |
| $K_{Kp}$ | $I_{Kp}$ activation |
| $K_m^{CMDN}$ | $Ca^{2+}$ half-saturation constant for calmodulin |
| $K_m^{CSQN}$ | $Ca^{2+}$ half-saturation constant for calsequestrin |
| $K_{mCa}$ | $Ca^{2+}$ half-saturation constant for $I_{NaCa}$ |
| $K_{mf_{Ca}}$ | $Ca^{2+}$ half-saturation constant for $f_{Ca}$ |
| $K_{mK1}$ | $K^+$ half-saturation constant for $I_{K1}$ |
| $K_{mKo}$ | $K^+$ half-saturation constant for $I_{NaK}$ |
| $K_{mNa}$ | $Na^+$ half-saturation constant for $I_{NaCa}$ |
| $K_{mNai}$ | $Na^+$ half-saturation constant for $I_{NaK}$ |
| $K_{mpCa}$ | Half-saturation constant for $I_{pCa}$ |
| $K_{mup}$ | $Ca^{2+}$ half-saturation constant for $J_{up}$ |
| $[K^+]_i$ | Intracellular $K^+$ concentration |
| $[K^+]_e$ | Extracellular $K^+$ concentration |
| $m$ | $I_{Na}$ activation gate |
| $[Na^+]_i$ | Intracellular $Na^+$ concentration |
| $[Na^+]_e$ | Extracellular $Na^+$ concentration |

| | |
|---|---|
| $\bar{P}_{Ca}$ | L-type $Ca^{2+}$ channel permeability to $Ca^{2+}$ |
| $\bar{P}_{CaK}$ | L-type $Ca^{2+}$ channel permeability to $K^{+}$ |
| $\bar{P}_{leak}$ | $Ca^{2+}$ leakage permeability between the sarcoplasmic reticulum and the myoplasm |
| $\bar{P}_{rel}$ | $Ca^{2+}$ maximal release permeability from the sarcoplasmic reticulum |
| $R$ | Ideal gas constant |
| $t$ | Time |
| $T$ | Temperature |
| $V_m$ | Membrabe voltage |
| $\Delta V_{max}$ | Maximum change in voltage |
| $\Delta V_{min}$ | Minimum change in voltage |
| $V_{myo}$ | Myoplasmic volume |
| $V_{SR}$ | Sarcoplasmic reticulum volume |
| $V_{up}$ | Maximal $Ca^{2+}$ uptake to the sarcoplasmic reticulum |
| $X_{Kr}$ | $I_{Kr}$ activation gate |
| $X_{Kr}^{\infty}$ | Steady-state $I_{Kr}$ activation |
| $X_{Ks}$ | $I_{Ks}$ activation gate |
| $X_{Ks}$ | Steady-state $I_{Ks}$ activation |
| $X_{to}$ | $I_{to}$ activation gate |
| $Y_{to}$ | $I_{to}$ inactivation gate |

# VITA

| | |
|---|---|
| Personal Background | Binaya Tuladhar<br>Kathmandu, Nepal<br>Son of Manik Tuladhar and Sumati Tuladhar |
| Education | Bachelor/Master of Science in Physics<br>Tribhuvan University, Kathmandu, Nepal, 1990<br>Master of Science in Physics<br>University of Massachusetts Lowell<br>Lowell, MA, USA, May 2011<br>Master of Science in Physics with Biophysics option<br>Texas Christian University, Fort Worth, TX, USA, May 2019 |
| Experience | Lecturer of Physics,<br>Tribhuvan University, Kathmandu, Nepal<br>August 1991–June 2005<br>Teaching Assistant, University of Massachusetts Lowell, MA, USA<br>September 2007–May 2011<br>Adjunct Faculty, Texas Christian University, Fort Worth, TX, USA<br>August 2012–December 2012<br>Teaching Assistant, Texas Christian University, Fort Worth, TX, USA<br>January 2013–July 2017 |
| Professional Membership | Nepal Physical Society |

ABSTRACT

A COMPARATIVE MODELING STUDY OF THE DOSE DEPENDENT EFFECTS OF ANTIARRHYTHMICS ON A CARDIAC CELL

by Binaya Tuladhar, M.S., 2019
Department of Physics and Astronomy
Texas Christian University

Hana M Dobrovolny, Associate Professor of Physics

Sudden cardiac death (SCD) in humans due to cardiac arrhythmia is one of the leading causes of mortality in the world. Antiarrhythmic drugs were developed to treat abnormal heart rhythms resulting from the irregular electrical activity of the heart. Several different classes of antiarrhythmic drugs, each primarily blocking a different ion channel, are currently available. It is essential to understand how these drugs affect the electrophysiological properties of cardiac cells. The main goal of our study is to understand how these drugs change the behavior of the ionic currents during the action potential at slower and faster heart rates in the ventricular cells of two different species.

In this paper, we use mathematical models of a human ventricular cell, the Bernus model and a canine ventricular cell, the Fox model, to study the response to three different classes of antiarrhythmic drugs: $Na^+$ channel blockers, $K^+$ channel blockers and $Ca^{2+}$ channel blockers. We compare the dose dependence of action potential duration (APD), rate dependence, hysteresis, restitution and the appearance of arrhythmias for the three classes of drugs. The Bernus model and the Fox model both predict that $Na^+$ channel blockers will have little effect on any electrophysiologic features except at high doses; $K^+$

channel blockers increase the APD, exhibit reverse rate-dependence and have a biphasic effect on the occurrence of arrhythmias as dose increases; and $Ca^{2+}$ channel blockers decrease APD, show reverse rate-dependence and decrease the occurrence of arrhythmias. The techniques developed in this study provide a method for examining predictions of antiarrhythmic effects using more complex cardiac models.

Electric restitution plays an important role in the function of the heart and is believed to determine the stability of heart rhythms. We investigate the effects of various antiarrhythmic drugs on restitution properties of APD of human and canine ventricular cells. Both dynamic and S1-S2 restitution protocol is implemented to study the slope of the restitution curves. Our study examines the maximum slope of these curves for three classes of antiarrhythmic drugs.